# Study and Miniaturisation of Antennas for Ultra Wideband Communication Systems

by

Lu Guo

A thesis submitted to the University of London for the degree of Doctor of Philosophy

School of Electronic Engineering and Computer Science

Queen Mary, University of London

United Kingdom

September 2009

*I hereby declare that the work presented in this thesis is my own and all references are cited accordingly.*

**TO MY PARENTS**

# Abstract

Wireless communications have been growing with an astonishing rate over the past few years and wireless terminals for future applications are required to provide diverse services. This rising demand prompts the needs for antennas able to cover multiple bandwidths or an ultrawide bandwidth for various systems.

Since the release by the Federal Communications Commission (FCC) of a bandwidth of 7.5 GHz (from 3.1 GHz to 10.6 GHz) for ultra wideband (UWB) wireless communications, UWB has been rapidly evolving as a potential wireless technology and UWB antennas have consequently drawn more and more attention from both academia and industries worldwide.

Unlike traditional narrow band antennas, design and analysis of UWB antennas are facing more challenges and difficulties. A competent UWB antenna should be capable of operating over an ultra wide bandwidth as assigned by the FCC. At the same time, a small and compact antenna size is highly desired, due to the integration requirement of entire UWB systems. Another key requirement of UWB antennas is the good time domain behaviour, i.e. a good impulse response with minimal distortion.

This thesis focuses on UWB antenna miniaturisation and analysis. Studies have been undertaken to cover the aspects of UWB fundamentals and antenna theory. Extensive investigations are also conducted on three different types of miniaturised UWB antennas.

The first type of miniaturised UWB antenna studied in this thesis is the loaded orthogonal half disc monopole antenna. An inductive load is introduced to broaden the impedance bandwidth as well as the pattern bandwidth, in other words, an equivalent size reduction is realised.

The second type of miniaturised UWB antenna is the printed half disc monopole antenna. By simply halving the original antenna and tuning the width of the coplanar ground plane, a significant more than 50% size reduction is achieved.

The third type of miniaturised UWB antenna is the printed quasi-self-complementary antenna. By exploiting a quasi-self-complementary structure and a built-in matching section, a small and compact antenna dimension is achieved.

The performances and characteristics of the three types of miniaturised UWB antennas are studied both numerically and experimentally and the design parameters for achieving optimal operation of the antennas are also analysed extensively in order to understand the antenna operations.

Also, time domain performance of the Coplanar Waveguide (CPW)-fed disc monopole antenna is examined in this thesis to demonstrate the importance of time domain study on UWB antennas.

# Acknowledgements

Over the past few years of my PhD study, I feel honoured and lucky to work with some of the most prestigious researchers in the Department of Electronic Engineering, Queen Mary, University of London. I would like to show my most cordial gratitude to those who have been helping me during the past few years. There would be no any progress without their generous and sincere support.

First of all, I would like to thank my supervisors Professor Clive Parini and Professor Xiaodong Chen, for their kind supervision and encouragement. I am impressed by their notable academic background and profound understanding of the subjects, which have proved to be immense benefits to me. It has been my great pleasure and honour to be under their supervision and work with them.

Second of all, I would like to thank Mr John Dupuy for his help in the fabrication and measurement of antennas I have designed during my PhD study. Also, a special acknowledgement goes to all of the staff for all the assistance throughout my graduate program.

Many thanks are contributed to my fellow colleagues and friends, Mrs Sheng Wang, Dr Bin Yang, Dr Zhao Wang, Dr Daohui Li, Dr Yue Gao, Dr Jianxin Liang, Dr Choo Chiau, Mr Masood Ur Rehman, Mr Zhenxin Zhu, Miss Shuxian Chen, Mr Xiaojing Wang and Mr Shihua Wang for their valuable discussions and feasible advices to my research.

I own a great deal to the Department of Electronic Engineering, Queen Mary, University of London for their financial support.

Finally, I must express my appreciation to my parents for their continuous care and understanding during the period of my study.

# Table of Contents

# List of Figures

# List of Tables

# List of Abbreviations

| | |
|---|---|
| 1G | First-Generation |
| 2G | Second-Generation |
| 3G | Third-Generation |
| 4G | Fourth-Generation |
| APT | Asia-Pacific Telecommunity |
| AWGN | Additive White Gaussian Noise |
| BW | BandWidth |
| CEPT | European Conference of Postal and Telecommunications Administrations |
| CMOS | Complementary Metal Oxide Semiconductor |
| CPW | Coplanar Waveguide |
| DAA | Detect and Avoid |
| DC | Direct Current |
| DS-UWB | Direct Sequence Ultra Wideband |
| DVD | Digital Video Disc |
| ECC | Electronic Communications Committee |
| EM | ElectroMagnetic |
| ETRI | Electronics and Telecommunications Research Institute |
| FBW | Fractional BandWidth |
| FCC | Federal Communications Commission |
| FIT | Finite Integration Technique |
| FR4 | Flame Retardant 4 |
| GPS | Global Positioning System |
| HDTV | High-Definition TV |

| | |
|---|---|
| IEEE | Institute of Electrical and Electronics Engineers |
| IFFT | Inverse Fast Fourier Transform |
| IP | Internet Protocol |
| ISI | Intersymbol Interference |
| ISM | Industrial Scientific and Medicine |
| ITU | International Telecommunication Union |
| LCD | Liquid Crystal Display |
| LED | Light Emitting Diode |
| LTCC | Low Temperature Co-fired Ceramic |
| MBOA | MultiBand OFDM Alliance |
| MB-OFDM | MultiBand Orthogonal Frequency Division Multiplexing |
| MIC | Ministry of Internal Affairs & Communications |
| MP3 | MPEG-1 Audio Layer 3 |
| OEM | Original Equipment Manufacturer |
| Ofcom | Office of Communications |
| OFDM | Orthogonal Frequency Division Multiplexing |
| PAM | Pulse Amplitude Modulation |
| PC | Personal Computer |
| PCB | Printed Circuit Board |
| PHY | Physical Layer |
| PLUS | Precision Location Ultra-wideband System |
| PPM | Pulse Position Modulation |
| PSD | Power Spectral Density |
| PVP | Personal Video Player |
| RF | Radio Frequency |
| RTLS | Real-Time Location System |
| SCA | Self-Complementary Antenna |

| | |
|---|---|
| SMA | SubMiniature version A |
| SNR | Signal-to-Noise Ratio |
| TGs | Task Groups |
| UFZ | UWB Friendly Zone |
| USB | Universal Serial Bus |
| UWB | Ultra Wideband |
| VSWR | Voltage Standing Wave Ratio |
| WBAN | Wireless Body Area Network |
| WGs | Work Groups |
| WLAN | Wireless Local Area Network |
| WPAN | Wireless Personal Area Network |
| WUSB | Wireless Universal Serial Bus |

# Chapter 1 Introduction

## 1.1 Introduction

With the advent of the information era, numerous advanced communication technologies have arisen during the past two decades, which, have greatly influenced and benefited every field of human society. The first-generation (1G) mobile communication technology only enabled analogue voice communication while the second-generation (2G) technology achieved digital voice communication. Currently, the third-generation (3G) technology can offer a wide range of high speed mobile services, including video calling, internet access, messaging, e-mail and information services. In the near future, the fourth-generation (4G) technology will be able to provide a comprehensive IP (Internet Protocol) solution where voice, data and streamed multimedia can be offered to users anytime and anywhere, and at higher data rate than former generations.

In the past few years, wireless personal area network (WPAN) has been attracting considerable interest and undergoing rapid development worldwide. A WPAN is a network for interconnecting devices around an individual person's workspace in which the connections are wireless. The future WPAN aims to achieve seamless operation among home or business devices and systems. In addition, fast data storage and exchange among these devices will also be realised. This demands a data rate which is much higher than what has been achieved in currently existing wireless technologies.

The maximum available data rate, or capacity, for the ideal band-limited additive white Gaussian noise (AWGN) channel is linked with the bandwidth and

signal-to-noise ratio (SNR) by Shannon-Nyquist criterion [1, 2], as given in equation 1.1.

$$C = B\log_2(1+SNR) \tag{1.1}$$

where $C$ represents the maximum transmission data rate, $B$ denotes the channel bandwidth.

Equation 1.1 illustrates that the transmission data rate can be raised by enlarging the bandwidth or amplifying the transmission power. Nevertheless, the signal power can't be easily increased as many portable devices are powered by battery and the potential interference with other radio systems should be also suppressed. Therefore, a huge frequency bandwidth will be the solution to realise a high data rate.

In 2002, the United States Federal Communications Commission (FCC) adopted the First Report and Order that validated the commercial operation of ultra wideband (UWB) technology [3]. Since then, UWB technology has been swiftly evolving as one of the most promising wireless technologies that provide the high bandwidth required by the latest and future portable home and office devices for multiple digital video and audio streams.

## 1.2 Review of the State-of-Art

Research and development on UWB systems have been progressing greatly. At the Freescale Technology Forum 2005, Freescale and Haier demonstrated a UWB-enabled LCD (Liquid Crystal Display) digital television and digital media server.

Figure 1.1: Haier's UWB-enabled LCD digital television and digital media server [4].

As shown in figure 1.1, the Haier television is a 37-inch, LCD HDTV (High-Definition TV). The Freescale UWB antenna is embedded inside the television and is invisible to the user. The UWB antenna is a flat planar design etched on a single metal layer of common Flame Retardant 4 (FR4) circuit board material. No extra equipment is required and consumers only need a power supply for the actual television. The digital media server presents a size of a standard digital video disc (DVD) player but includes personal video player (PVP) functionality, a DVD playback capability and a tuner, as well as the Freescale UWB solution to wirelessly stream media to the HDTV. The digital media server can be placed as far away as 20 metres from the actual HDTV, providing plenty of freedom in home theatre configuration and the transmission data rate is up to 110 megabits per second.

At the International Consumer Electronics Show in Las Vegas in January 2006, Belkin demonstrates its new CableFree USB (Universal Serial Bus) Hub, the industry's first USB Hub that does not need a cable to connect to the computer [5]. This hub allows people to place their laptop in the room while still maintaining wireless access to their USB devices, such as printers, scanners, hard drives, and MP3 (MPEG-1 Audio Layer 3) players. The CableFree USB Hub's wireless

functionality is enabled by Freescale Semiconductor's Ultra-Wideband technology.


Figure 1.2: Belkin's four-port CableFree USB Hub [5].

The Belkin's four-port hub, as shown in figure 1.2, is capable of high-speed wireless connectivity for any USB device without requiring software. The CableFree USB hub provides desktop computer users the freedom to put their USB devices in the room without running long cables. Laptop users benefit from the freedom to roam wirelessly with their laptop around the room while still retaining access to their stationary USB devices.

Recently, Time Domain Corporation, a world leader in ultra wideband product development, has introduced the thinnest active wearable UWB badge tag for real-time location system (RTLS) applications [6]. As displayed in figure 1.3, with a thickness of 6.8mm, height of 75mm and width of 37mm, the vertically-oriented, LED (Light Emitting Diode)-enabled PLUS (Precision Location Ultra-Wideband System) 2.0 Badge Tag can be easily attached to the collar, shirt pocket, lanyard or the belt. Users can confirm their arrival and status at a location or interaction with another person or equipments by the PLUS 2.0 Badge Tag, which

features a four-year battery life.


Figure 1.3: Time Domain's PLUS 2.0 Badge Tag [6].

## 1.3 Motivation

The UWB technology has undergone remarkable achievements during the past few years. In spite of all the promising prospects featured by UWB, there are still challenges in making this technology fulfill its full potential. One particular challenge is the UWB antenna.

In recent years, many varieties of UWB antennas have been proposed and investigated. They present a simple structure and UWB characteristics with nearly omni-directional radiation patterns. However, for some space-limited applications, UWB antennas need to feature a compact size while maintaining UWB characteristics. Therefore, miniaturisation of UWB antennas becomes an interesting research topic and deserves a comprehensive investigation and analysis.

In this thesis, three different miniaturisation approaches are applied to UWB antennas and all the miniaturised UWB antennas are investigated in detail in order to understand their operations. Furthermore, some quantitative guidelines are obtained

for designing these miniaturised UWB antennas.

In addition, a competent UWB antenna should also have good time domain characteristics. Unlike traditional narrow band systems, UWB systems usually employ short pulses to convey information. In other words, a huge bandwidth is occupied. In this case the antenna parameters will have to be treated as functions of frequency and will impose more significant impacts on the input signal. Moreover, successful transmission and reception of UWB signals entails minimisation of ringing, spreading and distortion of the pulses in the time domain. Therefore, it is indispensable and important to study antenna characteristics in the time domain. In this thesis, a Coplanar Waveguide (CPW)-Fed disc monopole antenna is exemplified to evaluate its time domain behaviour.

## 1.4 Organisation of the Thesis

This thesis is organised in eight chapters as follows:

Chapter 2 gives a brief introduction of UWB technology. The history and concept of UWB technology are reviewed. Its advantages as well as applications are also addressed. In addition, current regulations and standards are discussed.

Chapter 3 illustrates the principal requirements for a competent UWB antenna. A variety of widely-used and effective miniaturisation techniques for antennas are also discussed in this chapter.

Chapter 4 describes a study on a loaded orthogonal half disc monopole antenna. A pair of loading strips is introduced to broaden the bandwidth at the lower band. The key parameters that determine the antenna performance are investigated both numerically and experimentally to derive the design rules.

Chapter 5 addresses a design of printed half disc monopole. The operation

principle of the antenna is illustrated based on the investigation of the antenna performance and characteristic. The antenna configuration evolves from a CPW-Fed disc monopole antenna.

Chapter 6 presents novel and simple designs of printed quasi-self-complementary antennas. Printed on a dielectric substrate and fed by a 50Ω coaxial cable without using an extra matching circuit, planar antennas with the half disc self-complementary structure have been studied. The performance and characteristics of the antenna are investigated both numerically and experimentally to generate the design rules. In addition, an evolution of the proposed antenna is depicted to demonstrate the mechanism of the built-in CPW-like matching section.

Chapter 7 evaluates the time domain behaviour of the CPW-Fed disc monopole antenna. The performance of antenna system is analysed. Antenna response in both transmit and receive modes are studied. Furthermore, the received waveforms are assessed by the pulse fidelity.

Chapter 8 concludes the researches that have been undertaken in this thesis and some potential future works are also given in this chapter.

## References

[1] J. G. Proakis, “Digital Communications”, New York: McGraw-Hill, 1989.

[2] C. E. Shannon, “A Mathematical Theory of Communication”, *Bell Syst. Tech. J.*, vol. 27, pp. 379-423, 623-656, July & October 1948.

[3] FCC, First Report and Order 02-48. February 2002.

[4] http://www.freescale.com

[5] http://www.belkin.com

[6] http://www.timedomain.com

# Chapter 2 UWB Technology

UWB technology has been applied in aspects of radar, sensing and military communications during the past 20 years. Considerable research attention has been drawn since February 2002, when the FCC ruled that UWB can be used for data communications as well as radar and safety applications [1]. Since then, UWB technology has been swiftly progressing as a promising high data rate wireless communication technology for diverse applications.

This chapter presents a brief overview of UWB technology and elaborates its fundamentals, including UWB definition, advantages, applications, current regulations and standards.

## 2.1 Background

The concept of UWB was developed in the early 1960s through research in time domain electromagnetics, where impulse measurement techniques were adopted to characterise the transient behaviour of certain microwave networks [2]. In the late 1960s, impulse measurement techniques were employed for the design of wideband antennas, resulting in the development of short-pulse radar and communication systems [3]. In 1973, the first UWB communications patent was granted for a short-pulse receiver [4]. Through the late 1980s, UWB was referred to as carrier-free, baseband or impulse technology. The U.S. Department of Defence is believed to be the first to use the term ultra wideband in late 1980s. By 1989, UWB theory, techniques and many implementation methods had been developed for a broad range of applications, including radar, communications, positioning systems and so on.

However, most of the applications and development of UWB occurred in the military area or were funded by the U.S. government under classified programs [5, 6]. By the late 1990s, UWB technology had appeared more commercialised and its development had advanced greatly. Companies like Time Domain [7] and XtremeSpectrum [8] were founded around the idea of consumer communications using UWB.

A substantial change in UWB history took place in February 2002, when the FCC issued UWB rulings that provided the first radiation limitations for UWB transmission and allowed the operation of UWB devices on an unlicensed basis. According to the FCC rulings, UWB is defined as any wireless scheme that occupies either a fractional bandwidth greater than 20% or more than 500 MHz of absolute bandwidth. The fractional bandwidth is defined as $BW / f_c$, where $BW = f_H - f_L$ represents the -10 dB bandwidth and $f_c = (f_H + f_L)/2$ denotes the centre frequency. Here $f_H$ and $f_L$ indicate the upper frequency and the lower frequency, respectively, measured at -10 dB below the peak emission point. The FCC has also permitted the UWB radio transmissions in the unlicensed frequency band from 3.1 GHz to 10.6 GHz with a restricted transmit power of -41.3 dBm/MHz [1].

A UWB signal occupies extremely large bandwidth where the RF (Radio Frequency) energy is spread over an enormous spectrum. It is wider than any incumbent narrowband wireless system by orders of magnitude and its emitted power seen by other narrowband systems is a fraction of their own power. If the whole 7.5 GHz band is optimally utilised, the maximum achievable power to UWB transmitters is approximately 0.556 mW or less. This is barely a fraction of available transmit power in the industrial, scientific and medical (ISM) bands such as the WLAN (Wireless Local Area Network) IEEE (Institute of Electrical and Electronics

Engineers) 802.11a/b/g standards. This effectively confines the UWB scheme to indoor and short-range communications at high data rate or mid-range communications at low data rate. Applications such as wireless USB and WPANs have been proposed with hundreds of Mbps to several Gbps with distances ranging from 1 to 4 metres. For ranges beyond 20 metres, the achievable data rate by UWB is inferior to existing WLAN systems such as IEEE 802.11a/b/g [9].

## 2.2 UWB Transmission Schemes

Generally, UWB transmission schemes can be categorised into two main approaches: single-band and multiband.

A traditional UWB technology is based on single-band schemes adopting carrier-free or impulse radio communications [10, 11]. Impulse radio refers to the generation of a series of impulse-like waveforms, each of duration in the order of hundred of picoseconds. Each pulse spans a bandwidth of several gigahertz that must comply to the spectral mask requirements. The information is modulated directly into the sequence of pulses. Typically, one pulse carries the information for 1 bit. Data could be modulated using either pulse amplitude modulation (PAM) or pulse position modulation (PPM). Figure 2.1 shows a sequence of impulse-like waveforms, where $T_f$ is the frame interval, also known as the pulse repetition time, and $T_w$ is the duration of a monocycle. Typically, $T_f$ is 100 or 1000 times longer than the pulse width $T_w$. Multiple users can be supported using the time-hopping or direct-sequence spreading approaches. This type of transmission does not require the use of additional carrier modulation, as the pulse will propagate well in the radio channel. The technique is therefore a baseband signal approach. However, the single-band

system faces a challenging problem in building RF and analog circuits and in designing a low-complexity receiver that can capture sufficient multipath energy [12].

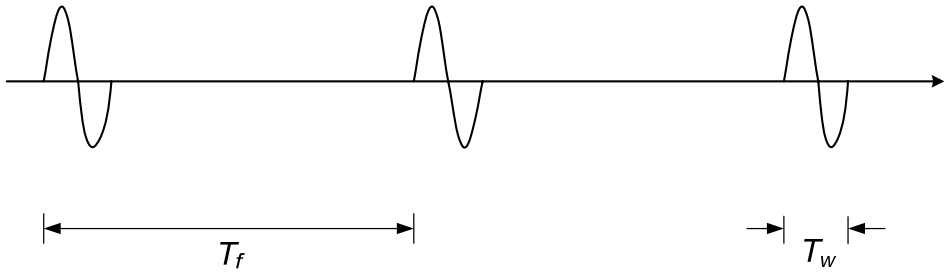


Figure 2.1: Pulse train with a low duty cycle, where $T_f$ is pulse repetition time and $T_w$ is pulse duration.

To overcome the disadvantage of single-band approaches, multiband approaches were proposed [13, 14]. Instead of using the entire UWB frequency band to convey information, the multiband technique divides the UWB frequency band from 3.1 to 10.6 GHz into several smaller bands, referred as subbands. Each subband has a bandwidth of at least 500 MHz to comply with the FCC definition of a UWB signal. Figure 2.2 illustrates a multiband UWB spectrum. In this example, each UWB signal occupies 500 MHz of bandwidth and eight of them cover the total bandwidth of 4 GHz. Each of these signals can be transmitted simultaneously to achieve a high data rate [12, 15].

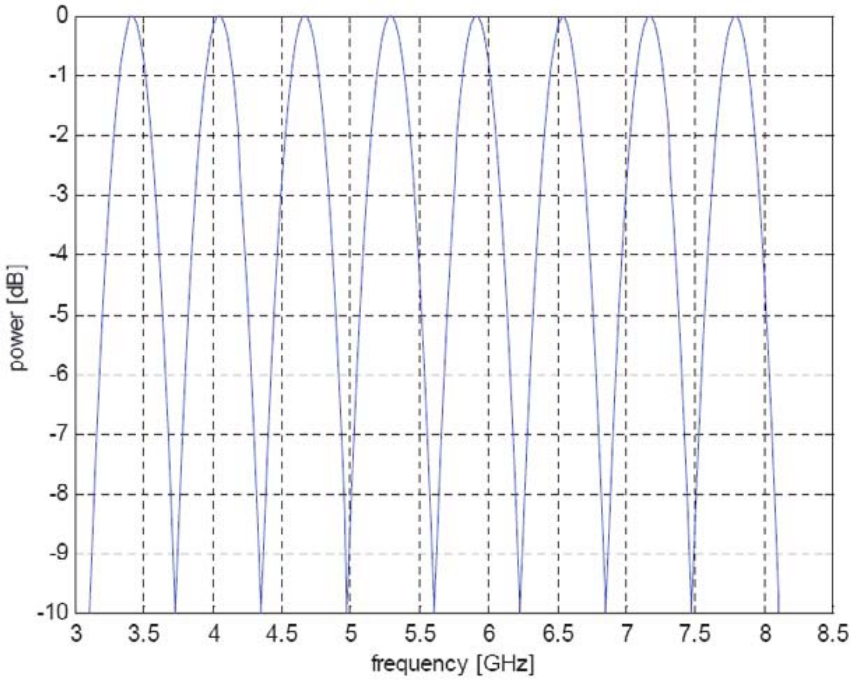


Figure 2.2: Multiband spectrum [15].

The signals can also be interleaved across subbands to maintain the transmitter power as if the large gigahertz bandwidth is utilised while allowing multiple users to transmit at the same time. Figure 2.3 depicts a time-domain representation of multiband UWB signals in which the signals at different centre frequencies are transmitted at different times. In the figure, the centre frequencies of the signals relative to the individual bands are shown in the vertical axis [12].

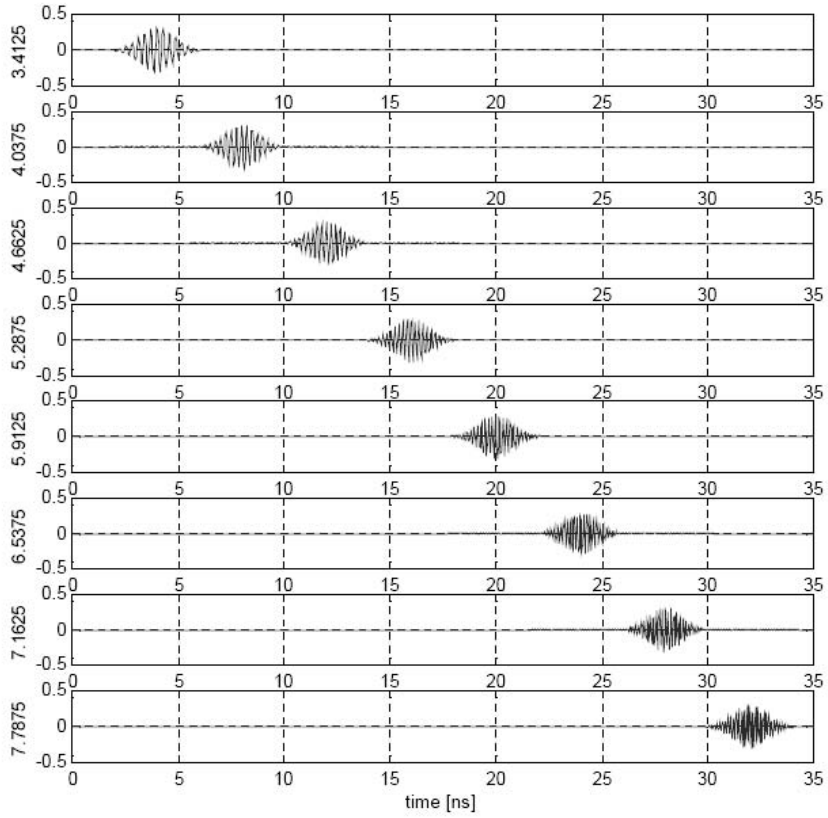


Figure 2.3: Multiband signals transmitted at different times [15].

With the multiband approach, the information can now be processed over a much smaller bandwidth, thereby reducing overall design complexity as well as improving spectral flexibility and worldwide compliance.

A multiband OFDM (MB-OFDM) approach that utilises a combination multiband approach and orthogonal frequency-division multiplexing (OFDM) technique was also proposed [16]. The OFDM technique is efficient at collecting multipath energy in highly dispersive channels, as is the case for most UWB channels [14]. Furthermore, OFDM allows each subband to be divided into a set of orthogonal narrowband channels (with a much longer symbol period duration). The main difference between multiband OFDM and traditional OFDM schemes is that the multiband OFDM symbols are not sent continually on one single frequency band; instead, they are interleaved over different subbands across both time and frequency.

Figure 2.4 illustrates the UWB multiband OFDM spectrum. The available UWB spectrum is divided into *S* subbands. Each subband occupies a bandwidth *BW* >500 MHz and the OFDM has *N* subcarriers. At each OFDM symbol period, the modulated symbol is transmitted over one of the *S* subbands. These symbols are time-interleaved across subbands. Multiple access to the multiband approach is enabled by the use of suitably designed frequency-hopping sequences over the set of subbands. A frequency synthesiser can be utilised to perform frequency hopping. By using proper time-frequency codes, a multiband system provides both frequency diversity and multiple access capability [12].

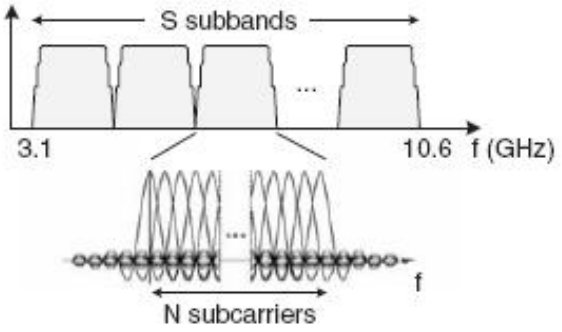


Figure 2.4: UWB multiband OFDM spectrum [12].

There are many trade-offs in the UWB approaches described above. The single-band approach benefits from a coding gain achieved through the use of time-hopping or direct-sequence spreading, exploiting Shannon's principle to a greater degree than does the multiband approach, offers greater precision for position location and realises better spectrum efficiency. However, it has less flexibility with regard to different worldwide spectral regulations and may be too broadband if other governments choose to restrict their UWB spectral allocations to smaller ranges than authorised by the FCC. On the other hand, the multiband approach is advantageous due to the ability for precise control of the transmitter power spectral density so as to

maximise the average power transmitted while meeting the spectral mask. It allows coexistence with flexible spectral coverage and is easier to adapt to different worldwide regulations. Furthermore, processing over a smaller bandwidth eases the requirement on analog-to-digital converter sampling rate and consequently facilitates greater digital processing. A comparison of key features of two UWB transmission schemes is shown in table 2-A [12, 17].

Table 2-A: Comparison of key features of two UWB transmission schemes.

| **Single-band schemes** | **Multiband-OFDM schemes** |
|---|---|
| Great precision for localisation | Flexible spectral coverage and easier to adapt to different worldwide regulations |
| High spectrum efficiency | Easier to be built in a single-chip solution |
| Does not require the use of additional carrier modulation, therefore low complexity | precise control of the transmitter power spectral density so as to maximise the average power transmitted while meeting the spectral mask |
| Less flexibility with regard to different spectral regulations | Reduced effects of intersymbol interference (ISI) |

## 2.3 Advantages of UWB

Owing to its ultra wideband nature, UWB communication systems present unique benefits that are attractive for radar and wireless communication applications. The primary advantages of UWB can be summarised as follows [18]:

(1) Potential for high data rate

(2) Multipath immunity

(3) Potential small size and low equipment cost

(4) High-precision ranging and localisation at the centimetre level

The extremely large bandwidth occupancy of UWB provides the potential of very high theoretical capacity, yielding very high data rates. This can be demonstrated by considering Shannon's capacity equation [19]:

$$C = B\log_2(1+\frac{S}{N}) \tag{2.1}$$

where $C$ is the maximum channel capacity, $B$ the signal bandwidth, $S$ the signal power and $N$ the noise power. Shannon's equation indicates that the capacity can be enhanced by either widening the signal bandwidth or increasing the signal power. Furthermore, it illustrates that capacity enhancement requires linear increases in bandwidth, while similar channel capacity enhancement would need exponential increases in signal power. Therefore, it can be seen from Shannon's equation that the UWB system exhibits a great potential for high-speed wireless communications.

Delivering information with ultra-short duration waveforms, UWB signals have low susceptibility to multipath interference. Multipath interference occurs when a modulated signal arrives at a receiver from various paths. Combining signals at the receiver can cause distortion of the signal received. The ultra-short duration of UWB waveforms provides a fine resolution of reflected pulses at the receiver. Therefore, UWB transmissions can resolve many paths and thus are rich in multipath diversity.

In single-band UWB scheme, no up / down-conversion is required at the transceivers, with the potential benefit of reducing the cost and size of the devices. In MB-OFDM UWB scheme, MB-OFDM technology is designed specifically to be built in low-cost CMOS (Complementary Metal Oxide Semiconductor) semiconductor processes. Single-chip CMOS integration of a UWB transceiver contributes directly to low cost, small size and low power.

The ultra-short duration of UWB waveforms gives rise to the potential ability of high-precision ranging and localisation. Together with good material penetration

properties, UWB signals offer opportunities for short-range radar applications such as rescue and anti-crime operations as well as in surveying and in the mining industry.

## 2.4 Applications of UWB

As mentioned in the previous section, UWB features some distinctive properties that make it attractive for various applications.

Multimedia communication is probably the obvious application due to the capability of high data rate delivery that is frequently acclaimed. The best proper scenario is likely to be WPANs in order to facilitate wireless devices connections and high speed image downloads in multipath rich environments. The high data rate WPANs can be defined as networks with a medium density of active devices per room (5 to 10) transmitting at data rates ranging from 100 to 500 Mbps within a distance of 20 metres [20]. The ultrawide bandwidth of UWB enables various WPAN applications, such as high-speed wireless universal serial bus (WUSB) connectivity for personal computers (PCs) and PC peripherals, high-quality real-time video and audio transmission, file exchange among storage systems and cable replacement for home entertainment systems. With the UWB technology, a user can bring a mobile device, such as a portable media player, in proximity to a content source, like a PC, laptop, or external hard drive. Once authentication and authorisation are completed, video files can be streamed onto the portable media player for later viewing. Figure 2.5 shows a typical application scenario where PC clusters interconnected through UWB [21].


Figure 2.5: PC clusters interconnected through UWB [21].

Different from conventional radar systems where targets are typically considered as point scatters, UWB radar pulses are shorter than the target dimensions. UWB reflections off the target exhibit not only changes in amplitude and time shift but also changes in the pulse shape. As a result, UWB waveforms present pronounced sensitivity to scattering relative to conventional radar signals. This property has been readily adopted by radar systems and can be extended to additional applications, such as underground, through-wall and ocean imaging, as well as medical diagnostics and border surveillance devices [18].

Sensor networks consist of a large number of nodes spread across a geographical area to be monitored. Depending on the specific application, the sensor nodes can be static, if deployed for, e.g., avalanche monitoring and pollution tracking, or mobile, if equipped on soldiers, firemen, or robots in military and emergency response situations. Key requirements for sensor networks operating in challenging environments include low cost, low power, and multifunctionality which can be met by using UWB technology. High data rate UWB communication systems are well capable of gathering and disseminating or exchanging an enormous quantity of

sensory data in a timely manner [22, 23].

Wireless Body Area Networks (WBANs) are networks whose nodes are usually placed close to the body on or in everyday clothing. A WBAN topology comprises many *transmit only sensor nodes*, that have to be very simple, low cost and extremely energy efficient, some *transceiver nodes*, that afford a somewhat higher complexity to sense and act, and few *high capability nodes*, e.g. master nodes with high computational capabilities and support for higher data rate. Compared to other wireless networks a WBAN has some distinct features and requirements. Due to the close proximity of the network to the body, electromagnetic pollution should be extremely low. Therefore, a noninvasive WBAN requires a low transmit power. Because of the rather simple hardware implementation and the low transmission power, UWB has consequently become one promising technology for the use in WBANs [24-26].

## 2.5 UWB Regulations and Standards

*A. UWB Regulations*

As mentioned previously, the UWB systems operate in a very huge bandwidth necessitating it to share the spectrum with other existing communication systems and consequently, interference may occur. The regulation of UWB radio spectrum is therefore necessary to establish a framework where UWB systems can peacefully co-exist with incumbent systems. For the regulation of UWB around the world there are many organisations and government entities that set rules and recommendations for UWB usage. The structure of international radio-communication regulatory bodies can be grouped into international, regional, and national levels.

The International Telecommunication Union (ITU) is an impartial,

international body where governments and the private sector work together on issues pertinent to telecommunication networks. The group that undertakes the work on UWB was created to study the compatibility between UWB and other communication systems. Most of telecommunication systems that occupy the allocated spectrum would prefer to keep UWB out of their frequency range.

At the regional level, the Asia-Pacific Telecommunity (APT) is an international body that sets recommendations and guidelines of telecommunications in the Asia-Pacific region. The European Conference of Postal & Telecommunications Administrations (CEPT) has created a task group under the Electronic Communications Committee (ECC) to draft a proposal regarding the use of UWB in Europe [17].

At the national level, the USA was the first country to authorise UWB for commercial use. In February 2002, the FCC has mandated that UWB radio transmission can legally operate in the range of 3.1 to 10.6 GHz, with the power spectral density (PSD) satisfying a specific spectral mask assigned by the FCC. In general, the spectral mask related with the FCC's UWB regulation was designed to prevent other spectrum users from undesirable interference caused by UWB operations. For wireless communications, the power levels regulated by the FCC are extremely low (i.e., -41.3 dBm/MHz), which permits UWB technology to overlay with existing services such as the GPS (Global Positioning System) and the WLAN [1, 27]. Figure 2.6 shows the FCC's indoor and outdoor emission masks.

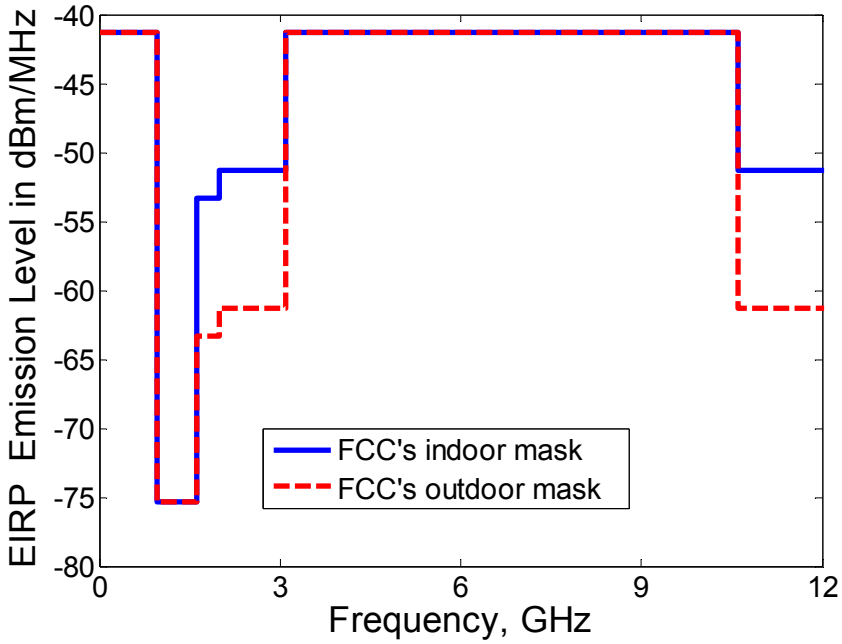


Figure 2.6: FCC's indoor and outdoor emission masks.

In the UK, the regulatory body, called the Office of Communications (Ofcom), opened a consultation on UWB matters in January 2005. The consultation consisted of 15 questions, asking opinions from those who are affected by the UWB technology. Ofcom sees UWB as a positive technology that if correctly regulated can bring economic growth to the UK. On August 13, 2007, Ofcom finally approved the use of ultra-wideband wireless technology without a license for use in the UK. Until 31 December 2010, 4.2 – 4.8 GHz band is allocated to UWB with no mitigation techniques required and the permitted transmission limits are -41.3 dBm/MHz. After 31 December 2010, 3.4 – 4.8 GHz band will be assigned to UWB with mitigation techniques required. A lower emission level of -70 dBm/MHz will be permitted [17, 28].

The regulatory body that set the policy on UWB in Japan is called the Ministry of Internal Affairs and Communications (MIC). The Japanese UWB radiation mask for indoor devices has two bands; from 3.4 to 4.8 GHz and from 7.25

to 10.25 GHz. For the 3.4-4.8 GHz band, it is required to use a technology to reduce interference with other radio systems. This interference mitigation technology is called Detect And Avoidance (DAA) [29] to ascertain the coexistence with incumbent systems and new services such as 4G systems. However, temporary measures are taken by now to permit the use of 4.2-4.8 GHz band without an interference reduction technology. It should be noted that no DAA is required for the band 7.25 – 10.25 GHz. Similar to the FCC mask, the power spectral density is limited to -41.3 dBm/MHz or lower on both bands [22].

In Korea, Electronics and Telecommunications Research Institute (ETRI) proposed an emission mask at a lot lower level than the FCC spectral mask. For the frequency range of 1-10 GHz, the Korean emission level is -66.5 dBm/MHz, which is about 25 dB lower than the FCC limit [22, 30].

In Singapore, the established UWB Friendly Zone (UFZ) allows test and trial of UWB technology by developers. The emission mask in the frequency range of 2.2-10.6 GHz is -35 dBm/MHz which is 6 dB higher than the FCC limit [22, 31].

The UWB proposals in Japan, Korea and Singapore against the FCC one are displayed in figure 2.7 [30].

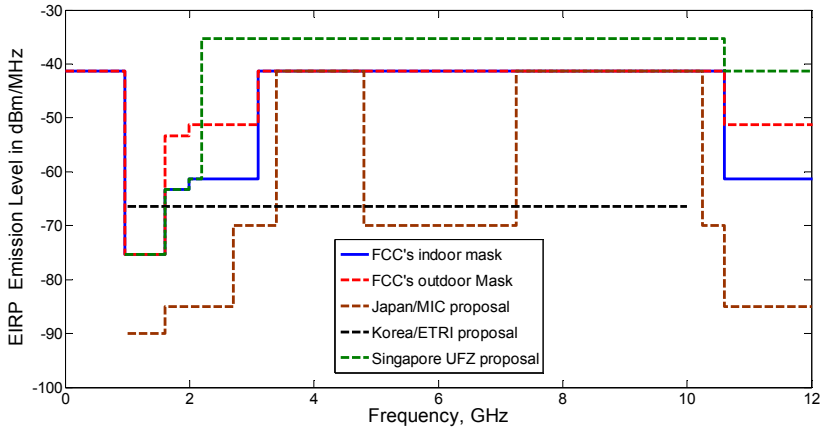


Figure 2.7: Proposed spectral masks in Aisa-Pacific (Reproduced from [30]).

*B. UWB Standards*

Different standards exist for different kind of technologies and processes. Standards are defined to provide uniform technical methods, processes, and understanding. Standards enable multi-vendor interoperability and allow competitive products to market quickly from different vendors. Especially in wireless communication systems, standards provide interoperability and interfaces for components and products from different vendors, so products can co-exist and co-work with each other without any problem [32].

In UWB matters, the IEEE is active in making standards. Within the IEEE 802 standard, the UWB standardisation activities initiate in the IEEE 802.15 Work Groups (WGs) for WPAN. The IEEE 802.15.3a (TG3a) and IEEE 802.15.4a (TG4a) are two Task Groups (TGs) within 802.15 WG that develop their standards based on UWB technology. The TG4a is focused on low rate alternative physical layer for WPANs. The technical requirements for the TG4a include low cost, low data rate, low complexity and low power consumption. The TG3a is aimed at developing high rate alternative physical layer for WPANs. The group targeted developing Physical Layer (PHY) standards to support data rates between 110 – 450 Mbps over short ranges (i.e., <10m) [32, 33]. There are two competitive proposals for the TG3a, i.e. the Direct Sequence UWB (DS-UWB) and the Multiband Orthogonal Frequency Division Multiplexing (MB-OFDM).

As introduced in the previous section, DS-UWB proposal is the conventional impulse radio approach to UWB communication, i.e. it employs short pulses which occupy a single band of several gigahertz for transmission. This proposal is mainly backed by Freescale and Motorola and its proponents have established their own group, namely, the UWB Forum [34].

MB-OFDM proposal is supported by MultiBand OFDM Alliance (MBOA) which merged with WiMedia Alliance in March 2005 and called WiMedia Alliance [35]. MB-OFDM combines the multiband approach together with the orthogonal frequency division multiplexing (OFDM) techniques, as described in the previous section.

After nearly three years of debates on technology and process issues, UWB PHY standardisation attempt failed in IEEE due to contrast between proposals supported by WiMedia Alliance and UWB Forum. Due to different basic modulation techniques of PHY, neither proposal's radio could communicate with the others, so both the radios can not co-exist. Finally, TG3a decided to disband the group in 2006 and decided to leave the issue of PHY to market [32]. In March, 2009, the Wimedia Alliance announced that they would hand over all current and future specification development of its version of UWB to the Bluetooth Special Interest Group, the Wireless USB Promoter Group and the USB Implementers Forum [36].

## 2.6 Summary

In this chapter, a general background of UWB technology is presented and its advantages, applications and current regulations and standards are also discussed. The future of UWB is promising and encouraging. However, the majority of the debate on UWB is around the question of whether it will incur detrimental interference to other existing systems and services. Wireless communications have always been regulated to avoid interference between different users of the spectrum. Since UWB occupies such a wide bandwidth, there are many users whose spectrum will be affected and they need to be assured that UWB will not cause undue interference to their existing services. Although UWB devices are restricted to

operate with a power level compliant with the emission mask, the concern about the potential interference will persist.

Due to its distinctive advantages, UWB technology can be used in a wide range of applications. First UWB implementations available in market are Wireless USB products. Universal Serial Bus (USB) is a very well adopted wired connectivity technology in PC market. Now, it is used in many consumer electronics devices also. UWB becomes the vehicle for unwiring USB through Wireless USB. First Certified Wireless USB products are in the form of dongles, which makes wired USB wireless. Companies like Alereon, Intel, NEC Electronics, Realtek Semiconductors, NXP Semiconductors, Staccato and Wisair are the leaders to provide silicon chips for Wireless USB products [32, 33]. Besides consumer products, UWB technology manufacturers can also see their products in test and measurement [22, 32] and medicine [17].

## References

[1] Federal Communications Commission, "Revision of Part 15 of the commission's rules regarding ultra-wideband transmission systems, first report and order", ET-Docket 98-153, FCC, Washington, DC, Feb. 2002.

[2] G. F. Ross, "The transient analysis of multiple beam feed networks for array systems", Ph.D. dissertation, Polytechnic Institute of Brooklyn, Brooklyn, NY, 1963.

[3] L. P. Ligthart, "Antennas and Propagation Measurement Techniques for UWB radio", *Wireless Personal Communications*, vol. 37, no. 3-4, May 2006, pp. 329-360.

[4] G. F. Ross, "Transmission and reception system for generating and receiving base-band duration pulse signals for short base-band pulse communication system", U.S. patent 3,728,632, Apr. 17, 1973.

[5] T. W. Barrett, "History of ultra wideband (UWB) radar and communications: pioneers and innovators", *Proceedings of Progress in Electromagnetics Symposium 2000 (PIERS2000)*, Cambridge, MA, July 5-14, 2000.

[6] C. L. Bennett and G. F. Ross, "Time-domain electromagnetics and its applications", *Proceedings of the IEEE*, vol. 66, no. 3, March, 1978, pp. 299-318.

[7] Time Domain. http://www.timedomain.com.

[8] XtremeSpectrum. http://www.xtremespectrum.com.

[9] I. Oppermann, "The role of UWB in 4G", *Kluwer Journal of Wireless Personal Communications*, vol. 29, pp. 121-133, 2004.

[10] M. Z. Win and R. A. Scholtz, "Impulse radio: how it works", *IEEE Commun. Lett*., vol. 2, no. 2, pp. 36-38, Feb. 1998.

[11] M. L. Welborn, "System considerations for ultra-wideband wireless networks", *Proc. IEEE Radio Wireless Conf*., pp. 5-8, August, 2001.

[12] W. Siriwongpairat and K. Liu, "Ultra-Wideband Communications Systems – MultiBand OFDM Approach", © 2007, John Wiley & Sons, Ltd.

[13] E. Saberinia and A. H. Tewfik, "Pulsed and non-pulsed OFDM ultra wideband wireless personal area networks", *Proc. IEEE Conf. Ultra Wideband Syst. Technol*., pp. 275-279, November, 2003.

[14] A. Batra et al., "Design of a multiband OFDM system for realistic UWB channel environments", *IEEE Trans. Microwave Theory Tech*., vol. 52, no. 9, pp. 2123-2138, September, 2004.

[15] Discrete Time Communications, "IEEE 802.15.3a 480Mbps wireless personal area networks: achieving a low complexity multi-band implementation", White Paper, January, 2003.

[16] A. Batra et al., "Multi-band OFDM physical layer proposal for IEEE 802.15 task

group 3a", IEEE P802.15-03/268r3, July, 2003.

[17] M. Ghavami, L. B. Michael and R. Kohno, "Ultra Wideband – signals and systems in communication engineering 2nd ed.", © 2007, John Wiley & Sons, Ltd.

[18] T. Kaiser et al., "UWB Communications Systems: A Comprehensive Overview", © 2006, Hindawi Publishing Corporation.

[19] J. G. Proakis, "Digital Communications, 4th ed.", McGraw-Hill, New York, 2001.

[20] R. Prasad and L. Munoz, "WLANs and WPANs towards 4G Wireless", © 2003, Artech House, Inc.

[21] "Ultra-Wideband (UWB) Technology Enabling high-speed wireless personal area networks", Intel White Paper, http://www.intel.com.

[22] H. Nikookar and R. Prasad, "Introduction to Ultra Wideband for Wireless Communications", © 2009, Springer Science+Business Media B.V.

[23] R. Kraemer and M. Katz, "Short-Range Wireless Communications-Emerging Technologies and Applications", © 2009, John Wiley & Sons, Ltd.

[24] P. Hall and Y. Hao, "Antennas and Propagation for Body-Centric Wireless Communications", © 2006, Artech House, Inc.

[25] H. Ghannoum, R. Errico, C. Roblin and X. Begaud, "Characterization of the UWB On-Body Propagation Channel", *The first European Conference on Antennas and Propagation (EuCAP 2006)*, Nice, France, 6-10 November, 2006.

[26] A. Fort, C. Desset, P. De Doncker, P. Wambacq and L. Van Biesen, "An ultra-wideband body area propagation channel model – From statistics to implementation", *IEEE Trans. Microw. Theory Tech*., vol. 54, no. 4, pp. 1820-1826, April, 2006.

[27] A. Safarian and P. Heydari, "Silicon-Based RF Front-Ends for Ultra Wideband Radios" © 2008, Springer Science+Business Media B.V.

[28] "Decision to make The Wireless Telegraphy (Ultra-Wideband Equipment)

(Exemption) Regulations 2007", http://www.ofcom.org.uk.

[29] "Detect and Avoid Technology – for Ultra Wideband (UWB) Spectrum Usage", Wisair White Paper, http://www.wisair.com.

[30] Y. Rahayu, T. Rahman, R. Ngah and P. Hall, "Ultra Wideband Technology and Its Applications", *International Conference on Wireless and Optical Communications Networks (WOCN 2008)*, Surabaya, Indonesia, 5-7 May, 2008.

[31] K. Siwiak and D. McKeown, "Ultra-Wideband Radio Technology", © 2004, John Wiley & Sons, Ltd.

[32] S. Jogi and M. Choudhary, "Ultra Wideband Demystified – Technologies, Applications, and System Design Considerations", © 2009, River Publishers.

[33] R. Aiello and A. Batra, "Ultra Wideband Systems – Technologies and Applications", © 2006, Elsevier Inc.

[34] UWB Forum, http://www.uwbforum.org.

[35] WiMedia Alliance, http://www.wimedia.org.

[36] "WiMedia folds: hands UWB spec to Bluetooth, USB groups", WiMedia Alliance, http://www.wimedia.org.

# Chapter 3 UWB Antennas and Miniaturisation

The primary objective of this thesis is to design and investigate miniaturised and compact UWB antennas. Before the study, it is essential to understand the unique aspects of UWB antenna designs as well as potential miniaturisation techniques for UWB antennas. In this chapter, the main requirements and challenges for a competent UWB antenna are firstly discussed and then some general approaches of UWB antenna miniaturisation are presented.

## 3.1 Requirements and Challenges of UWB Antennas

Over the past few years UWB communications have received much attention. Research and development of UWB communications has been advancing rapidly due to promising communication and ranging capabilities of this technology as well as the recognition of significance of UWB technology by the FCC and other regulatory bodies. The major step in the development of UWB technology for wireless communications is the antenna. As in the case of conventional wireless communication systems, an antenna also plays a vital role in UWB systems. However, due to the enormous bandwidth occupied by the UWB system, there are more challenges and difficulties in designing a UWB antenna than its narrow band counterpart.

Firstly, the ultra wide frequency bandwidth is the main factor distinguishing a UWB antenna from other antennas. According to the FCC, a UWB antenna should possess an absolute bandwidth greater than 500 MHz or a fractional bandwidth of at least 20% [1, 2].

Secondly, the performance of a UWB antenna is required to be consistent across the whole operational band. Ideally, antenna impedance matching, radiation patterns and gains should be stable over the entire band [3, 4]. Sometimes, it is also desired that the UWB antenna offers the band-notched characteristic to co-exist with other narrow band devices and services occupying the same working band [5-8].

Thirdly, directional or omni-directional radiation characteristics are demanded depending on different situation and application. Omni-directional patterns are normally desirable in mobile communications [9-12]. For radar and other directional systems where high gain is required, directional radiation properties are preferred [13-16].

Fourthly, a suitable antenna should be small and compact enough to be embedded in UWB terminals especially in mobile and portable devices [17, 18]. It is also highly preferred that the antenna features low profile and compatibility for easy integration with printed circuit board (PCB) construction. Additionally, compact and miniature antennas are particularly imperative in UWB WBANs applications [19-22].

Fifthly, a good antenna design should optimise the overall system performance. For instance, the antennas need to be designed properly in order to make the overall device (antenna and RF front end) complies with the power emission mask regulated by the FCC and offer a low return loss ($S_{11}$) so maximising the power usage [3, 23, 24].

Finally, a UWB antenna should have good time domain characteristics. For the narrow band case, it is approximated that an antenna has the same performance over the relative narrow bandwidth and the basic parameters, such as gain and return loss, vary little across the operational band. In contrast, UWB systems usually employ short pulses to deliver information. In other words, a huge bandwidth has

been occupied. Thus the antenna can't be treated as a "spot filter" anymore but a "band-pass filter". In this case the antenna parameters will have to be treated as functions of frequency and will impose more significant impacts on the input signal. Furthermore, a successful transmission and reception of UWB signals entails minimisation of ringing, spreading and distortion of the pulses in the time domain. Therefore, it is indispensable and important to study antenna characteristics in the time domain [25-30].

## 3.2 Miniaturisation of UWB Antennas

### 3.2.1 Fundamental Limitations for Electrically Small Antennas

An electrically small antenna is the one which fits inside a sphere of radius $r = 1/k$ where $k$ is the wave number and equal to $2\pi/\lambda$. The limits on electrically small antennas are obtained by assuming that the entire antenna structure (with a largest linear dimension of 2*r*), and its transmission line and oscillator are all enclosed within a sphere of radius *r* [31, 32], as shown in figure 3.1.

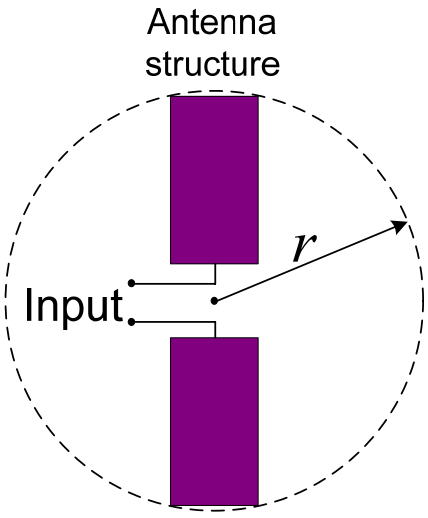


Figure 3.1: Antenna within a sphere of radius *r*.

The fundamental limitations for electrically small antennas were studied first by Chu [33] and subsequently by Harrington [34], so they are called Chu-Harrington limitations. Chu's approach uses spherical wave functions to describe the field and calculate the quality factor Q.

When $kr < 1$, the quality Q of a small antenna can be expressed as [35]:

$$Q = \frac{1 + 2(kr)^2}{(kr)^3[1 + (kr)^2]} \cdot e_{rad} \tag{3.1}$$

where $e_{rad}$ is the radiation efficiency of the antenna.

Equation 3.1 shows the relationships between the quality factor Q and the antenna size as well as the radiation efficiency. Since the Q grows rapidly as the antenna size decreases, the result relates the lowest attainable Q to the maximum dimension of an electrically small antenna. Because the antenna fractional bandwidth FBW is the reciprocity of Q [35], as shown in equation 3.2, the increasing Q with reducing size $r$ indeed implies a fundamental limitation on the widest achievable bandwidth FBW.

$$FBW = \frac{1}{Q} \tag{3.2}$$

Therefore, the antenna size, quality factor, bandwidth and radiation efficiency are interrelated and there is no complete freedom to independently optimise each one. Thus, there is always a compromise between them to obtain an optimal antenna performance [36].

It has been realised recently that most of UWB monopoles operate in the resonating modes at low operating frequencies and in the travelling wave modes supported by the tapered slots at high operating frequencies. The transition from the resonating modes to travelling waves is achieved through the overlapping of the resonating harmonics after tuning the feeding and the ground plane [37]. Supporting

the overlapped multiple harmonics on a UWB monopole is a way to approach the minimum attainable Q and resulted in a flourish of development of various compact UWB monopoles.

### 3.2.2 Approaches of UWB Antenna Miniaturisation

As discussed in the previous section, small and compact size of a UWB antenna is highly desirable due to their ease of integration into space-limited systems. During the past few years, some research efforts have been made towards miniaturisation of UWB antennas and various designs have been proposed to realise a reduction in antenna size while retaining sufficient antenna performance [38-41].

For example, Zhining Chen et al. design a small swan-shaped UWB antenna as shown in figure 3.2. By cutting a rectangular notch vertically from the printed radiator and asymmetrically attaching a strip to the radiator, the antenna has achieved a -10 dB $|S_{11}|$ bandwidth over 2.9 – 11.6 GHz with a small size of 25mm×25mm. This novel design also features a reduced ground plane effect and therefore mitigates severe practical engineering problems such as design complexity and deployment difficulty [38].

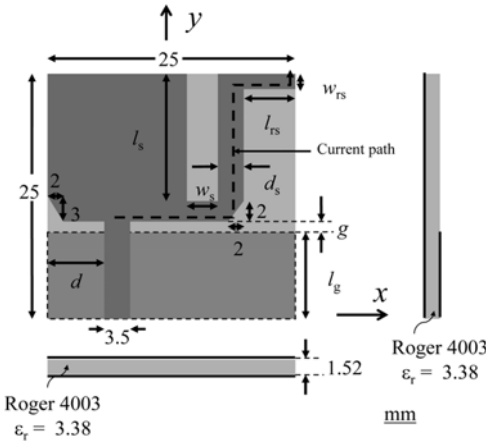


Figure 3.2: Geometry of swan-shaped UWB antenna [38].

Another miniaturised UWB antenna design is also proposed as depicted in figure 3.3. The microstrip-fed elliptical monopole is etched on a substrate with $\varepsilon_r = 2.3$. A top-loading structure on the backside of the substrate is introduced to provide additional inductance or capacitance to reduce the antenna size. Furthermore, the shape of elliptical radiator is modified to improve the impedance matching at the higher end of the frequency band. The final design features a 25mm×26mm physical size and covers a -10 dB $|S_{11}|$ bandwidth over 2.4 – 10.6 GHz without exhibiting significant degradation in efficiency [39].

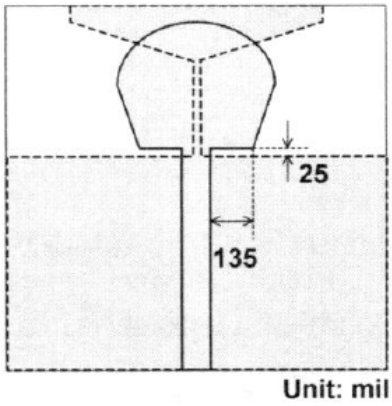


Figure 3.3: Geometry of top-loading elliptical antenna [39].

Further miniaturisation can be realised by employing substrate with a high dielectric constant. Although a high dielectric constant substrate is susceptible to surface wave excitation, which degrades the radiation pattern and reduces the efficiency of the antennas, it might be suppressed if the electrical thickness of the substrate is small. An example of such antenna is displayed in figure 3.4. The radiating element uses the intersection of elliptical structures and is etched on a high dielectric constant substrate with $\varepsilon_r = 10.2$ and thickness of 0.64mm, corresponding to electrical thickness of 0.03λ at the highest frequency. The antenna presents a physical dimension of 20mm×26mm and exhibits a -10 dB impedance bandwidth

from 3.1 GHz to 15 GHz [40].

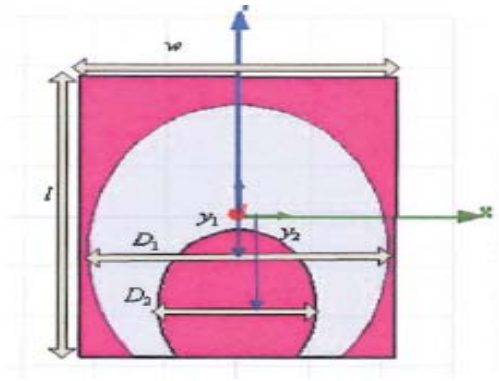


Figure 3.4: Geometry of high-dielectric constant substrate antenna [40].

Moreover, by applying a Klopfenstein taper on the slot line formed by ground plane and radiator, a microstrip line fed elliptical card UWB antenna presents a quite small size of 40mm×20mm, covering a wide impedance bandwidth from 3 GHz to more than 11 GHz [41]. Also, a feeding mechanism is proposed in this design by using a microstrip line on the other side of the substrate and connecting the line to the elliptical element by a via. Figure 3.5 depicts the configuration of the proposed antenna.

Figure 3.5: Configuration of elliptical card UWB antenna [41].

## 3.3 Summary

As is the case in narrowband systems, antennas also play a vital role in UWB systems and face more strict requirements.

Several techniques have been proposed to miniaturise UWB antennas.

Dielectric loading is an effective way to reduce antenna size but at the expense of surface wave excitation and high Q which will degrade the antenna efficiency and bandwidth. Reactive loading can bring down the lowest frequency by increasing the effective length of the antenna but may cause low efficiency due to loading loss. Topology optimisation can to some extent reduce the antenna size without above mentioned detrimental effects but the miniaturisation factor is limited and the procedure is not generic.

Undoubtedly, the other aspects of the UWB antenna performance, such as radiation pattern, phase linearity, group delay and time domain characteristics should be also taken into account in different applications. These issues impose further constraints to the UWB antenna design and there often exists some tradeoffs between them and the antenna size. There is thus a need for a comprehensive study of UWB antennas, both in design for compactness and for wideband pulse performance.

## References

[1] Hans Schantz, "The Art and Science of Ultrawideband Antennas", © 2005, Artech House, Inc.

[2] B. Allen et al., "Ultra-wideband Antennas and Propagation for Communications, Radar and Imaging", © 2006, John Wiley & Sons, Ltd.

[3] H. Arslan, Z. Chen and M. Benedetto, "Ultra Wideband Wireless Communication", © 2006, John Wiley & Sons, Ltd.

[4] M. Ghavami, L. B. Michael and R. Kohno, "Ultra Wideband – signals and systems in communication engineering 2nd ed.", © 2007, John Wiley & Sons, Ltd.

[5] Y. Cho, K. Kim, D. Choi, S. Lee and S. Park, "A Miniature UWB Planar Monopole Antenna With 5-GHz Band-Rejection Filter and the Time-Domain

Characteristics", *IEEE Transaction on Antennas and Propagation*, vol. 54, no. 5, May 2006, pp. 1453-1460.

[6] J. Qiu, Z. Du, J. Lu and K. Gong, "A Planar Monopole Antenna Design With Band-Notched Characteristic", *IEEE Transaction on Antennas and Propagation*, vol. 54, no. 1, January 2006, pp. 288-292.

[7] N. Choi, C. Jung, J. Byun, F, Harackiewicz, M. Park, Y. Chung, T. Kim and B. Lee, "Compact UWB Antenna With I-Shaped Band-Notch Parasitic Element for Laptop Applications", *IEEE Antennas and Wireless Propagation Letters*, vol. 8, 2009, pp. 580-582.

[8] C. Sim, W. Chung and C. Lee, "A Circular-Disc Monopole Antenna with Band-Rejection Function for Ultrawideband Application", *Microwave and Optical Technology Letter*, vol. 51, no. 6, pp. 1607-1613, June 2009.

[9] A. Abbosh and M. Bialkowski, "Design of Ultrawideband Planar Monopole Antennas of Circular and Elliptical Shape", *IEEE Transaction on Antennas and Propagation*, vol. 56, no. 1, January 2008, pp. 17-23.

[10] J. Liang, C. Chiau, X. Chen and C. G. Parini, "Study of a Printed Circular Disc Monopole Antenna for UWB Systems", *IEEE Transaction on Antennas and Propagation*, vol. 53, no. 11, November 2005, pp. 3500-3504.

[11] S. Choi, K. Hamaguchi and R. Kohno, "Small Printed CPW-Fed Triangular Monopole Antenna for Ultra-Wideband Applications", *Microwave and Optical Technology Letter*, vol. 51, no. 5, pp. 1180-1182, May 2009.

[12] Q. Wu, R. Jin, J. Geng and M. Ding, "Printed Omni-Directional UWB Monopole Antenna With Very Compact Size", *IEEE Transaction on Antennas and Propagation*, vol. 56, no. 3, March 2008, pp. 896-899.

[13] M. Mokhtaari and J. Bornemann, "Directional Ultra-Wideabnd Antennas in

Planar Technologies", *Proceedings of the 38th European Microwave Conference (EuMC 2008)*, Amsterdam, Netherlands, 27-31, October, 2008.

[14] Y. Kwag, A. Hassanein and D. Edwards, "A High-Directive Bowtie Radar Antenna with A Pyramidal Reflector for Ultra Wideband Radar Imaging Applications", *Microwave and Optical Technology Letter*, vol. 51, no. 2, pp. 387-390, February 2009.

[15] A. Abbosh, H. Kan and M. Bialkowski, "Design of Compact Directive Ultra Wideband Antipodal Antenna", *Microwave and Optical Technology Letter*, vol. 48, no. 12, pp. 2448-2450, December 2006.

[16] M. Peyrot-Solis, G. Galvan-Tejada and H. Jardon-Aguilar, "Parametric Study of A UWB Parallel-Plate Monopole Antenna for Operation in the 5- to 20-GHz Band", *International Journal of RF and Microwave Computer-Aided Engineering*, vol. 18, no. 5, September 2008, pp. 389-396.

[17] F. Viani, L. Lizzi, R. Azaro and A. Massa, "A Miniaturized UWB Antenna for Wireless Dongle Devices", *IEEE Antennas and Wireless Propagation Letters*, vol. 7, 2008, pp. 714-717.

[18] Z. Chen and T. See, "Small UWB Antennas for Wireless USB Dongle Attached to Laptop Computer", *IEEE International Workshop on Antenna Technologies: Small and Smart Antennas Metamaterials and Applications (IWAT 2007)*, Cambridge, U.K, 21-23 March, 2007.

[19] T. See and Z. Chen, "Experimental Characterization of UWB Antennas for On-Body Communications", *IEEE Transaction on Antennas and Propagation*, vol. 57, no. 4, April 2009, pp. 866-874.

[20] M. Klemm and G. Troester, "Textile UWB Antennas for Wireless Body Area Networks", *IEEE Transaction on Antennas and Propagation*, vol. 54, no. 11,

November 2006, pp. 3192-3197.

[21] T. See, A. Alomainy, Y. Hao and Z. Chen, "On-Body Characterisation of A Compact Planar UWB Antenna", *The first European Conference on Antennas and Propagation (EuCAP 2006)*, Nice, France, 6-10 November, 2006.

[22] K. Yazdandoost and R. Kohno, "UWB Antenna for Wireless Body Area Network", *Proceedings of Asia-Pacific Microwave Conference 2006 (APMC2006)*, Yokohama, Japan, 12-15 December, 2006.

[23] C. Lin, Y. Kan, L. Kuo and H. Chuang, "A Planar Triangular Monopole Antenna for UWB Communication", *IEEE Microwave and Wireless Components Letters*, vol. 15, no. 10, October 2005, pp. 624-626.

[24] Y. Duroc, A. Ghiotto, T. Vuong and S. Tedjini, "On the Characterization of UWB Antennas", *International Journal of RF and Microwave Computer-Aided Engineering*, vol. 19, no. 2, March 2009, pp. 258-269.

[25] S. Cheng, P. Hallbjorner and A. Rydberg, "Printed Slot Planar Inverted Cone Antenna for Ultrawideband Applications", *IEEE Antennas and Wireless Propagation Letters*, vol. 7, 2008, pp. 18-21.

[26] X. Wu and Z. Chen, "Comparison of Planar Dipoles in UWB Applications", *IEEE Transaction on Antennas and Propagation*, vol. 53, no. 6, June 2005, pp. 1973-1983.

[27] W. Wiesbeck, G. Adamiuk and C. Sturm, "Basic Properties and Design Principles of UWB Antennas", *Proceedings of the IEEE*, vol. 97, no. 2, February 2009, pp. 372-385.

[28] T. Vuong, A. Ghiotto, Y. Duroc and S. Tedjini, "Design and Characteristics of A Small U-Slotted Planar Antenna for IR-UWB", *Microwave and Optical Technology Letter*, vol. 49, no. 7, pp. 1727-1731, July 2007.

[29] J. Zhang and F. Wang, "Study of A Double Printed UWB Dipole Antenna", *Microwave and Optical Technology Letter*, vol. 50, no. 12, pp. 3179-3181, December 2008.

[30] M. Gopikrishna, D. Krishna, C. Aanandan, P. Mohanan and K. Vasudevan, "Design of A Microstrip Fed Step Slot Antnena for UWB Communication", *Microwave and Optical Technology Letter*, vol. 51, no. 4, pp. 1126-1129, April 2009.

[31] C. Balanis, "Antenna Theory Analysis and Design", © 2005, John Wiley & Sons, Ltd.

[32] J.S.Mclean, "A Re-Examination of the Fundamental Limits on the Radiation Q of Electrically Small Antennas," *IEEE Trans. Antennas & Propagat*., vol. 44, pp. 672-676, May 1996.

[33] L.J.Chu, "Physical limitations of omnidirectional antennas", *J. Appl. Phys*., vol. 19, December 1948, pp. 1163-1175.

[34] R.F.Harrington, "Effect of antenna size on gain, bandwidth and efficiency", *J. Res. Nat. Bur. Stand*., vol. 64D, January-February 1960, pp. 1-12.

[35] R.C.Hansen, "Fundamental Limitations in Antennas", *Proceedings of the IEEE*, vol. 69, no. 2, February 1981, pp. 170-182.

[36] R. Aiello and A. Batra, "Ultra Wideband Systems Technologies and Applications", © 2006, Elsevier Inc.

[37] X. Chen, J. Liang, L. Guo, P. Li, C.C.Chiau and C.G. Parini, "Planar UWB monopoles and their operation", *The first European Conference on Antennas and Propagation (EuCAP 2006)*, Nice, France, 6-10 November, 2006.

[38] Z.Chen, T.See and X.Qing, "Small Printed Ultrawideband Antenna with Reduced Ground Plane Effect", *IEEE Transactions on Antennas and Propagation*, vol. 55, no. 2, February 2007, pp. 383-388.

[39] T.Yang, W.A.Davis and W.L.Stutzman, "Small Planar Ultra-wideband antenna with top-loading", *2005 IEEE Antennas and Propagation Society International Symposium*, pp. 479-482, July 2005.

[40] A.M.Abbosh, M.E.Bialkowski, M.V.Jacob and J.Mazierska, "Design of a compact ultra wideband antenna", *Microwave and Optical Technology Letter*, vol. 48, pp. 1515-1518, August 2006.

[41] K. Bahadori and Y. Rahmat-Samii, "An Elliptic-Card UWB Antenna for Wireless Communications", *The first European Conference on Antennas and Propagation (EuCAP 2006)*, Nice, France, 6-10 November, 2006.

# Chapter 4 Loaded Orthogonal Half Disc Monopole Antenna

As mentioned in chapter 3, UWB antenna design and analysis are confronting more challenges and difficulties than its narrow band counterparts. Firstly, UWB antennas should have ultra wide impedance bandwidth and stable patterns across the bandwidth. Secondly, UWB antennas should feature a small and compact size in order to make it suitable for portable devices. Thirdly, UWB antennas should possess an omni-directional radiation pattern across the entire frequency band for mobile communications. In this chapter, a loaded orthogonal half disc monopole antenna is studied. A pair of loading strips is introduced to broaden the bandwidth at the lower band. The loading effects as well as the ground plane dimension on the antenna performance and characteristics are investigated both numerically and experimentally. It is demonstrated that a massive 68.8% equivalent size reduction in volume can be realised in the loaded orthogonal half disc monopole antenna. Good agreement has been obtained between the simulation and the measurement.

## 4.1 Introduction

For antennas to fulfil UWB technology requirement, various monopole-like UWB antennas have been proposed due to their attractive merits of simple configuration and ease of fabrication and numerous techniques have been exploited to broaden their bandwidth as well as improving their performance. The square planar monopole with symmetrical bevelling [1], the diamond-like vertical monopole antenna [2] and the circular disc monopole [3] can all achieve impedance bandwidths covering the

entire UWB band, i.e. from 3.1 GHz to 10.6 GHz. However, they all exhibit physically large dimensions and suffer radiation pattern distortions at higher frequencies with about 10 dB gain variation in the azimuthal plane.

P.V.Anob and K.P.Ray constructed an orthogonal square monopole antenna with a semi-circular base [4], which not only features a wide impedance bandwidth but also shows an omni-directional pattern across the whole frequency band. This antenna also presents a physical size of 450mm×450mm×46mm in volume.

In this study, three main objectives are to be achieved. Firstly, an antenna which has both the ultra-wide impedance and the radiation pattern bandwidth is to be designed. Secondly, the impedance bandwidth as well as the pattern bandwidth is to be further broadened by exploiting the loading technique in order to meet the requirements defined by the FCC. Finally, the antenna's physical size is to be miniaturised by shrinking the ground plane so as to make it more suitable for portable devices.

This chapter will be organised as follows. An original orthogonal half disc monopole antenna fed by a 50Ω coaxial cable is firstly studied. It can yield a -10 dB measured impedance bandwidth from 4.6 GHz to 11 GHz. In order to cover the entire UWB band allocated by the FCC, i.e. 3.1 GHz to 10.6 GHz, a loading technique is then introduced to increase the bandwidth at the lower band. The loading effects on the antenna performance and characteristics are investigated both numerically and experimentally. It has been shown that an improvement on the antenna performance can be achieved by using this loading method. In addition, it is also found that the size of the ground plane can be largely reduced. The loaded orthogonal half disc monopole antenna exhibits an impedance bandwidth from 2.99 GHz to 11.05 GHz while its radiation patterns remain omni-directional across the

entire band.

## 4.2 Original Orthogonal Half Disc Monopole Antenna

### 4.2.1 Antenna Geometry

The original antenna studied in this chapter consists of two orthogonal half circular copper discs, a ground plane and a coaxial cable feeding, as shown in figure 4.1. *r* is the radius of the half disc, *W* and *L* denote the width and the length of the ground plane, respectively. *h* is the feed gap between the half discs and the ground plane. In this study, a 50Ω coaxial cable is used to feed the antenna.

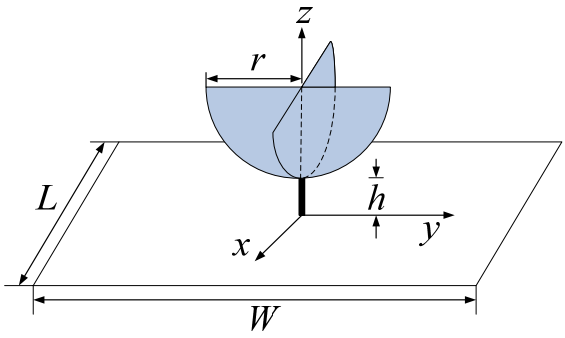


(a) The coordinate system

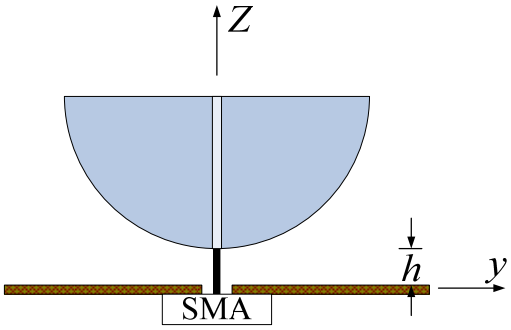


(b) Side view

Figure 4.1: Geometry of the original orthogonal half disc monopole antenna.

### 4.2.2 Performance and Characteristics

The simulations are performed using the CST Microwave StudioTM package, which utilizes the Finite Integration Technique (FIT) for electromagnetic computation. It is found in simulations that $r$, $h$, $W$ and $L$ are the key parameters that influence the antenna's performance. These parameters can be optimised to achieve a maximum bandwidth. A prototype of the orthogonal half disc monopole antenna with original design, i.e. $r$=12.5mm, $h$=0.7mm, $W$=$L$=100mm, was built and tested, as shown in figure 4.2. The return loss was measured in an anechoic chamber by using a HP 8720ES network analyser.

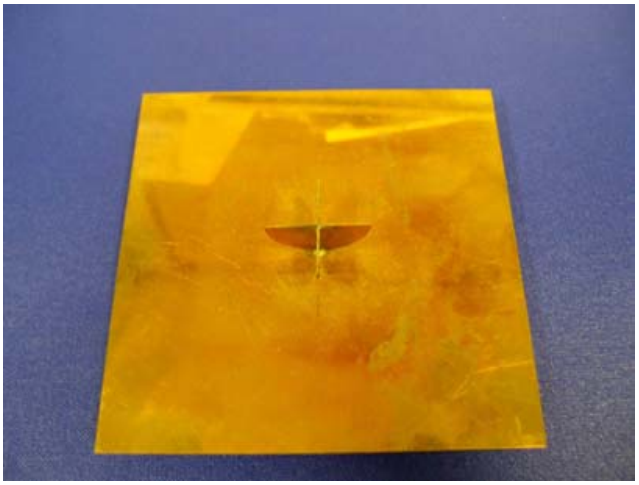

Figure 4.2: Photo of the orthogonal half disc monopole antenna with original design.

Figure 4.3 illustrates the simulated and measured $|S_{11}|$ curves. The measured $|S_{11}|$ curve agrees very well with the simulated one in the entire frequency band range. It is shown that there is an obvious local minimum occurring at around 6 GHz in both the simulation and the measurement. Generally speaking, the -10 dB impedance bandwidth spans a wide frequency range. The simulated bandwidth ranges from 4.4 GHz to 11.3 GHz and it is confirmed in the experiment, with only a slight deviation, from 4.6 GHz to 11 GHz.

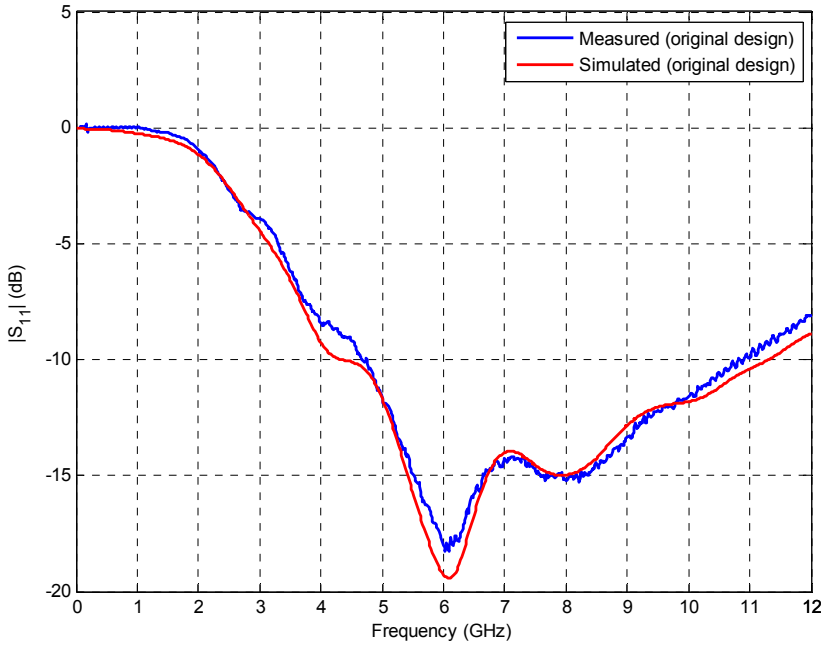


Figure 4.3: Simulated (red line) and measured (blue line) $|S_{11}|$ curves of the original antenna design.

The measured and simulated radiation patterns at 4.4 GHz, 6.03 GHz, 8 GHz and 11 GHz are plotted in figure 4.4, figure 4.5, figure 4.6 and figure 4.7, respectively.

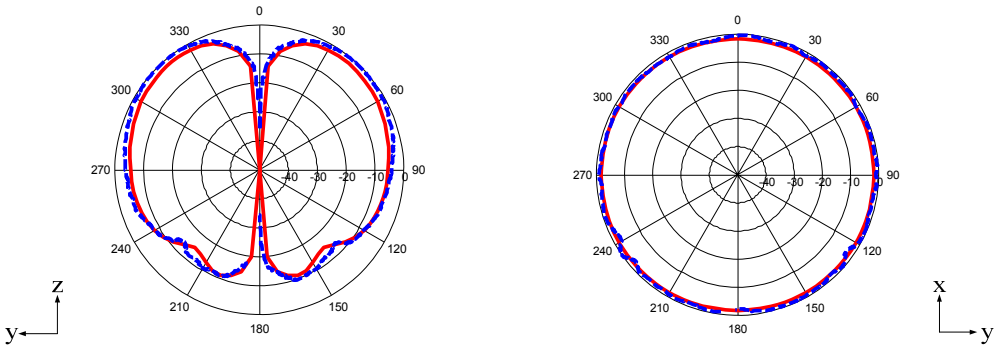


(a) *z-y* plane (b) *x-y* plane

Figure 4.4: Simulated (red line) and measured (blue line) radiation patterns at 4.4 GHz.

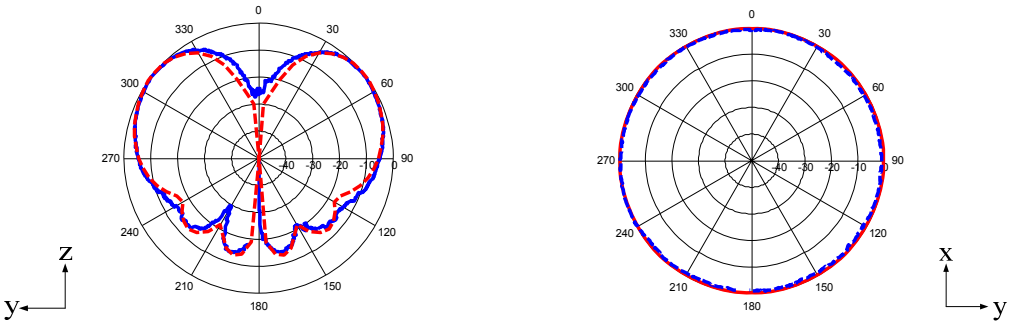


(a) *z-y* plane (b) *x-y* plane

Figure 4.5: Simulated (red line) and measured (blue line) radiation patterns at 6.03 GHz.

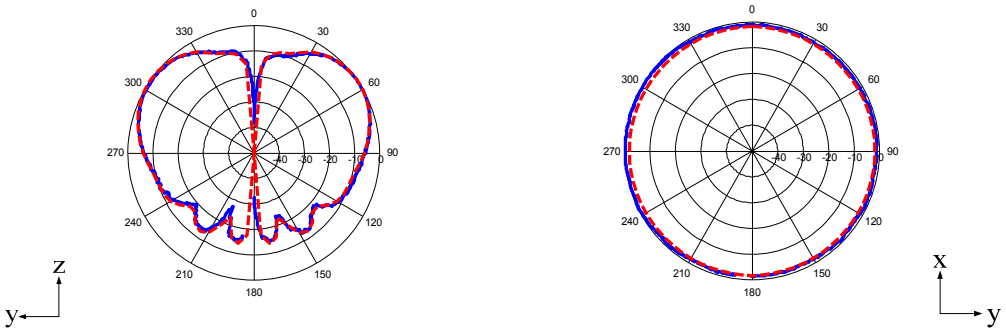


(a) *z-y* plane (b) *x-y* plane

Figure 4.6: Simulated (red line) and measured (blue line) radiation patterns at 8 GHz.

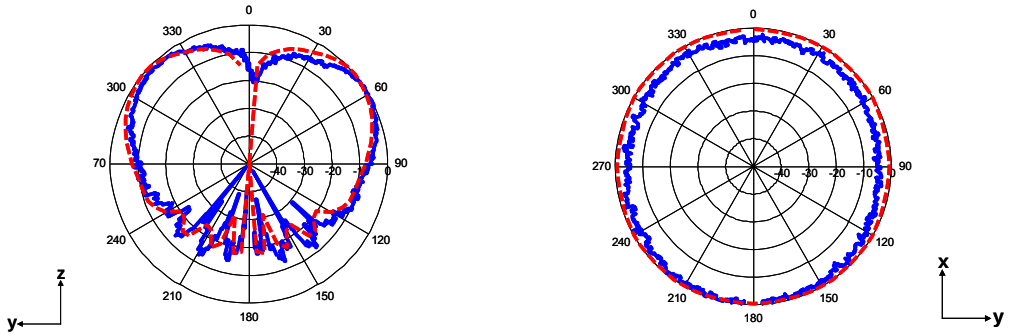


(a) *z-y* plane (b) *x-y* plane

Figure 4.7: Simulated (red line) and measured (blue line) radiation patterns at 11 GHz.

In the *z*-*y* plane (figure 4.4 (a), figure 4.5 (a), figure 4.6 (a) and figure 4.7 (a)), the patterns have large back lobes at lower frequencies. With the increase of the frequency, the back lobes become smaller and split into minor ones. In the *x*-*y* plane, the patterns are omni-directional at low band and mid band (as shown in figure 4.4 (b), figure 4.5 (b) and figure 4.6 (b)) and slightly distorted at high band (as displayed in figure 4.7 (b)). The simulated peak gain of the original antenna is displayed in figure 4.8, it is seen that a satisfactory gain level is achieved across the whole band.

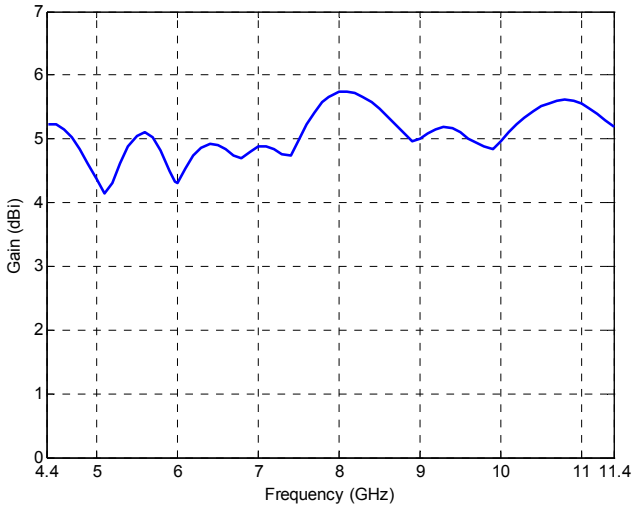


Figure 4.8 Simulated peak gain of the original antenna.

## 4.3 Improved Design with One Loading Strip

### 4.3.1 Antenna Geometry

As the bandwidth of the original orthogonal half disc monopole antenna does not fully satisfy the requirements defined by the FCC, i.e. 3.1 GHz – 10.6 GHz, a loading strip is introduced to improve the $|S_{11}|$ performance at the lower band. The configuration of the improved antenna design with one loading strip is shown in figure 4.9.

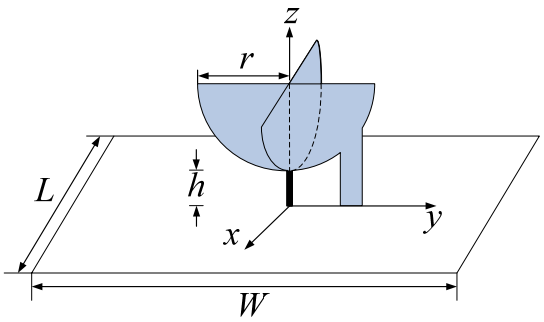


(a) The coordinate system

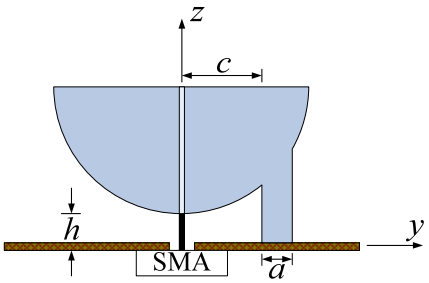


(b) Side view

Figure 4.9: Geometry of the improved antenna design with one loading strip.

The loading is a copper strip inserted between the semi-circular disc and the ground. The loading strip is featured by two major parameters, i.e. width *a* and position *c*, respectively. It has been shown in the simulation that the operating bandwidth of the modified antenna with one loading strip is critically dependent on the strip width *a* and the position *c*, so both parameters should be optimised for a maximum bandwidth. Also, the ground plane size on the antenna performance will be evaluated.

### 4.3.2 Effect of Loading Strip Position

Figure 4.10 displays the simulated $|S_{11}|$ curves for different loading strip positions (*c*=3, 5, 7, and 9mm) when both *W* and *L* are fixed at 100mm, *a* at 0.5mm, *r* at

12.5mm and *h* at 0.7mm, respectively.

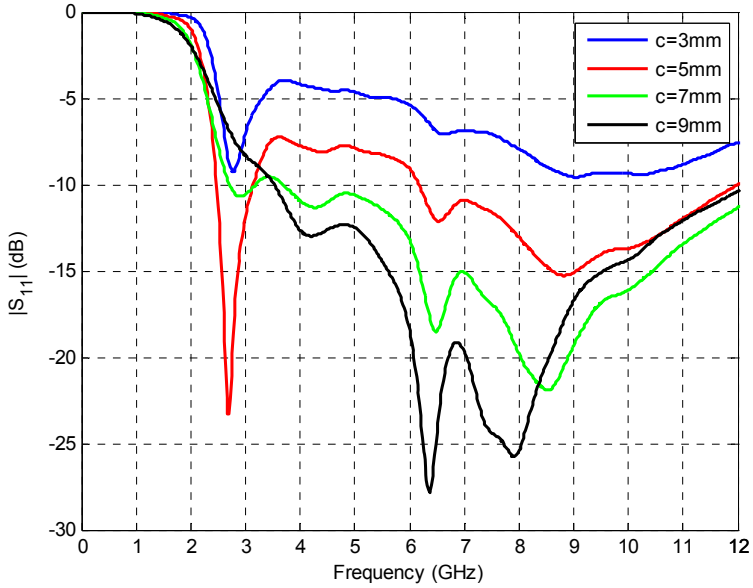


Figure 4.10: Simulated $|S_{11}|$ curves of the improved antenna with one loading strip for different loading strip positions with $a$=0.5mm, $r$=12.5mm, $h$=0.7mm and $W$=$L$=100mm.

It can be seen in figure 4.10 that the $|S_{11}|$ curves have similar overall patterns for four different loading strip positions. However, the -10 dB operating bandwidth of the antenna varies dramatically with the variation of the loading strip position $c$. In addition, the first local minimum is enhanced with the increase of $c$ up to 5mm and becomes less prominent with the further increase of $c$ and eventually disappears when $c$=9mm. The optimal loading strip position is found to be at $c$=7mm with the bandwidth spanning an ultra wide frequency range from 2.7 GHz to greater than 12 GHz, much broader than the original design.

### 4.3.3 Effect of Loading Strip Width

Another design parameter influencing the antenna operation is the width of the loading strip $a$. The simulated $|S_{11}|$ curves with $r$=12.5mm, $h$=0.7mm, $W$=$L$=100mm

and optimal loading strip position *c* of 7mm for various widths a are presented in figure 4.11.

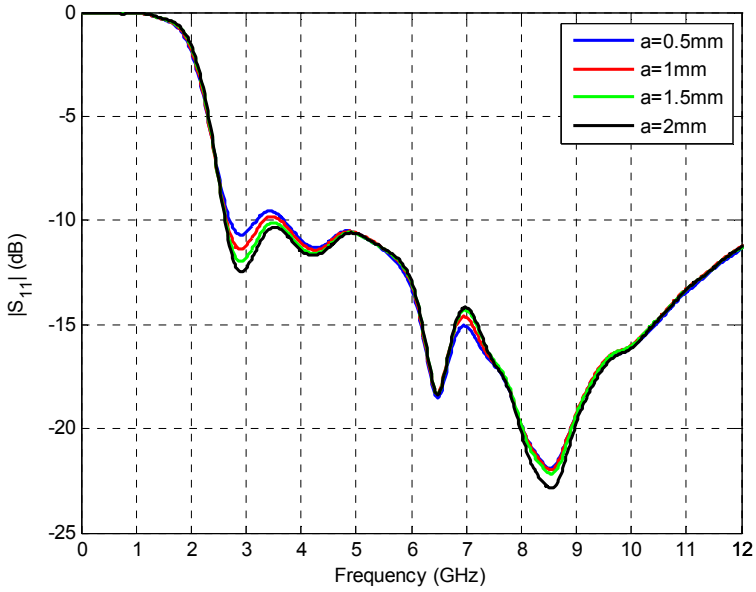


Figure 4.11: Simulated $|S_{11}|$ curves of the improved antenna with one loading strip for different loading strip widths with *c*=7mm, *r*=12.5mm, *h*=0.7mm and *W*=*L*=100mm.

It is noticed in figure 4.11 that the $|S_{11}|$ curves also feature quite similar shapes for four different loading strip widths. Nevertheless, the -10 dB bandwidth of the antenna changes with different *a*, particularly at the lower frequency band. The optimal loading strip width is found to be at *a*=2mm with the bandwidth covering an ultra wide frequency range from 2.64 GHz to more than 12 GHz.

### 4.3.4 Effect of the Ground Plane Size

As discussed above, the optimal design so far has been achieved with *r*=12.5mm, *h*=0.7mm *c*=7mm and *a*=2mm while the ground plane remains an original size of 100mm×100mm. In this subsection, a ground size reduction will be conducted in order to make the antenna more compact. The effects of different ground sizes on the

antenna performance are plotted in figure 4.12.

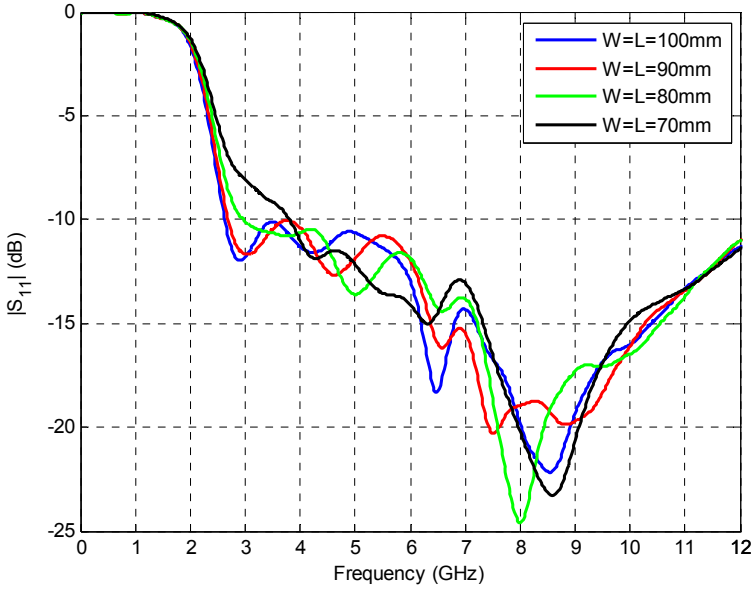


Figure 4.12: Simulated $|S_{11}|$ curves of the improved antenna with one loading strip for different ground plane sizes with $c$=7mm, $a$=2mm, $r$=12.5mm and $h$=0.7mm.

According to figure 4.12, it is evident that the $|S_{11}|$ performances gradually deteriorate with the decrease of the ground plane size. The -10 dB operating bandwidth of the antenna alters significantly with the variation of the ground plane dimension at the lower end. It is also noted that the first local minimum is shifted up with the reduction of the ground plane. Therefore, the ground plane exhibits a major influence on the lower end of the bandwidth. The ground plane size can be at most shrunk to 80mm × 80mm so as to maintain the bandwidth required by the FCC.

## 4.4 Improved Design with Two Loading Strips

### 4.4.1 Antenna Geometry

In the last section, the modified antenna with one loading strip has been analysed. Some primary parameters that influence antenna performance have been discussed

and optimised to obtain the maximum bandwidth and an optimal design with $r$=12.5mm, $a$=1.5mm, $c$=7mm, $h$=0.7mm and $W$=$L$=80mm has been achieved. It has been demonstrated that the loading technique is feasible for the frequency bandwidth enlargement. However, as can be seen clearly, this configuration is not symmetrical hence the radiation patterns at higher frequencies will not retain omni-directional attributes. Consequently, another loading strip will be invited and positioned symmetrically opposite the semi-circular disc, as shown in figure 4.13.

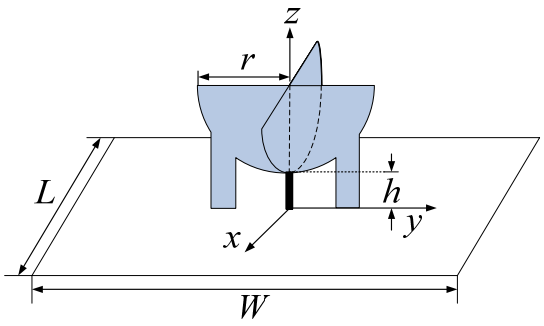


(a) The coordinate system

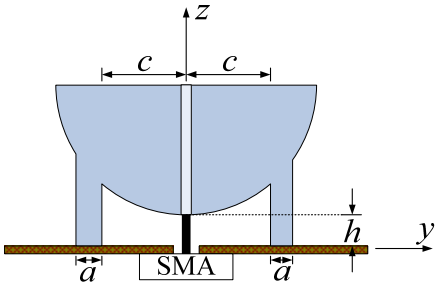


(b) Side view

Figure 4.13: Geometry of the improved antenna design with two loading strips.

With a similar analysis in the last section, a parametric study on the improved antenna design with two loading strips is performed to acquire the optimal bandwidth.

### 4.4.2 Effect of Loading Strip Position

As shown in figure 4.14, when *r* is fixed at 12.5mm, *h* at 0.7mm, *a* at 1.5mm and both *W* and *L* at 100mm, the performance of the improved antenna with two loading strips is also quite sensitive to the loading strip position *c*.

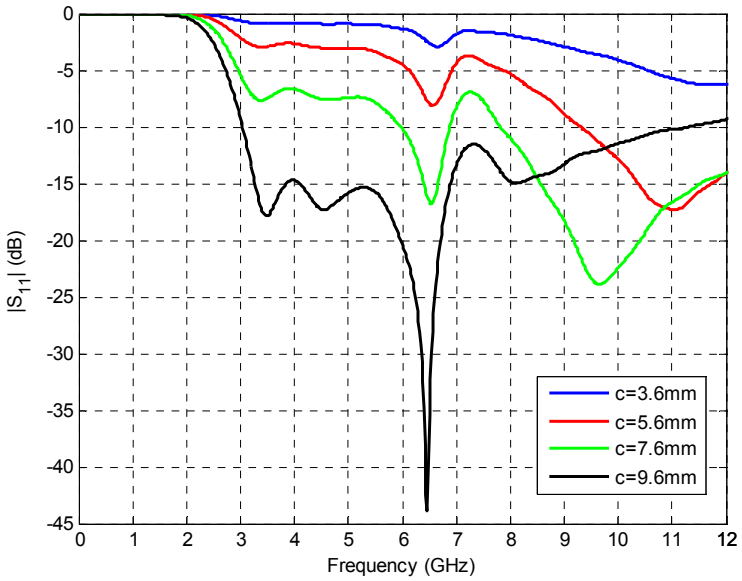


Figure 4.14: Simulated $|S_{11}|$ curves of the improved antenna with two loading strips for different loading strip positions with *a*=1.5mm, *r*=12.5mm, *h*=0.7mm and *W*=*L*=100mm.

It is presented in figure 4.14 that the $|S_{11}|$ curves again have a shape resemblance for four different loading strip positions although the -10 dB operating bandwidth of the antenna fluctuates dramatically with the alteration of the loading strip position *c*. In addition, the first local minimum becomes remarkable with the increase of the loading strip position *c*. The optimised loading strip position is found to be at *c*=9.6mm with the bandwidth covering an ultra wide frequency range from 3.04 GHz to 11.32 GHz.

### 4.4.3 Effect of Loading Strip Width

As the same as the improved antenna design with one loading strip, another design parameter affecting the antenna's operation is the width of the loading strip *a*. The simulated $|S_{11}|$ curves with *r*=12.5mm, *h*=0.7mm, *W*=*L*=100mm and optimal loading strip position *c* of 9.6mm for different widths a are displayed in figure 4.15.

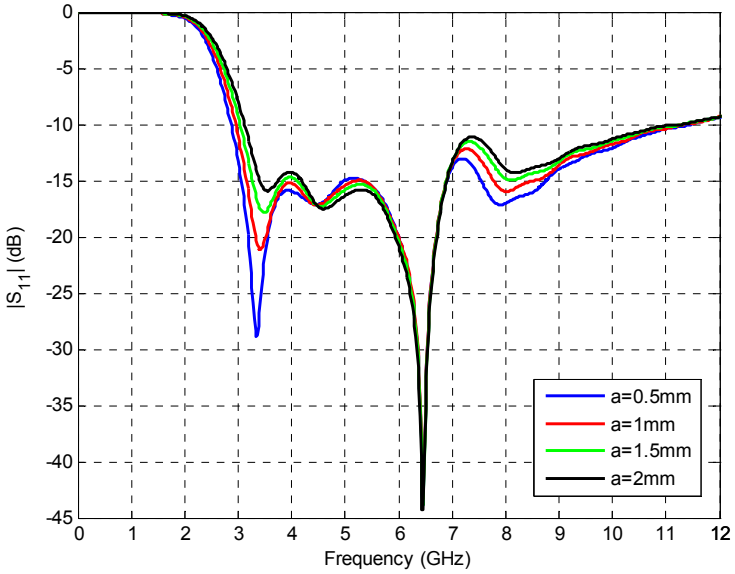


Figure 4.15: Simulated $|S_{11}|$ curves of the improved antenna with two loading strips for different loading strip widths with *c*=9.6mm, *r*=12.5mm, *h*=0.7mm and *W*=*L*=100mm.

It is observed in figure 4.15 that the $|S_{11}|$ curves also feature similar shapes for four various loading strip widths and the -10 dB bandwidth of the antenna changes slightly with different *a* at the lower frequency band. The loading strip width is optimised to be at *a*=0.5mm with the bandwidth spanning an ultra wide frequency range from 2.87 GHz to 11.47 GHz.

### 4.4.4 Effect of the Ground Plane Size

As discussed in the previous section, a ground plane size reduction can also be

realised for the improved antenna design with two loading strips to make the antenna more compact. The effects of different ground dimensions on the antenna performance are depicted in figure 4.16.

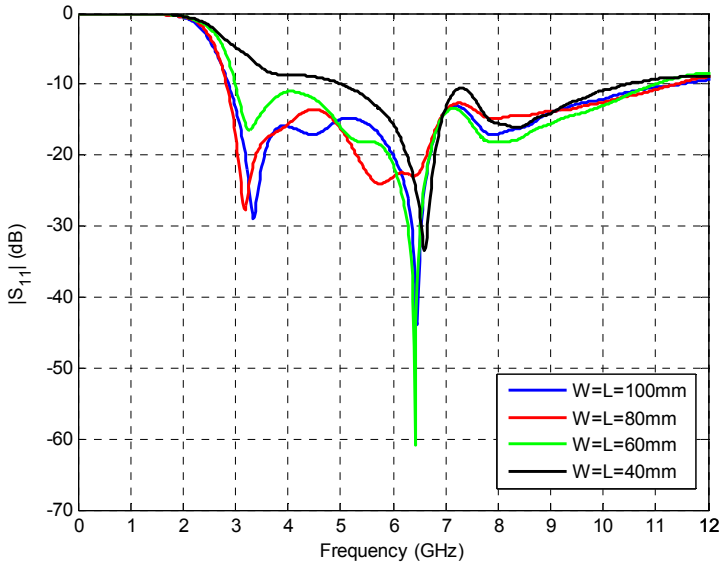


Figure 4.16: Simulated $|S_{11}|$ curves of the improved antenna with two loading strips for different ground plane sizes with $c$=9.6mm, $a$=0.5mm, $r$=12.5mm and $h$=0.7mm.

As can be clearly seen in figure 4.16, the $|S_{11}|$ characteristics gradually degrade with the reduction of the ground plane. The -10 dB impedance bandwidth of the antenna varies little with the variation of the ground plane dimension from $W$=$L$=100mm down to $W$=$L$=60mm. However, a significant bandwidth cut is observed when $W$=$L$=40mm. It is also noticed that the first local minimum occurs around 3 GHz except the scenario of $W$=$L$=40mm, where the first local minimum almost vanishes. Therefore, the ground plane size can be at most decreased to $W$=$L$=60mm so as to retain the bandwidth required by the FCC.

### 4.4.5 Effect of the Half Disc Dimension

It has been so far established that the loading strip position and width together with

the ground plane all play important roles on the antenna bandwidth. Besides, an interesting phenomenon in figure 4.14, 4.15 and 4.16 is noticed that the first local minimum always appears at around 3.2 GHz for different loading strip positions and widths, and ground plane sizes when the half disc radius is fixed at 12.5mm. In fact, the quarter wavelength at the first local minimum frequency (23.4mm) is just close to the diameter of the half disc.

Figure 4.17 exhibits the simulated $|S_{11}|$ curves for different dimensions of the half disc with their respective optimal designs, which are given in table 4-A. It can be seen that the ultra wide impedance bandwidth can be obtained in all of these designs.

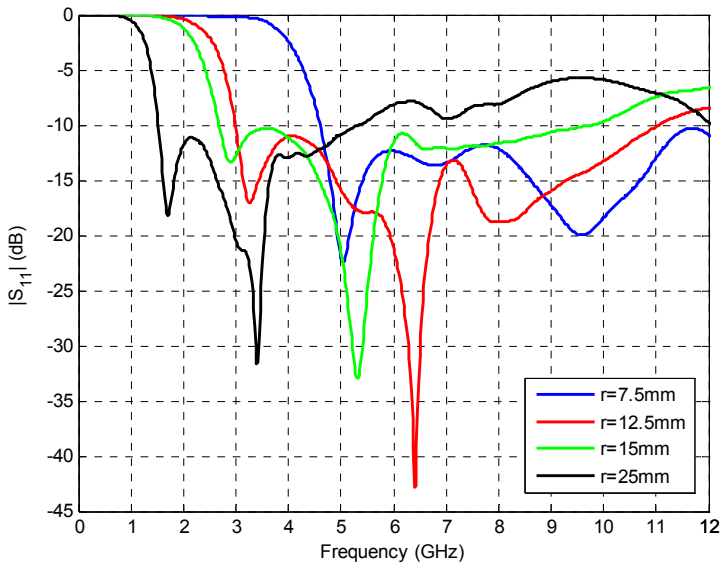


Figure 4.17: Simulated $|S_{11}|$ curves for different disc dimensions of the improved antenna with two loading strips in the optimal designs.

The relationship between the half disc diameters and the first local minimums is also listed in table 4-A. It is demonstrated that the first local minimum frequency is determined by the radius of the half disc as well as the perimeter *S* of the closed loop formed by A-B-C-D-A, as shown in figure 4.18, which approximately corresponds to the three tenth wavelength at this frequency. *S* can be calculated based on the loading

strip position *c*, as shown in equation 4.1. The optimal loading strip width *a* is 0.5mm for all cases and the optimal ground size *W* is just more than twice the diameter of the half disc.

$$S = \frac{tg^{-1}\left(\frac{c}{\sqrt{r^2 - c^2}}\right) \times \pi \times r}{180} + c + 2h + r - \sqrt{r^2 - c^2} \qquad (4.1)$$

Table 4-A is thus a good summary of the design rules for achieving the ultra wide impedance bandwidth in a loaded orthogonal half disc monopole antenna.

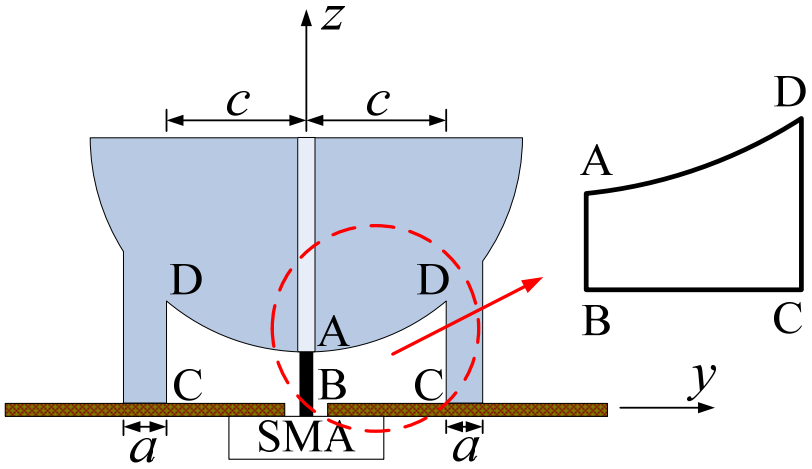


Figure 4.18: Closed loop formed by A-B-C-D-A.

Table 4-A: Optimal design parameters of the loaded orthogonal half disc monopole antenna and relationship between the diameter as well as perimeter *S* and the first local minimum frequency.

| Diameter $2r$ (mm) | 15 | 25 | 30 | 50 |
|---|---|---|---|---|
| First local minimum $f_1$ (GHz) | 5.04 | 3.26 | 2.9 | 1.7 |
| Wavelength $\lambda$ at $f_1$ (mm) | 59.52 | 92.02 | 103.45 | 176.47 |
| $2r / \lambda$ | 0.25 | 0.27 | 0.29 | 0.28 |
| Optimal $S$ | 18.61 | 26.43 | 30.26 | 42.46 |
| $S / \lambda$ | 0.31 | 0.29 | 0.29 | 0.24 |
| Optimal $a$ (mm) | 0.5 | 0.5 | 0.5 | 0.5 |
| Optimal $W$ (mm) | 45 | 60 | 60 | 110 |
| $W / \lambda$ | 0.76 | 0.65 | 0.58 | 0.62 |

## 4.4.6 Performance and Characteristics

A prototype of the improved antenna with two loading strips with optimal design, i.e. $r$=12.5mm, $c$=9.6mm, $a$=0.5mm, $h$=0.7mm and ground size $W$=$L$=60mm, was fabricated and tested in the Antenna Measurement Laboratory at Queen Mary, University of London, as shown in figure 4.19. It is noticed that the ground size has been diminished from $W$=$L$=100mm to $W$=$L$=60mm, thus the physical size reduction in volume is 64%.

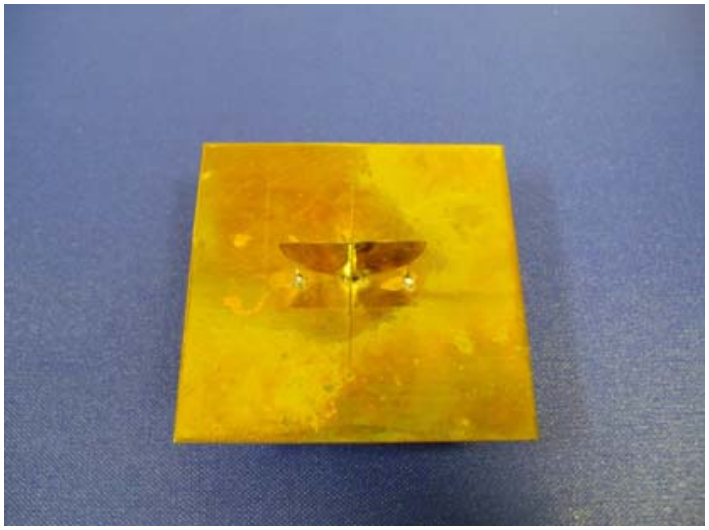

Figure 4.19: Photo of the improved antenna with two loading strips with optimal design.

Figure 4.20 displays the simulated and the measured $|S_{11}|$ curves. The measured $|S_{11}|$ curve again agrees well with the simulated one across the whole frequency band range. It is clearly shown that apart from the local minimum at around 6 GHz there is another obvious local minimum occurring around 3.2 GHz due to the loading. This local minimum is optimally enhanced and hence leads to the broadened frequency bandwidth at the lower end. Generally speaking, the -10 dB bandwidth spans a wide frequency range in both the simulation and the measurement. The simulated bandwidth ranges from 2.99 GHz to 11.05 GHz. This UWB characteristic of the improved antenna is confirmed in the experiment, with a slight variance, from 2.91 GHz to 11.86 GHz.

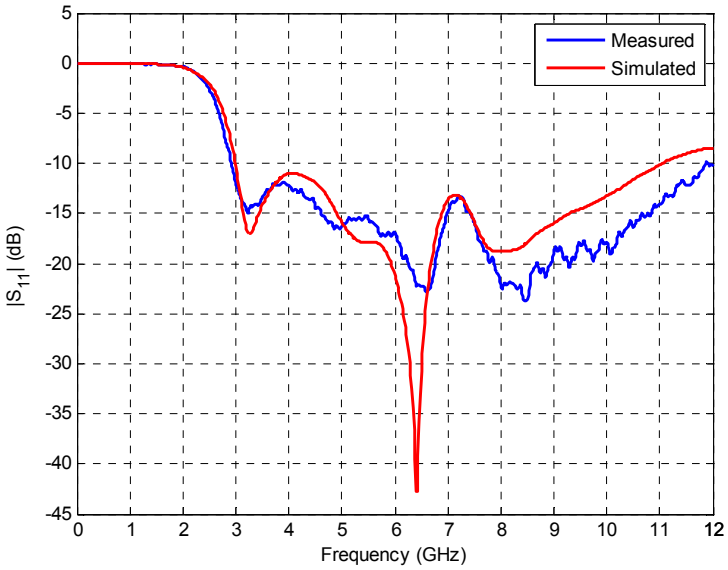


Figure 4.20: Simulated (red line) and measured (blue line) $|S_{11}|$ curves of the improved antenna design with two loading strips.

The measured and simulated radiation patterns at 3.1 GHz, 5.97 GHz, 7.88 GHz and 11 GHz are plotted in figure 4.21, figure 4.22, figure 4.23 and figure 4.24, respectively.

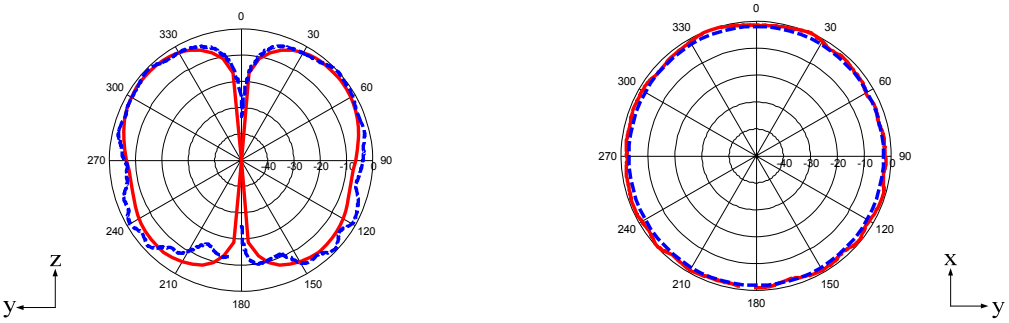


(a) *z-y* plane (b) *x-y* plane

Figure 4.21: Simulated (red line) and measured (blue line) radiation patterns at 3.1 GHz.

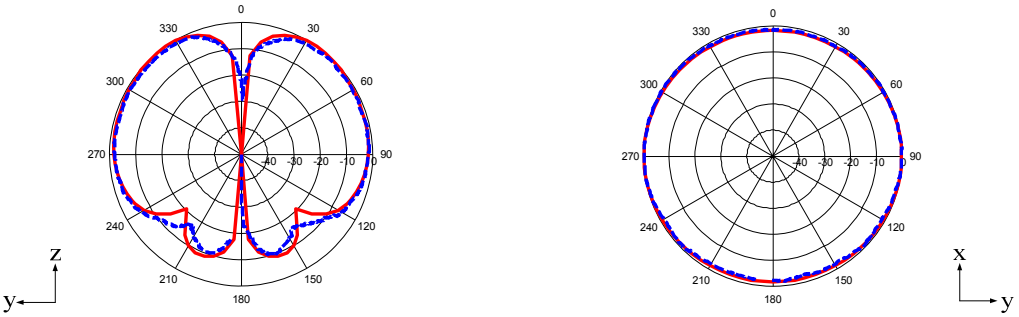


(a) *z-y* plane (b) *x-y* plane

Figure 4.22: Simulated (red line) and measured (blue line) radiation patterns at 5.97 GHz.

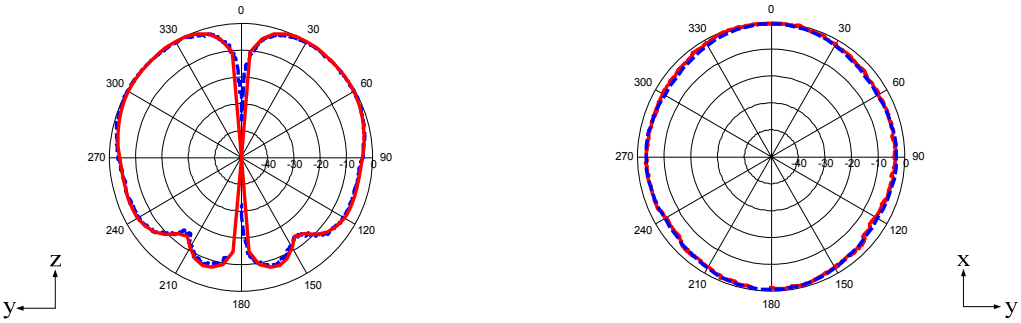


(a) *z-y* plane (b) *x-y* plane

Figure 4.23: Simulated (red line) and measured (blue line) radiation patterns at 7.88 GHz.

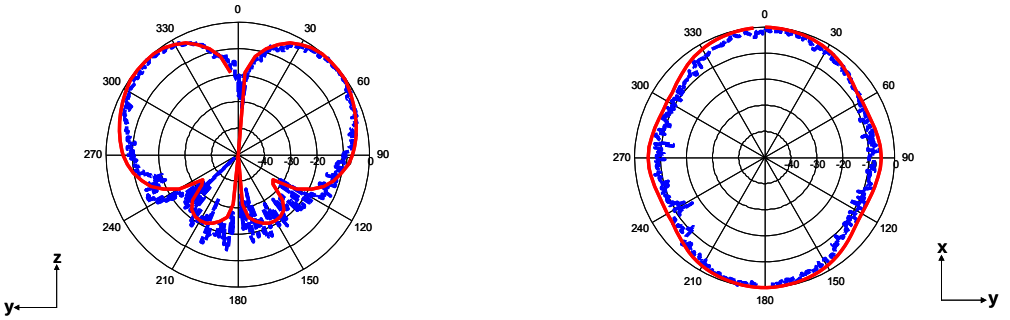


(a) *z-y* plane (b) *x-y* plane

Figure 4.24: Simulated (red line) and measured (blue line) radiation patterns at 11 GHz.

It is observed that in the *z-y* plane (figure 4.21 (a), figure 4.22 (a), figure 4.23 (a) and figure 4.24 (a)), the patterns have a donut-like shape at lower frequencies. With

the increase of the frequency, the back lobes again become smaller and split into minor ones. In the *x-y* plane, the patterns are omni-directional at low band and mid band (as shown in figure 4.21 (b), figure 4.22 (b) and figure 4.23 (b)) and slightly distorted at high band (as depicted in figure 4.24 (b)). Figure 4.25 depicts the simulated peak gain of the improved antenna. It is noticed that a satisfactory gain level is achieved across the whole band.

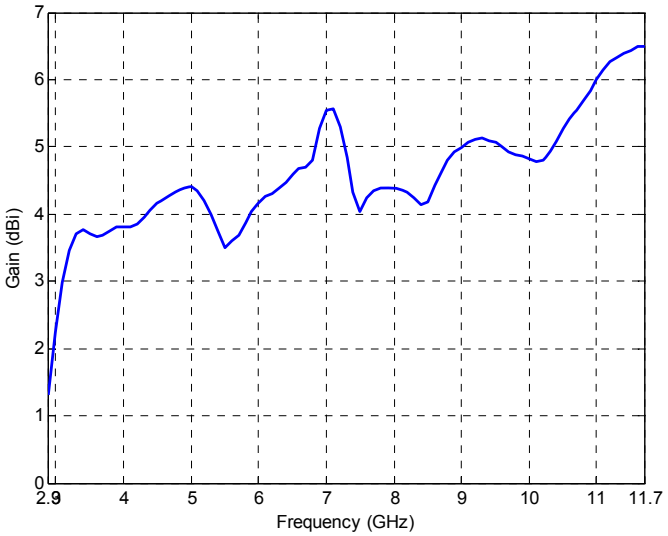


Figure 4.25 Simulated peak gain of the improved antenna.

Figure 4.26 shows the comparison of simulated $|S_{11}|$ curves of the original antenna of figure 4.1 and the improved antenna with two loading strips. As can be seen clearly, with the loading technique applied, the lower end of the bandwidth has been brought down from 4.4 GHz to 2.99 GHz while maintaining the same disc dimension. In other words, the electrical dimension of the antenna has been miniaturised from $0.37\lambda \times 0.37\lambda \times 0.19\lambda$ to $0.25\lambda \times 0.25\lambda \times 0.13\lambda$, where $\lambda$ is the lower end of the bandwidth, therefore the equivalent size reduction in volume is 68.8%.

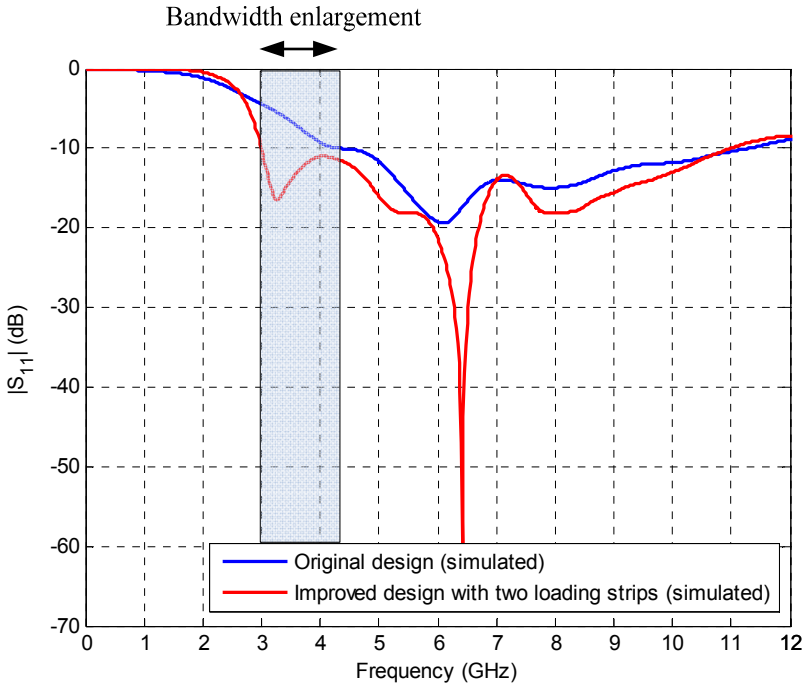


Figure 4.26: Comparison of $|S_{11}|$ curves of the original antenna design and the improved antenna design with two loading strips.

To gain some insights into the loading technique, an input impedance characteristics comparison between the original design and improved design with two loading strips is illustrated in figure 4.27. For a straightforward contrast purpose, the ground plane dimension remains $W$=$L$=100mm, same with the original one.

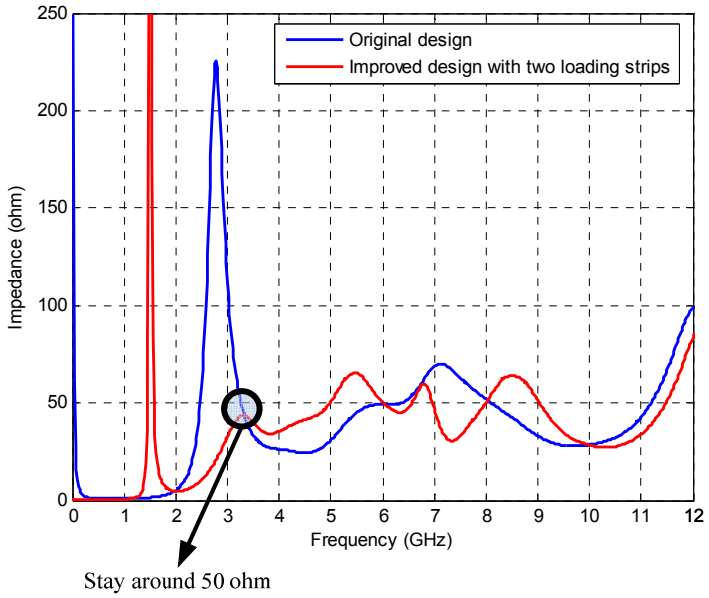


(a) Resistance *R*

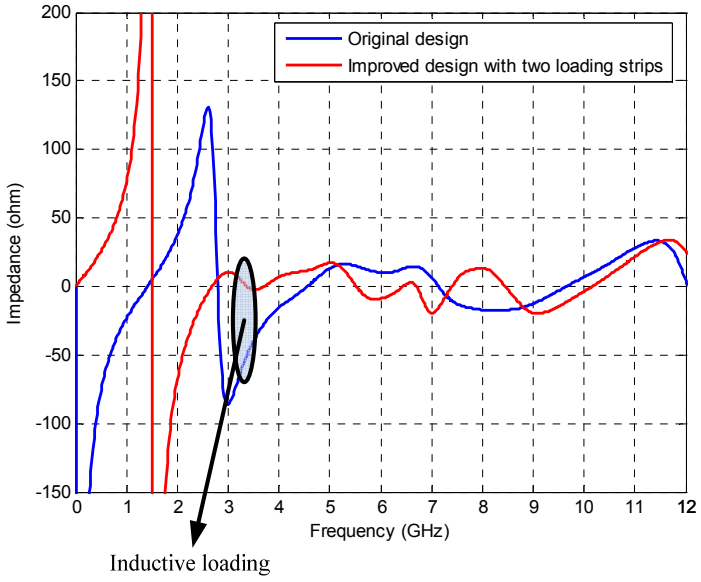


(b) Reactance *X*

Figure 4.27: Comparison of simulated input impedance curves of the original antenna design and the improved antenna design with two loading strips.

As shown in figure 4.27, the input resistance *R* is close to 50Ω while the input reactance *X* is far from zero at 3.25 GHz for the original design, therefore the

input impedance is mismatched to 50Ω. When loading strips applied to the original design, the input reactance *X* varies from previously -50Ω to around 0Ω at 3.25 GHz, which means a resonance is generated at this frequency. In contrast, the input resistance still stays around 50Ω when loading strips added, as shown in figure 4.27 (a), hence the resonance is enhanced with a 50Ω coaxial cable feed and leads to the broadened frequency bandwidth at the lower end.

The typical current distributions on the original design and the improved design with two loading strips close to the first local minimum frequencies are plotted in figure 4.28.

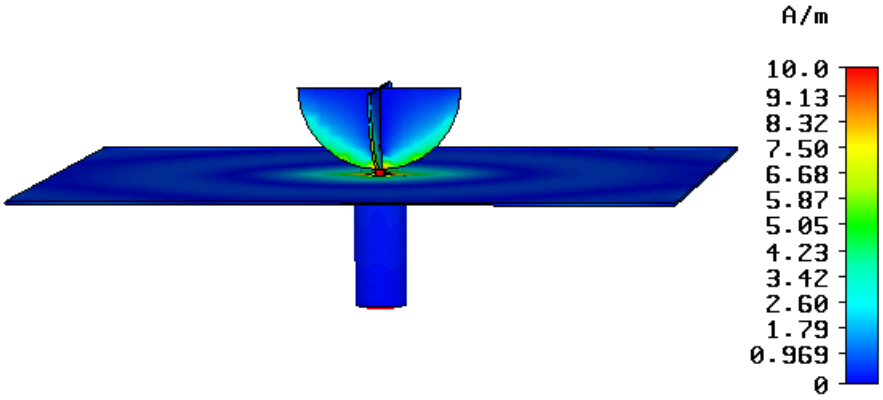


(a) Current distribution at 6 GHz of the original design

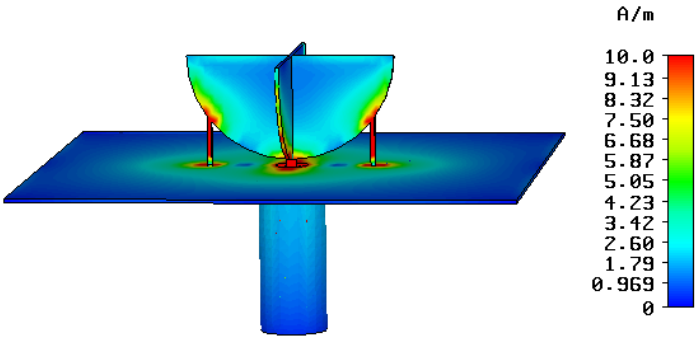


(b) Current distribution at 3.2 GHz of the improved design with two loading strips

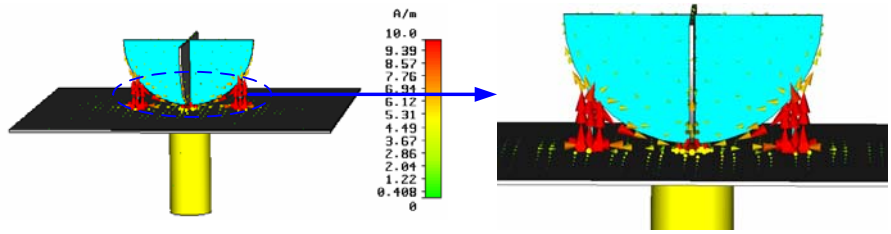


(c) Current distribution at 3.2 GHz of the improved design with two loading strips in vector plot

Figure 4.28: Simulated current distributions of the original design and the improved design with two loading strips.

Figure 4.28 (a) shows the current pattern near the first local minimum at 6 GHz of the original antenna. It is clearly seen that the current is primarily distributed along the edges of two orthogonal half discs and part of the ground plane only close to the feeding region, which indicates the viability of the ground plane reduction. Figure 4.28 (b) illustrates the current distribution near the first local minimum at 3.2 GHz of the improved design with two loading strips. It is evident that apart from current paths on the fringes of two orthogonal half discs, a strong current flowing is also spotted along two loading strips. This validates the effectiveness of the loading technique, which prolongs the current flowing route. In addition, it is found in figure 4.28 (c) that the introduction of loading strips forms a closed-loop current flowing, whose circumference approximately corresponds to the three tenth wavelength at this frequency, as stated in subsection 4.4.5.

## 4.5 Summary

This chapter has presented an investigation into the operation of the loaded orthogonal half disc monopole antenna. It has been shown that the loading strip width $a$, position $c$ and ground size are the three major parameters that determine the performance of the loaded orthogonal half disc monopole antenna. The ground plane

can be appropriately decreased in order to make the antenna more compact. The enhancement of the first local minimum due to the loading technique leads to the broadened bandwidth at the lower frequency band. Both simulation and measurement have demonstrated that the loaded orthogonal half disc monopole antenna can achieve an ultra wide bandwidth, covering the FCC defined UWB frequency band. It is also observed that the radiation patterns are omni-directional over the entire operating band. Most importantly, the loaded orthogonal half disc monopole antenna has achieved 68.8% equivalent size reduction in volume compared with the original design. The results have proved that this loaded orthogonal half disc monopole antenna is suitable for future UWB applications.

## References

[1] M. Ammann and Z. Chen, "Wideband monopole antennas for multi-band wireless systems", *IEEE Antennas and Propagation Magazine*, vol. 45, no. 2, April 2003, pp. 146-150.

[2] S. Khan, L. Ti, J. Hu and S. He, "A Diamond-Like Vertical Monopole Antenna for Ultra-Wideband Communication", *Microwave and Optical Technology Letters*, vol. 49, no. 10, October 2007, pp. 2443-2446.

[3] J. Liang, C.C.Chiau, X. Chen and J. Yu, "Study of A Circular Disc Monopole Antenna for Ultra Wideband Applications", *2004 International Symposium on Antennas and Propagation*, August 17-21, 2004, Sendai, Japan.

[4] Anob.P.V, K.P.Ray and G. Kumar, "Wideband Orthogonal Square Monopole Antennas with Semi-Circular Base", *2001 IEEE Antenna and Propagation Society International Symposium*, Boston, Massachusetts, July 8-13, 2001, vol. 3, pp. 294-297.

# Chapter 5 Printed Half Disc Monopole Antenna

In chapter 4, a loaded orthogonal half disc monopole antenna has been proposed and studied. It is revealed that the antenna miniaturisation can be achieved by applying the loading technique. In this chapter, a printed half disc monopole antenna is investigated. The configuration of the antenna has evolved from a printed CPW-Fed circular disc monopole antenna. By simply halving the original UWB circular disc antenna and adjusting the coplanar ground width, the ultra wide impedance bandwidth can be retained. Interestingly, it is found that an even wider impedance bandwidth at the lower end is obtained in the half disc monopole antenna design. The important parameters that influence the antenna performance and characteristics will be studied both numerically and experimentally. It is manifested that a 65% physical size reduction in area compared to the original antenna design can be realised using a printed half disc monopole antenna. The mechanism of the miniaturised antenna is also illustrated to understand its operation.

## 5.1 Introduction

During the past few years, considerable progresses have been made towards miniaturisation of UWB antennas. In [1], a LTCC (Low Temperature Co-fired Ceramic) based bevelled planar monopole antenna which exploits its structural symmetry can achieve a -10 dB bandwidth of 8.25 GHz and a significant 40% reduction in size is realised. In [2], an *E*-plane cut dual layer part-shielded strip line fed UWB monopole is constructed by removing a symmetrical section of a

previously developed design. The antenna has a dimension of 34.25mm × 12.5mm with its -10 dB bandwidth featuring more than the 3 GHz – 10.6 GHz needed for the UWB communication systems and a noticeable 42% size reduction from the original antenna has been achieved.

In this chapter, a novel design of printed half disc monopole antenna is proposed for UWB applications. The geometry of the antenna has stemmed from an original printed CPW-Fed circular disc monopole antenna. The original antenna design is firstly described and it can offer a -10 dB impedance bandwidth covering the entire UWB band allocated by the FCC, i.e. 3.1 GHz – 10.6 GHz. By simply halving the original design and tuning the width of the coplanar ground plane, a wider impedance bandwidth at the lower end can be achieved. Main parameters that affect the antenna performance are investigated both numerically and experimentally. Also, the mechanism of the printed half disc monopole antenna is illustrated to gain some insights into its operation.

## 5.2 Original Printed CPW-Fed Disc Monopole Antenna

### 5.2.1 Antenna Geometry

The original printed CPW-Fed disc monopole antenna has a single layer-metallic structure, as shown in figure 5.1. A circular disc monopole with a radius of $r$ and a $50\Omega$-CPW are printed on the same side of a dielectric substrate. $W_f$ is the width of the metal strip and $g$ is the gap between the strip and the coplanar ground plane. $W$ and $L_1$ represent the width and the length of the ground plane, respectively, $h$ is the feed gap between the disc and the ground plane. In this study, a dielectric substrate with a thickness of $H$=1.6mm and a relative permittivity of $\varepsilon_r$=3 was chosen, so $W_f$

and $g$ are fixed at 4mm and 0.33mm, respectively, in order to obtain $50\,\Omega$ impedance.

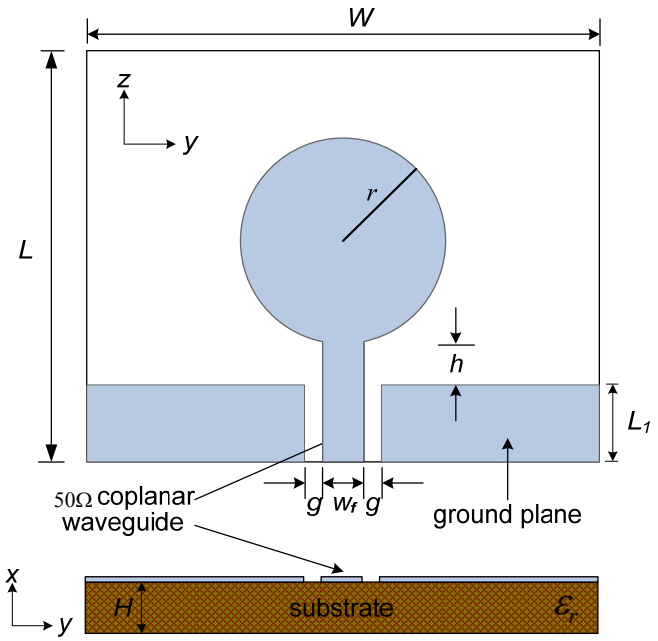


Figure 5.1: Geometry of the CPW-Fed circular disc monopole antenna.

## 5.2.2 Performance and Characteristics

The simulations are performed using the CST Microwave StudioTM package, which utilizes the Finite Integration Technique for electromagnetic computation. A prototype of the CPW-Fed circular disc monopole antenna with optimal design, i.e. $r$=12.5mm, $h$=0.3mm, $W$=47mm, $L$=40mm and $L_1$=10mm, was built and tested in the Antenna Measurement Laboratory at Queen Mary, University of London, as shown in figure 5.2. The $|S_{11}|$ were measured in an anechoic chamber by using a HP 8720ES network analyser.

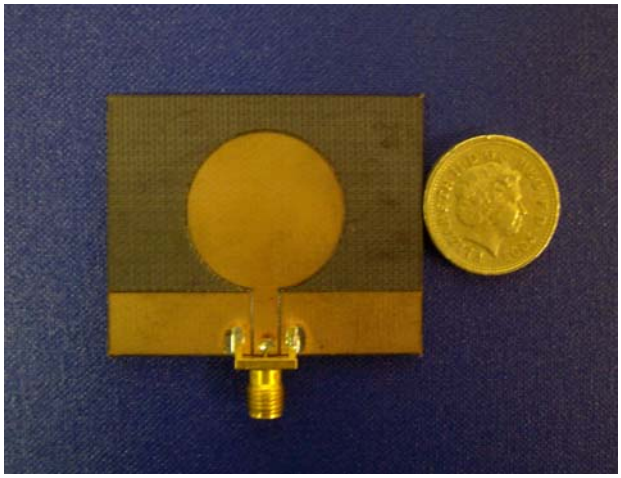

Figure 5.2: Prototype of the CPW-Fed circular disc monopole with $r$=12.5mm, $h$=0.3mm, $W$=47mm, $L$=40mm and $L_1$=10mm.

Figure 5.3 displays the simulated and the measured $|S_{11}|$ curves. The measured $|S_{11}|$ curve agrees reasonably with the simulated one across the whole band. Generally speaking, the -10dB bandwidth occupies an ultra wide frequency range in both the simulation and the measurement. The measured bandwidth of the CPW-Fed circular disc monopole antenna spans from 2.73 GHz to 15.4 GHz.

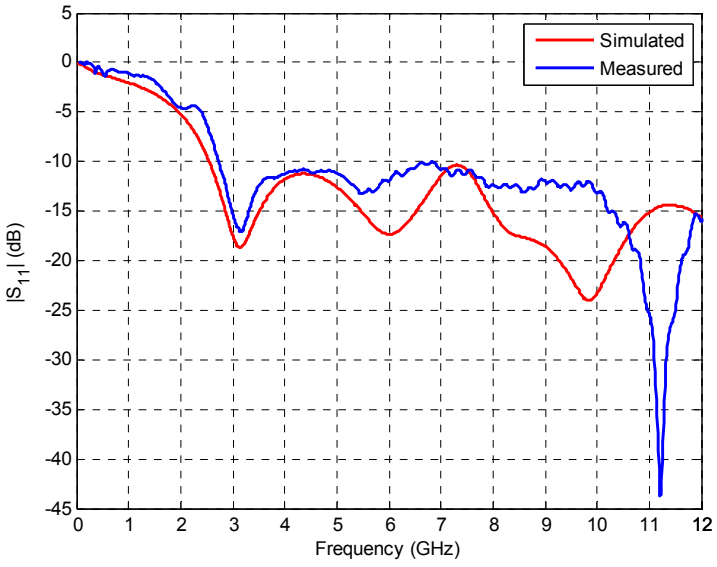


Figure 5.3: Simulated (red line) and measured (blue line) $|S_{11}|$ curves of the CPW-Fed circular disc monopole with $r$=12.5mm, $h$=0.3mm, $W$=47mm, $L$=40mm and $L_1$=10mm.

The measured and simulated radiation patterns at 3 GHz, 5.6 GHz, 8.8 GHz and 10.6 GHz are plotted in figure 5.4, figure 5.5, figure 5.6 and figure 5.7, respectively.

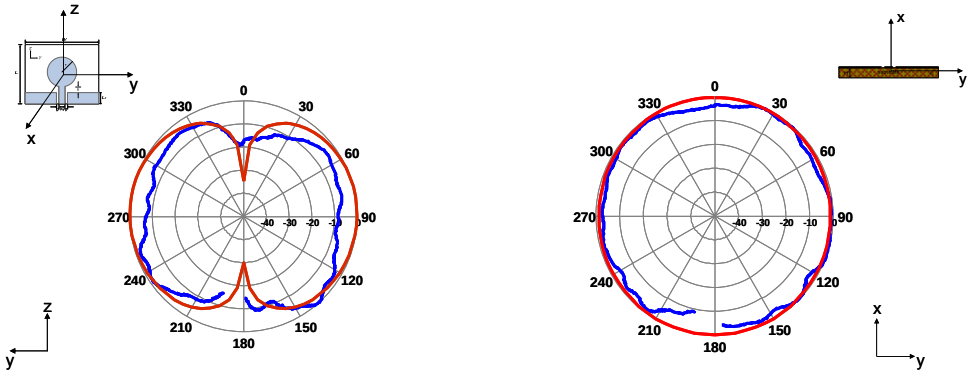


(a) *z*-*y* plane (*E*-plane) (b) *x*-*y* plane (*H*-plane)

Figure 5.4: Simulated (red line) and measured (blue line) radiation patterns of the CPW-Fed circular disc monopole at 3 GHz.

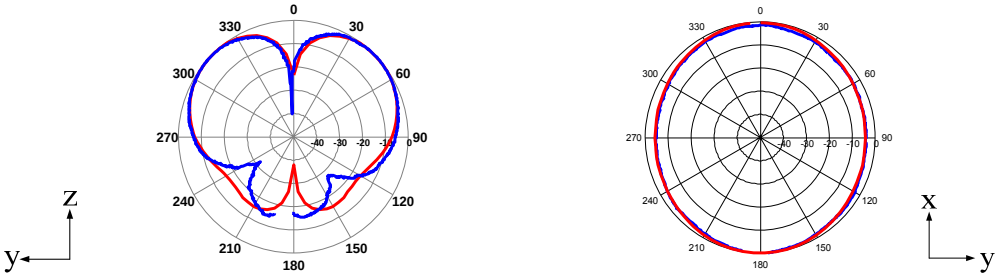


(a) *z*-*y* plane (*E*-plane) (b) *x*-*y* plane (*H*-plane)

Figure 5.5: Simulated (red line) and measured (blue line) radiation patterns of the CPW-Fed circular disc monopole at 5.6 GHz.

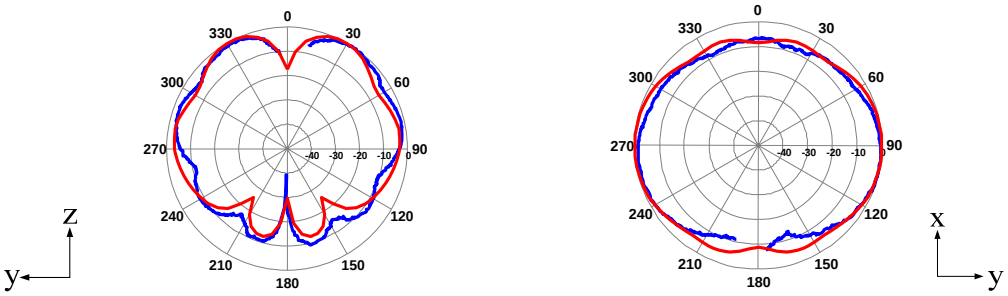


(a) *z*-*y* plane (*E*-plane) (b) *x*-*y* plane (*H*-plane)

Figure 5.6: Simulated (red line) and measured (blue line) radiation patterns of the CPW-Fed circular disc monopole at 8.8 GHz.

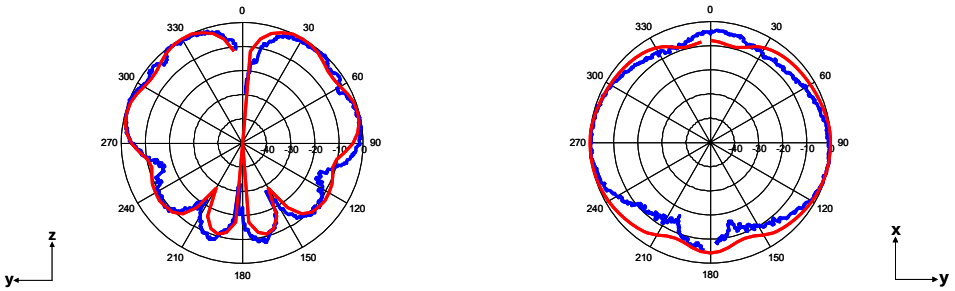


(a) *z*-*y* plane (*E*-plane) (b) *x*-*y* plane (*H*-plane)

Figure 5.7: Simulated (red line) and measured (blue line) radiation patterns of the CPW-Fed circular disc monopole at 10.6 GHz.

As shown in figure 5.4 – figure 5.7, the measured radiation patterns are similar with those obtained in the simulation. The *E*-plane (*z*-*y* plane) patterns have large back lobes at lower frequencies. With the increase of the frequency, the back lobes become smaller, splitting into many minor ones, while the front lobes start to form humps and notches. It is also noticed that the *H*-plane (*x*-*y* plane) pattern is omni-directional at low frequency (3 GHz) and only distorted at higher frequencies (the gain relative to the peak radiated signal direction being reduced less than 10dB in most directions). So the radiation patterns are generally omni-directional over the entire band, like a traditional monopole antenna.

## 5.3 Printed Half Disc Monopole Antenna

### 5.3.1 Antenna Geometry

As displayed in figure 5.8, the printed half disc monopole antenna is obtained by simply halving the full circular disc monopole antenna, as shown in figure 5.1.

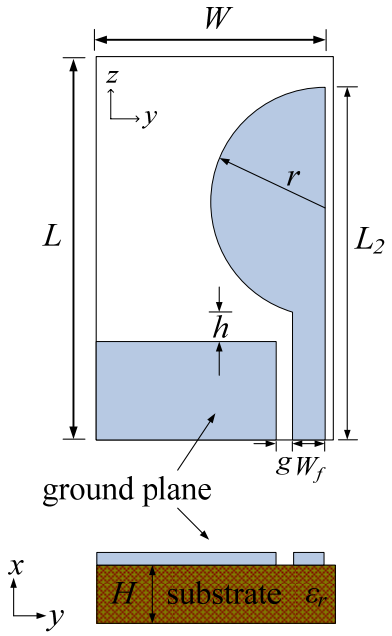


Figure 5.8: Geometry of the printed half disc monopole antenna.

It has been observed in the simulation that the operating bandwidth of the printed half disc monopole antenna is primarily dependent on the ground plane width *W* and the half disc size *r*, so both parameters should be optimised for a maximum bandwidth.

### 5.3.2 Effect of Ground Plane Width

Figure 5.9 displays the simulated $|S_{11}|$ curves for different ground width (*W*=23.5, 20, 16, and 14mm) when *r* is fixed at 12.5mm.

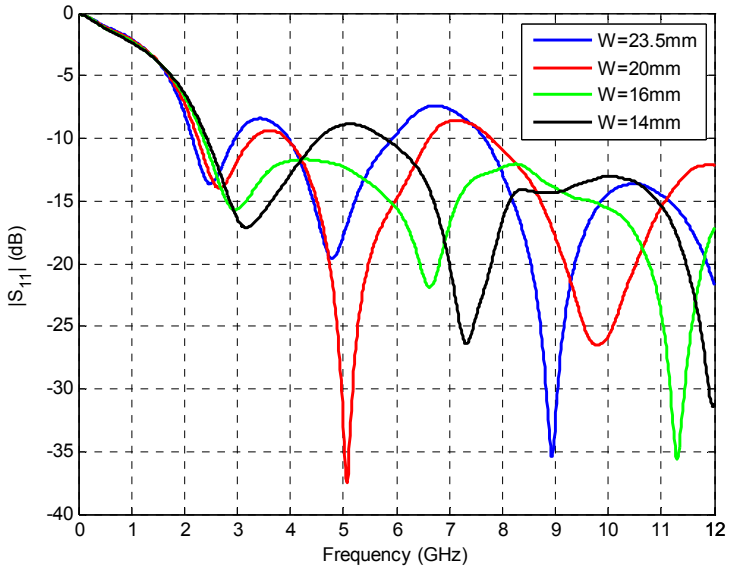


Figure 5.9: Simulated $|S_{11}|$ curves of the printed half disc monopole antenna for different ground widths with $r$=12.5mm.

It can be seen in figure 5.9 that the alteration of the ground plane width shifts all the resonance modes across the entire frequency band and the -10 dB operating bandwidth of the antenna changes dramatically with the variation of the ground plane width $W$. It is interesting to notice that the -10 dB bandwidth is reduced when the width of ground is either too wide or too narrow and $W$=23.5mm is a special scenario when the original design is just simply chopped in half. The optimal ground plane width is found to be at $W$=16mm with the bandwidth covering an ultra wide frequency range. This phenomenon can be explained when the ground plane width is either decreased or increased from its optimal dimension, consequently the current distribution on the upper edge of the ground plane also changes. This corresponds to a decrease or increase of the inductance of the antenna if it is treated as a resonating circuit, which leads to the first resonance mode either up-shifted or down-shifted in the spectrum. In addition, this variation of inductance causes the higher frequency harmonics to be unequally shifted. Hence, the change of the ground plane width

makes some resonances become not so closely spaced across the spectrum and weakens the overlapping between them. Therefore, the impedance matching is worse in these frequency ranges.

### 5.3.3 Effect of Half Disc Dimension

It is also observed in simulations that the antenna's performance is quite sensitive to the size of the half disc *r*, or alternatively can be represented as an overall length $L_2$, as shown in figure 5.8. Figure 5.10 exhibits the simulated $|S_{11}|$ curves for different dimensions of the half disc with their respective optimal designs, which are given in table 5-A. It can be seen that the ultra wide impedance bandwidth can be obtained in all of these designs.

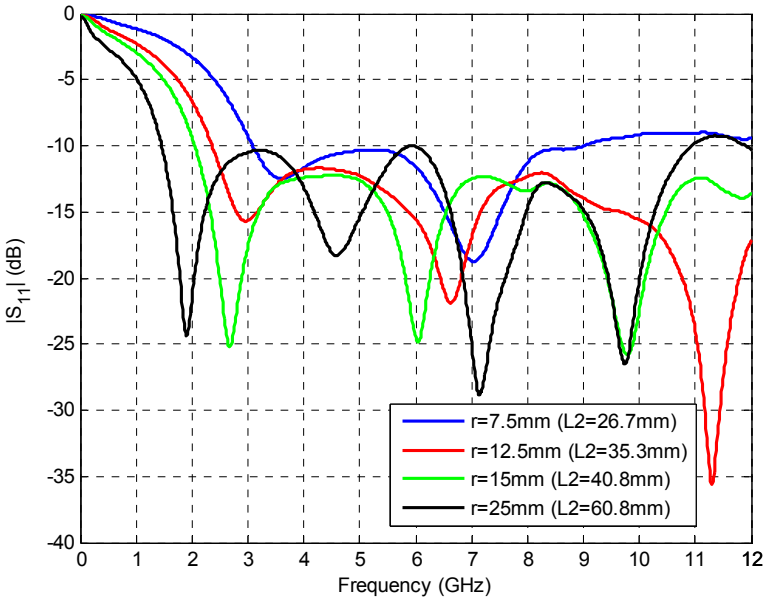


Figure 5.10: Simulated $|S_{11}|$ curves for different disc dimensions of the half circular disc in the optimal designs.

The relationship between the half disc diameters 2*r*, overall length $L_2$, ground plane width *W* and the first local minimums is also listed in table 5-A. It is

demonstrated that the first local minimum frequency is determined by the ground plane width $W$ plus the overall length $L_2$, which approximately corresponds to the half wavelength at this frequency. It is also found that the optimal overall length $L_2$ is just around twice the ground plane width $W$. Table 5-A is therefore a good summary of the design rules for achieving the ultra wide impedance bandwidth in a printed half disc monopole antenna.

Table 5-A: Optimal design parameters of the printed half disc monopole antenna and relationship between the diameter 2*r*, overall length $L_2$, ground plane width $W$ and the first local minimum frequency.

| Diameter 2*r* (mm) | 15 | 25 | 30 | 50 |
|---|---|---|---|---|
| Optimal $L_2$ (mm) | 26.7 | 35.3 | 40.8 | 60.8 |
| Optimal $W$ (mm) | 12 | 16 | 18 | 31 |
| First local minimum $f_1$ (GHz) | 3.6 | 2.96 | 2.67 | 1.9 |
| Wavelength at $f_1$ (mm) | 83.33 | 101.35 | 112.36 | 157.89 |
| $L_2 / \lambda$ | 0.32 | 0.35 | 0.36 | 0.38 |
| $W / \lambda$ | 0.14 | 0.16 | 0.16 | 0.19 |
| $(L_2 + W) / \lambda$ | 0.46 | 0.51 | 0.52 | 0.57 |
| $L_2 / W$ | 2.23 | 2.21 | 2.27 | 1.96 |

### 5.3.4 Antenna Performance

A prototype of the printed half disc monopole antenna with optimal design, i.e. $r$=12.5mm, $L_2$ =35.3mm and $W$=16mm, was fabricated and tested in the Antenna Measurement Laboratory at Queen Mary, University of London, as shown in figure 5.11.

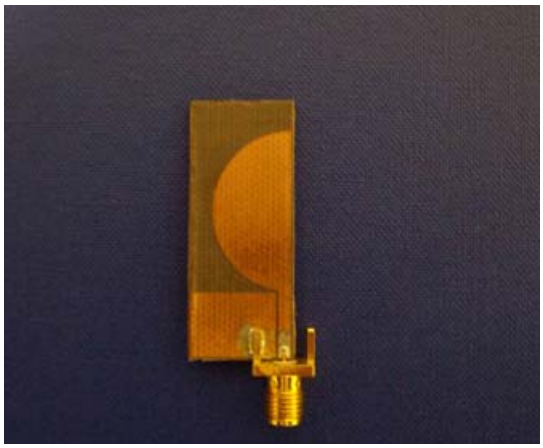

Figure 5.11: Photo of the printed half disc monopole antenna with optimal design.

Figure 5.12 displays the simulated and the measured $|S_{11}|$ curves. The measured $|S_{11}|$ curve agrees reasonably with the simulated one across the whole frequency band. The minor discrepancy is due to the effect of the feeding cable since the antenna size is small. The measured -10 dB $|S_{11}|$ bandwidth of the miniaturised antenna ranges from 1.94 GHz to 11.6 GHz.

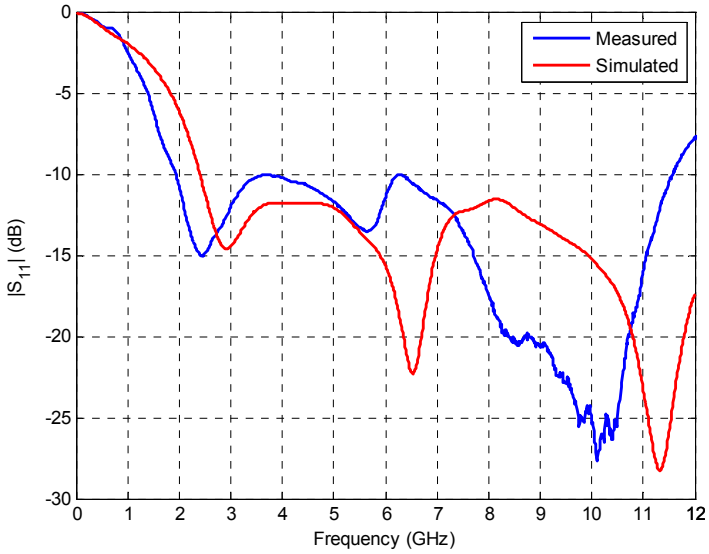


Figure 5.12: Simulated (red line) and measured (blue line) $|S_{11}|$ curves of the printed half disc monopole antenna.

The measured radiation patterns at 2.45 GHz, 5.64 GHz and 10 GHz are plotted in figure 5.13, figure 5.14 and figure 5.15, respectively. It is observed in figure 5.13 that the *E*-plane (*z*-*x* plane) pattern has a large back lobe while the *H*-plane (*x*-*y* plane) pattern is close to omni-directional. In figure 5.14 and figure 5.15, it is noticed that in the *H*-plane the pattern is distorted due to the asymmetrical structure of the antenna. Figure 5.16 plots the simulated peak gain of the printed half disc monopole antenna, it is seen that the antenna has achieved a satisfactory gain level across the band.

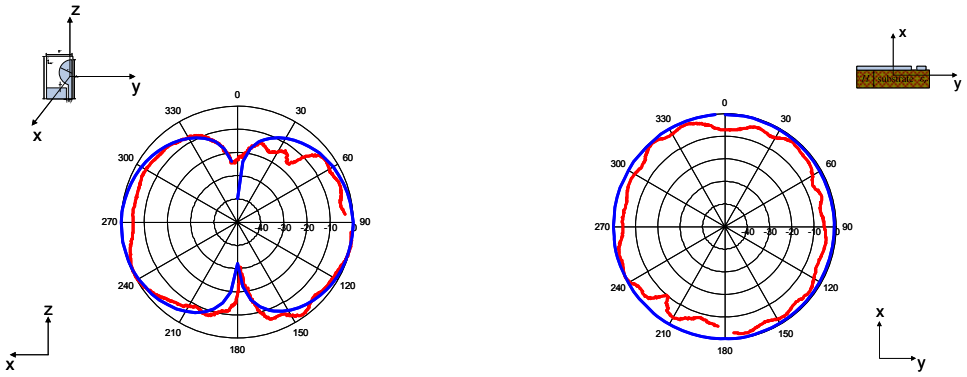


(a) *z-x* plane (b) *x-y* plane

Figure 5.13: Measured (red line) and simulated (blue line) radiation patterns of the printed half disc monopole antenna at 2.45 GHz.

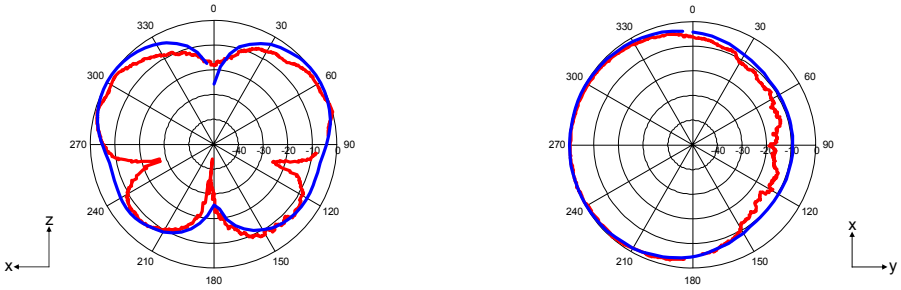


(a) *z-x* plane (b) *x-y* plane

Figure 5.14: Measured (red line) and simulated (blue line) radiation patterns of the printed half disc monopole antenna at 5.64 GHz.

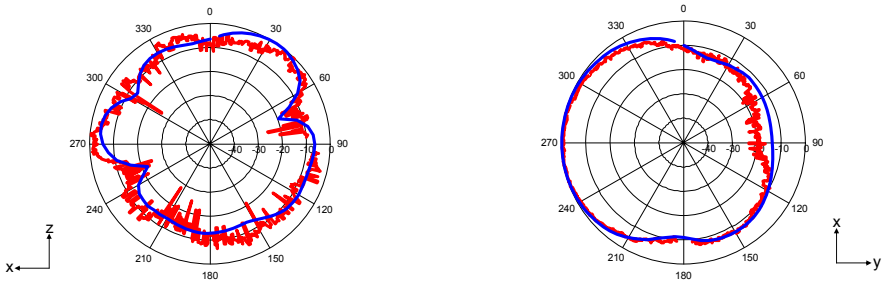


(a) *z-x* plane (b) *x-y* plane

Figure 5.15: Measured (red line) and simulated (blue line) radiation patterns of the printed half disc monopole antenna at 10 GHz.

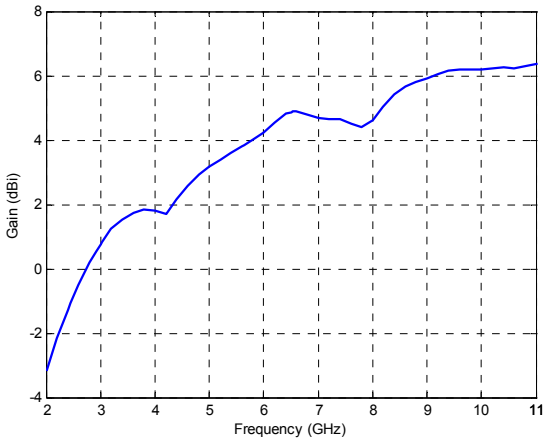


Figure 5.16 Simulated peak gain of the printed half disc monopole antenna.

### 5.3.5 Antenna Characteristics

Printed half disc monopole antenna has been demonstrated to exhibit UWB characteristic with reasonable radiation patterns. It is essential to acquire some insights into its operation.

Figure 5.17 illustrates the simulated $|S_{11}|$ curve of the optimal design of the antenna together with its corresponding input impedance.

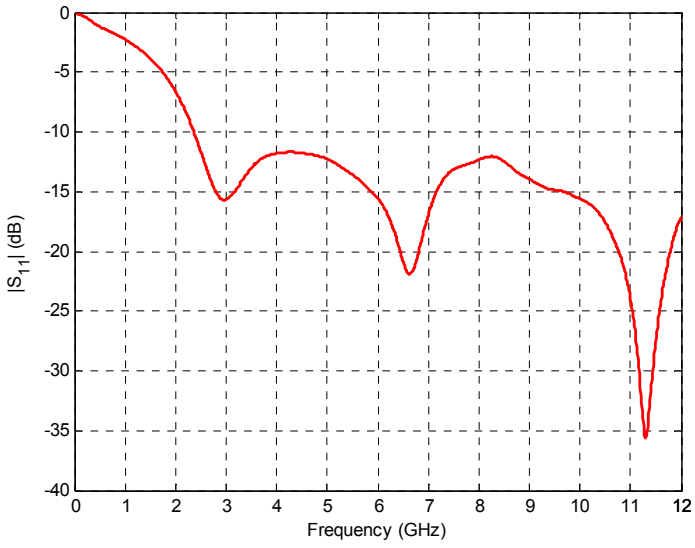


(a) Simulated $|S_{11}|$ of the optimal design of the antenna

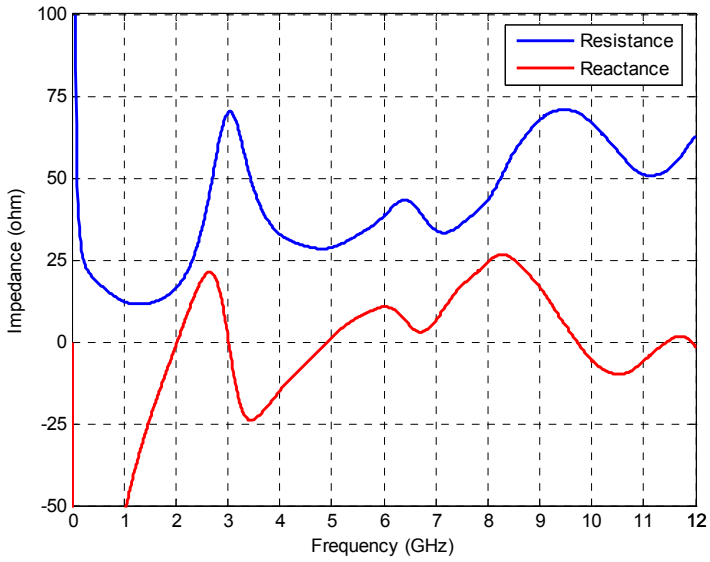


(b) Simulated input impedance curve of the optimal design of the antenna

Figure 5.17: Simulated $|S_{11}|$ curve of the optimal design of the antenna and its corresponding input impedance.

As shown in figure 5.17, the first local minimum emerges at around 2.92 GHz, the second local minimum at 6.53 GHz and the third one at 11.32 GHz. The overlapping of these local minimums which are closely spaced across the spectrum leads to an ultra wide -10 dB bandwidth.

The $|S_{11}|$ or input impedance can only depict the performance of an antenna as a lumped load at the end of the feeding line. The elaborated electromagnetic behaviour of the antenna can only be revealed by examining the current distributions or radiation patterns. The typical current distributions on the antenna close to the local minimum frequencies are displayed in figure 5.18.

Figure 5.18 (a) exhibits the current pattern near the first local minimum at 2.92 GHz. The current distribution near the second local minimum at 6.53 GHz is plotted in figure 5.18 (b), representing approximately a second order harmonics. Figure 5.18 (c) presents the third order harmonics at 11.32 GHz. These current

distributions support the standpoint that the overlapping of closely spaced resonance modes results in the UWB characteristic of the antenna. The resonances are clearly seen on the edges of both the ground plane and the half circular disc at these three frequencies.

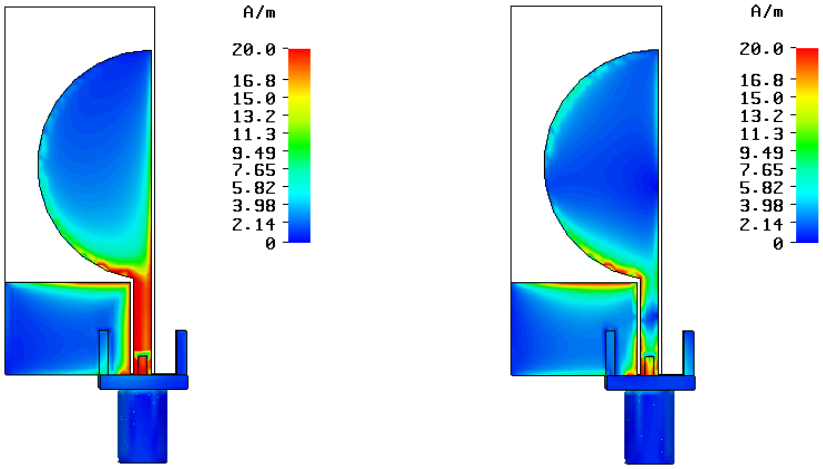


(a) at 2.92 GHz




(b) at 6.53 GHz

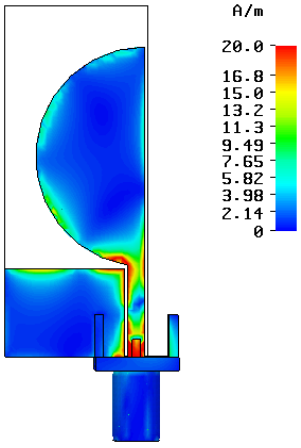


(c) at 11.32 GHz

Figure 5.18: Simulated current distributions of the optimal design of the printed half disc monopole antenna.

The simulated 3D radiation patterns close to these local minimums are illustrated in figure 5.19. The radiation pattern resembles a donut, similar to a dipole pattern, at the first resonance frequency, as shown in figure 5.19 (a). At the second harmonic, the pattern exhibits an asymmetrical pinched donut with the gain increase

around $\theta = 45^{\circ}$ in figure 5.19 (b). At the third harmonic, the pattern is squashed in *x*-direction and becomes more irregular with maximum gain forming around *z*-direction, as shown in figure 5.19 (c). It is also noticed that the *H*-plane patterns are almost omni-directional at lower resonance (1st harmonic) and become distorted at the higher harmonics (2nd and 3rd harmonics).

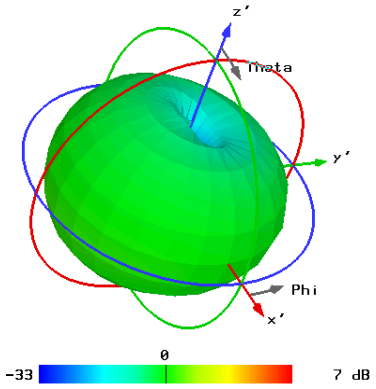


(a) at 2.92 GHz

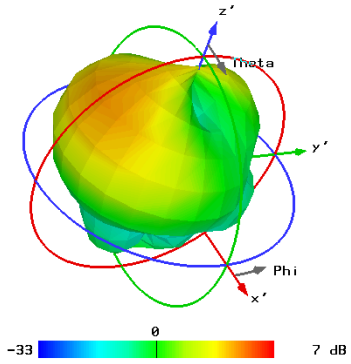


(b) at 6.53 GHz

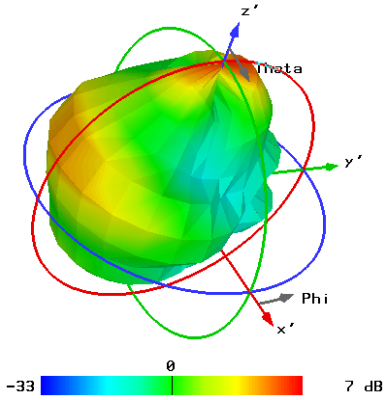


(c) at 11.32 GHz

Figure 5.19: Simulated 3D radiation patterns of the optimal design of the printed half disc monopole antenna.

### 5.3.6 Operating Principle

It has been demonstrated that the overlapping of closely spaced resonance modes in the printed half disc monopole antenna results in an ultra wide -10 dB bandwidth.

At the low frequency end (the first local minimum) when the wavelength is

larger than the antenna size, the input / receiving signal can easily 'couple' into the antenna structure hence it behaves in an oscillating mode, i.e. a standing wave. With the increase of the frequency, the antenna begins to operate in a hybrid mode of standing and travelling waves.

At the high frequency end, the travelling wave appears more influential to the antenna operation since the EM wave needs to travel down to the antenna structure which is large in terms of the wavelength.

For the printed half disc monopole antenna, the slot formed by the bottom edge of the disc and the ground plane (as shown in figure 5.20 Region A) with an appropriate size can support travelling wave quite well. Therefore an optimally designed printed half disc monopole antenna can present an ultra wide -10 dB bandwidth. The operation principle of printed half disc monopole is depicted as the schematic shown in figure 5.21.

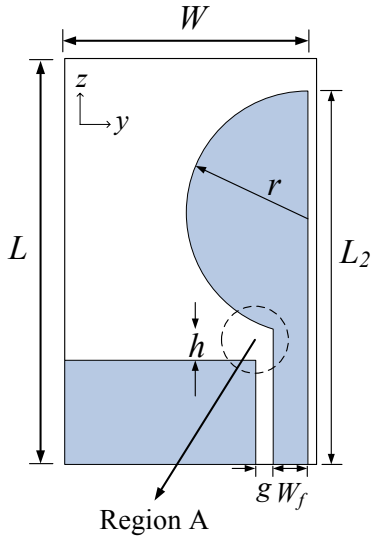


Figure 5.20: The slot (Region A) formed by the bottom edge of the disc and the ground plane.

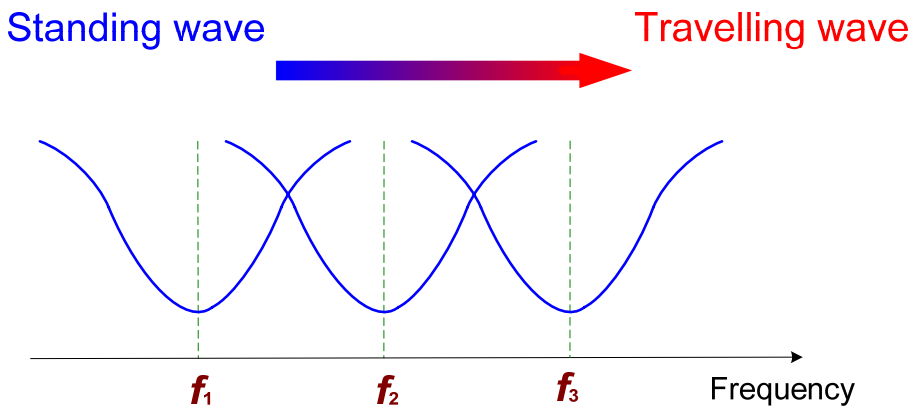


Figure 5.21: Operation principle of printed half disc monopole antenna.

Interestingly, it is also noticed that the printed half disc monopole antenna has an even wider impedance bandwidth than its full disc counterpart at the lower band in both the simulation and the measurement. The reason for this phenomenon will be investigated as follows.

Firstly, the circular disc monopole antenna is just simply chopped in half, as shown in figure 5.22 and a $|S_{11}|$ comparison is displayed in figure 5.23.

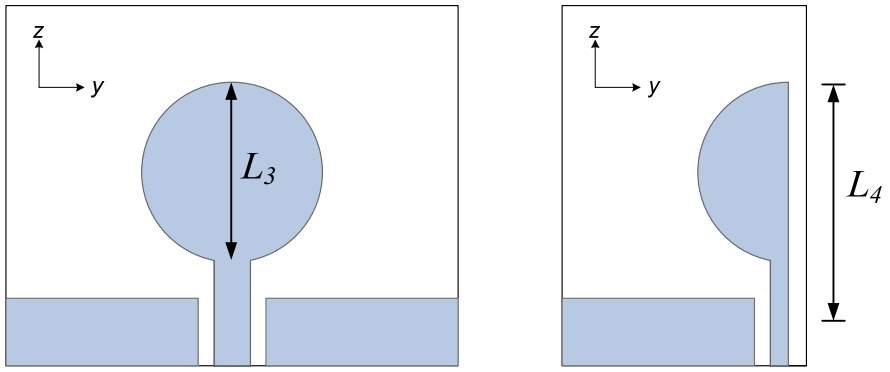


Figure 5.22: (a) Full disc monopole and (b) Simply chopped half monopole.

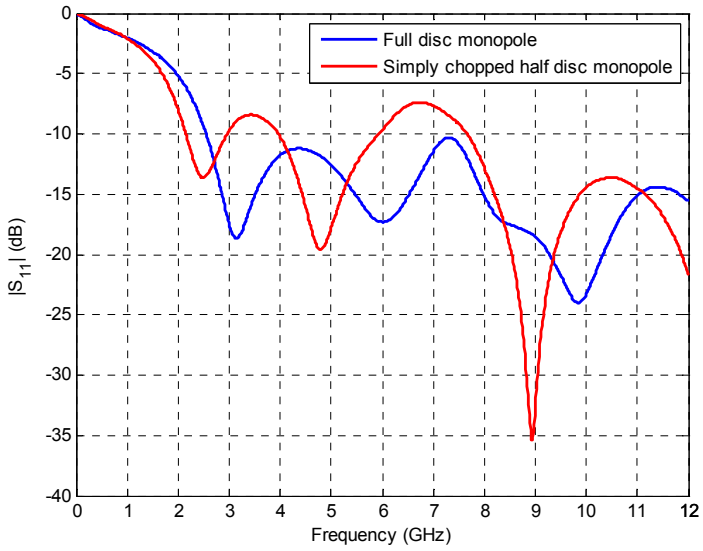


Figure 5.23: $|S_{11}|$ of the full disc and half disc monopole antenna.

As can be seen in figure 5.23, the first local minimum is shifted down from 3.1 GHz to 2.46 GHz despite overall return loss pattern being degraded. The deviation of the first local minimum is caused by the increase of the effective current path (from $L_3$ to $L_4$), which is illustrated in figure 5.22. For the full disc case, the current is mainly distributed along the edge of circular disc and its first local minimum is approximately determined by the diameter $L_3$ ($\approx \lambda/4$). For the half disc monopole case, apart from a clear current flow on the left-hand side circular disc edge, another obvious current path is also excited along the length $L_4$ ($\approx \lambda/4$), which is a bit longer than $L_3$ as depicted in figure 5.22 (b). For clarity, a current distribution plot is employed to illustrate the phenomenon.

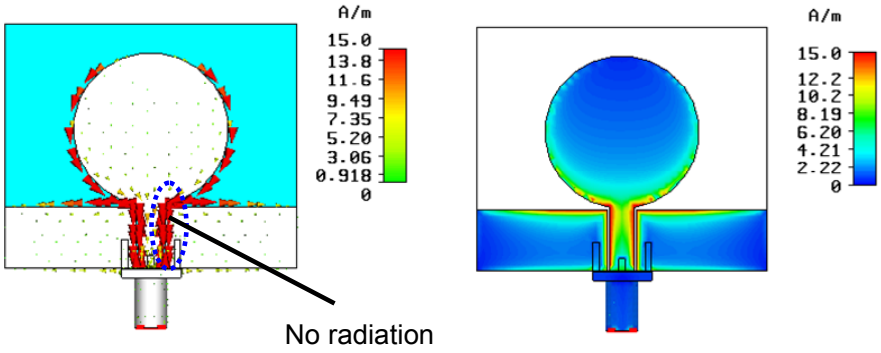


(a)

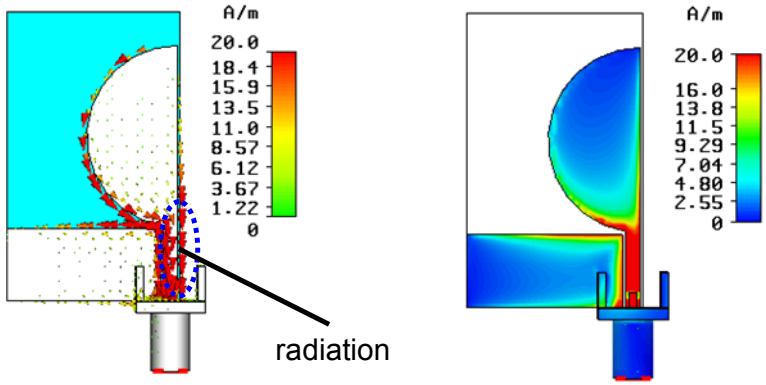


(b)

Figure 5.24: Current distribution (a) Full disc monopole antenna and (b) Half disc monopole antenna.

It is seen in figure 5.24 that an additional current path is introduced due to the removal of the right-hand side ground plane for the half disc monopole scenario. However, for the full disc monopole case, there is a regular CPW transmission line mode and no extra current route is generated.

To further verify this mechanism for the improvement at the lower end of the impedance bandwidth of the half disc monopole, a ground plane on the other side of disc is gradually introduced in different length $L_5$, as shown in figure 5.25.

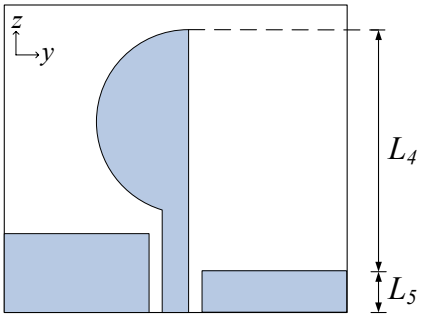


Figure 5.25: The sweep of the ground plane.

A $|S_{11}|$ comparison is given in figure 5.26, red, green and blue curves standing for $L_5$ =4mm, $L_4$ =31.3mm; $L_5$ =7mm, $L_4$ =28.3mm; and $L_5$ =10mm, $L_4$ =25.3mm, respectively. It is noticed that with the increase of the ground length $L_5$, the first local minimum also increases as listed in table 5-B. So, when the added ground plane length is levelled with the other half, the first local minimum frequency is close to that of the full disc.

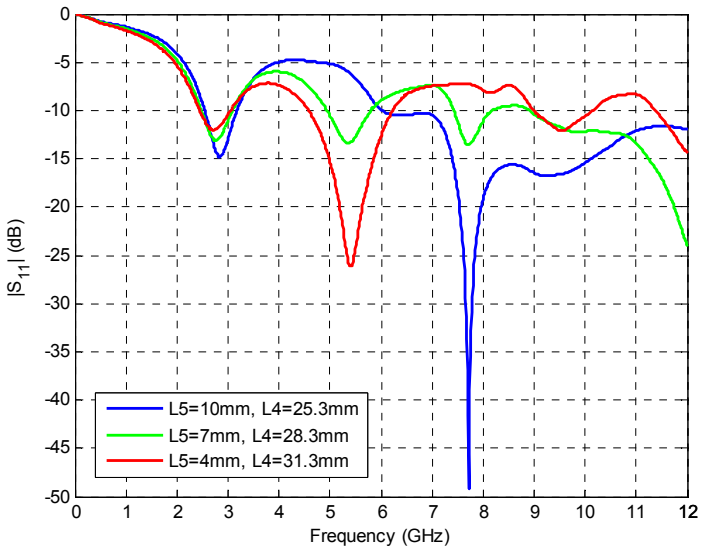


Figure 5.26: $|S_{11}|$ comparison of the ground plane sweep.

Table 5-B: The relationships between $L_4$, $L_5$ and the first local minimums.

| | $L_5$=4mm, $L_4$=31.3mm | $L_5$=7mm, $L_4$=28.3mm | $L_5$=10mm, $L_4$=25.3mm | $L$=25 mm (full disc) |
|---|---|---|---|---|
| First local minimum $f_1$ | 2.72 GHz | 2.76 GHz | 2.84 GHz | 3.01 GHz |
| Wavelength $\lambda$ at $f_1$ | 110.3mm | 108.7mm | 105.6mm | 99.7mm |
| $L_4 / \lambda$ | 0.28 | 0.26 | 0.24 | 0.25 |

## 5.4 Summary

This chapter has presented an investigation into the printed half disc monopole antenna. It has been shown that a significant 65% physical size reduction can be achieved for the printed disc monopole antenna for UWB systems by simply halving the original antenna and tuning the width of the coplanar ground plane. The miniaturised half disc monopole antenna features an even wider impedance bandwidth at the lower band. It has been revealed that the prolonged current path due to the removal of the right-hand side ground plane contributes to the wider impedance bandwidth at the lower end. The results show this half disc monopole is a good candidate for the future UWB applications.

## References

[1] M.Sun and Y.P.Zhang, "Miniaturization of Planar Monopole Antennas for Ultrawide-Band Applications", *IEEE International Workshop on Antenna Technology: Small Antennas and Novel Metamaterials*, 21-23, March 2007, Cambridge, U.K.

[2] B.Sanz-Izquierdo and J.C.Batchelor, "E-Plane Cut UWB Monopole", *2007*

*Loughborough Antennas & Propagation Conference (LAPC'07)*, Loughborough, UK, 2-3 April 2007.

# Chapter 6 Printed Quasi-Self-Complementary UWB Antenna

In chapter 3 and 4, a loaded orthogonal half disc monopole antenna and a printed half disc monopole antenna have been proposed and investigated. It is demonstrated that the antenna miniaturisation can be achieved by either applying the loading technique or exploiting original antenna's symmetry. In this chapter, printed quasi-self-complementary UWB antennas are studied for size reduction. Printed on a dielectric substrate and fed by a 50 Ω coaxial cable, planar antennas with a half disc complementary structure have been exhibited to offer an ultra wide -10 dB impedance bandwidth with reasonable radiation properties. The performance and characteristics of the proposed antennas are investigated both numerically and experimentally. Good agreement is achieved between the simulation and the measurement. It is also manifest that a massive 74% equivalent size reduction in area can be realised in the printed CPW-Fed quasi-self-complementary antenna compared with the original CPW-Fed disc monopole design. For the microstrip line-fed quasi-self-complementary antenna, it features both physically and electrically small dimensions with 16mm×25mm in physical size and 0.24λ in electrical size, respectively.

## 6.1 Introduction

The self-complementary antenna (SCA), firstly proposed by Mushiake [1, 2], has claimed a broad impedance bandwidth. Theoretically, a self-complementary antenna possesses the constant input impedance 188.5 Ω , independent of the source

frequency and the antenna configuration. To briefly demonstrate the principle of SCA, consider the slot antenna shown in figure 6.1 (a) and the complementary dipole antenna shown in figure 6.1 (b).

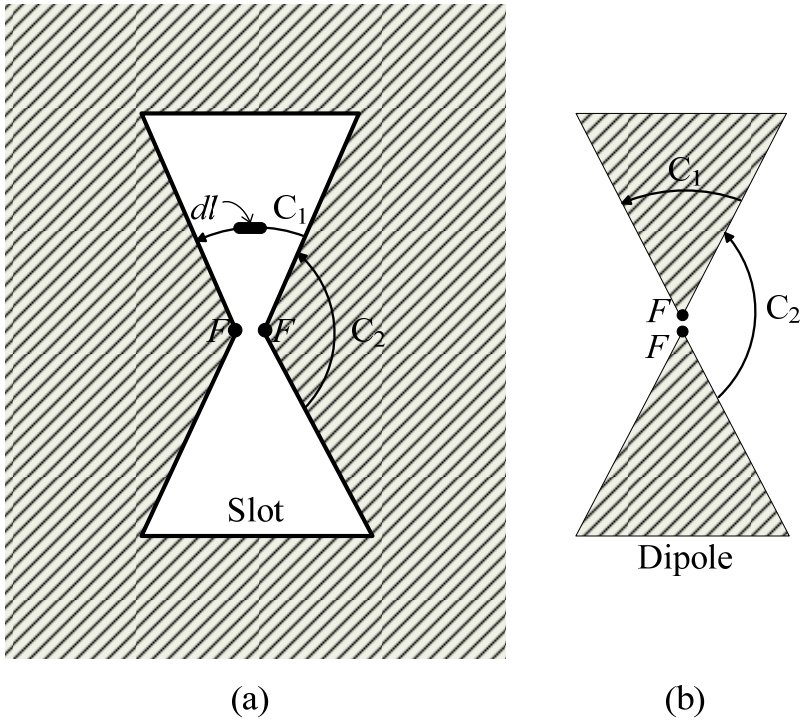


Figure 6.1: Slot antenna (a) and complementary dipole antenna (b).

The terminals of each antenna are denoted by *FF*, and it is assumed that they are separated by an infinitesimal distance. It is also assumed that the slot and dipole are cut from an infinitesimally thin, plane, perfectly conducting sheet.

Put a generator connect to the terminals of the slot. The driving-point impedance $Z_s$ at the terminals is the ratio of the terminal voltage $V_s$ to the terminal current $I_s$. Assume $E_s$ and $H_s$ are the electric and magnetic fields of the slot at any point *P*. Then the voltage $V_s$ at the terminals *FF* of the slot is given by the line integral of $E_s$ over the path $C_1$ (Figure 6.1 (a)) as $C_1$ approaches zero. Therefore,

$$V_s = \lim_{C_1 \to 0} \int_{C_1} E_s \cdot dl \tag{6.1}$$

where d**l** is the infinitesimal vector element of length dl along the contour or path $C_1$. The current $I_s$ at the terminals of the slot is:

$$I_s = 2 \lim_{C_2 \to 0} \int_{C_2} H_s \cdot dl \tag{6.2}$$

The path $C_2$ is just outside the metal sheet and parallel to its surface. The factor 2 enters because only half the line integral is taken, the line integral over the other side of the sheet being equal by symmetry.

As for the complementary dipole antenna, place a generator connect to the terminals of the dipole. The driving-point impedance $Z_d$ at the terminals is the ratio of the terminal voltage $V_d$ to the terminal current $I_d$. Assume $E_d$ and $H_d$ are the electric and magnetic fields of the dipole at any point *P*. Then the voltage at the dipole terminals is:

$$V_d = \lim_{C_2 \to 0} \int_{C_2} E_d \cdot dl \tag{6.3}$$

and the current is:

$$I_d = 2 \lim_{C_1 \to 0} \int_{C_1} H_d \cdot dl \tag{6.4}$$

However,

$$\lim_{C_2 \to 0} \int_{C_2} E_d \cdot dl = Z_0 \lim_{C_2 \to 0} \int_{C_2} H_s \cdot dl \tag{6.5}$$

and

$$\lim_{C_1 \to 0} \int_{C_1} H_d \cdot dl = \frac{1}{Z_0} \lim_{C_1 \to 0} \int_{C_1} E_s \cdot dl \tag{6.6}$$

where $Z_0$ is the intrinsic impedance of the surrounding medium. Substituting (6.2)

and (6.3) in (6.5) yields:

$$V_d = \frac{Z_0}{2} I_s \tag{6.7}$$

Substituting (6.1) and (6.4) in (6.6) gives:

$$V_s = \frac{Z_0}{2} I_d \tag{6.8}$$

Multiplying (6.7) and (6.8) yields:

$$\frac{V_s}{I_s}\frac{V_d}{I_d} = \frac{{Z_0}^2}{4} \tag{6.9}$$

or:

$$Z_s Z_d = \frac{{Z_0}^2}{4} \tag{6.10}$$

Equation (6.10) indicates that the terminal impedance $Z_s$ of a slot antenna is equal to quarter of the square of the intrinsic impedance of the surrounding medium divided by the terminal impedance $Z_d$ of the complementary dipole antenna [3].

It is seen in (6.10) that the product of the impedances of two complementary antennas is the constant ${Z_0}^2/4$. If the antenna is its own complement, frequency-independent impedance behaviour is achieved. This is the self-complementary property, in which the antenna and its complement are identical. A self-complementary structure can be made to exactly overlay its complement through translation and / or rotation. The value of impedance follows directly from (6.10), as noted by Mushiake:

$$Z = Z_s = Z_d = \frac{Z_0}{2} = 188.5\Omega \tag{6.11}$$

Therefore, self-complementary antennas have the constant input impedance 188.5Ω, independent of the source frequency and the antenna structure.

During the past few years, the concept of SCA has been applied to create wideband antennas and subsequently research efforts have been made towards SCA designs and analysis. A self-complementary antenna formed by a monopole and a slot has been proposed and investigated in [4] and a printed self-complementary spiral antenna was presented in [5]. In spite of all the promising prospects provided by these SCAs, it has to be noted that a matching network is essential to transform the input impedance from 188.5Ω to 50Ω in order to integrate the antenna with the RF front end. This has constrained the bandwidth of this type of antenna. For instance, Wong [6] proposes a broadband printed quasi-self-complementary antenna which is excited by a mini 50Ω coaxial line, thus avoiding the bulky matching circuit. However, the bandwidth of this antenna is only appropriate for 5.2 / 5.8 GHz WLAN operation but not for ultra-wideband applications.

In this chapter, a novel design of printed quasi-self-complementary antenna fed by a 50Ω coaxial cable without an extra matching network is proposed for UWB applications. The parameters that affect the performance of the antenna are analysed both numerically and experimentally in order to understand the operation of the antenna. Also, an evolution of the proposed antenna is depicted to demonstrate the mechanism of the built-in CPW-like matching section. It has been illustrated that the optimal design of this type of antenna can yield an ultra wide impedance bandwidth with reasonable radiation properties. In addition, a microstrip line-fed quasi-self-complementary antenna is also proposed and studied. This antenna features an even smaller size, 16mm×25mm in physical size and 0.24λ in electrical size, respectively.

## 6.2 CPW-Fed Quasi-Self-Complementary Antenna

### 6.2.1 Antenna Design and Performance

The quasi-self-complementary antenna studied in this section has a single layer-metallic structure, as displayed in figure 6.2. A half circular disc and a half circular slot are printed on the same side of the dielectric substrate (in this study, the substrate of thickness 1.6mm and relative permittivity 3.0 was used). *L* and *W* denote the length and the width of the dielectric substrate, respectively. In addition, a CPW-like matching section is added to connect the half circular disc with the SMA (SubMiniature version A) coaxial connector. The dimension of the half circular slot is chosen to be the same as the half circular disc with a radius of *r*=12.5mm. *h* is the height of the feed gap between the bottom of the half circular disc and the ground. *s* represents the spacing between the central strip and the slotted ground. The simulations are performed using the CST Microwave Studio™ package for electromagnectic computation.

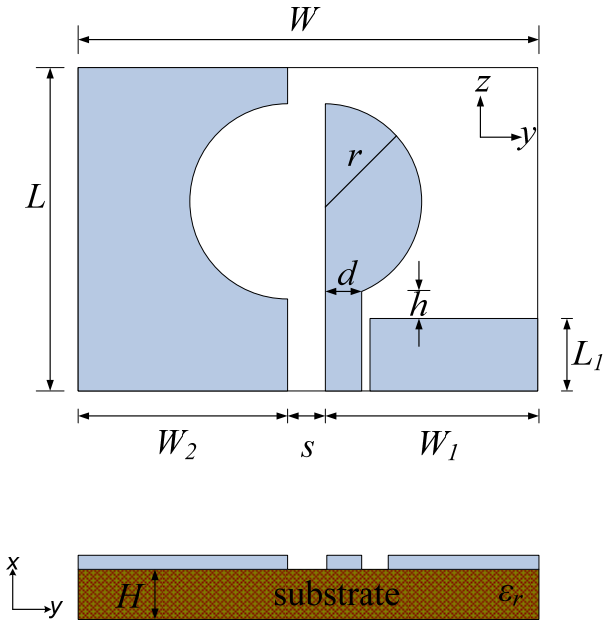


Figure 6.2: Geometry of proposed quasi-self-complementary antenna.

A prototype of the quasi-self-complementary antenna with optimal design, i.e. $r$=12.5mm, $h$=0.3mm, $W$=51.5mm, $L$=40mm, $W_1$ =20.7mm, $W_2$ =28.77mm, $L_1$=10mm, $s$=2.03mm and $d$=2mm, was built and tested in the Antenna Measurement Laboratory at Queen Mary, University of London, as shown in figure 6.3. The $|S_{11}|$ were measured in an anechoic chamber by using a HP 8720ES network analyser.

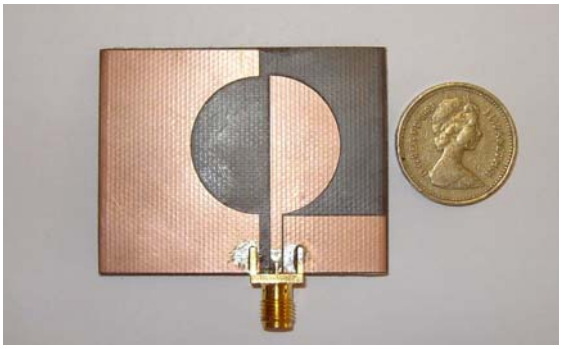

Figure 6.3: Photo of the quasi-self-complementary antenna with its optimal design.

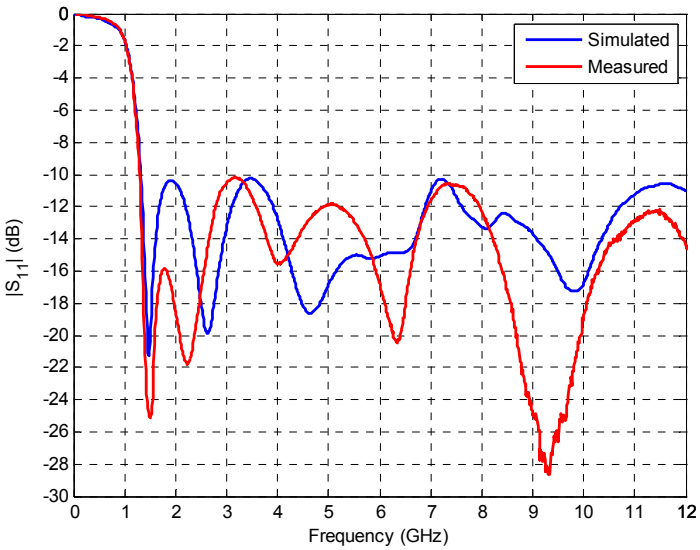


Figure 6.4: Measured and simulated $|S_{11}|$ curves of the quasi-self-complementary antenna with its optimal design.

As illustrated in figure 6.4, the measured $|S_{11}|$ curve agrees well with the simulated one in the entire UWB frequency band. The measured -10 dB $|S_{11}|$ bandwidth of the quasi-self-complementary antenna ranges from 1.3 GHz to 13.1

GHz. Most importantly, it is also noticed that the antenna size (footprint width *W*) at the lowest frequency (1.3 GHz) is $0.22\lambda$. Comparing with current UWB antenna designs published in the literature, this quasi-self-complementary antenna offers a rather small size, for example, 36 % reduction in area compared to [7].

The radiation patterns of the antenna at the frequencies close to the local minimums have been measured inside an anechoic chamber. The measured and simulated radiation patterns at 1.47 GHz, 2.63 GHz, 4.64 GHz, 8.1 GHz and 9.83 GHz (the theoretical local minimums) are plotted in figure 6.5 – figure 6.9, respectively.

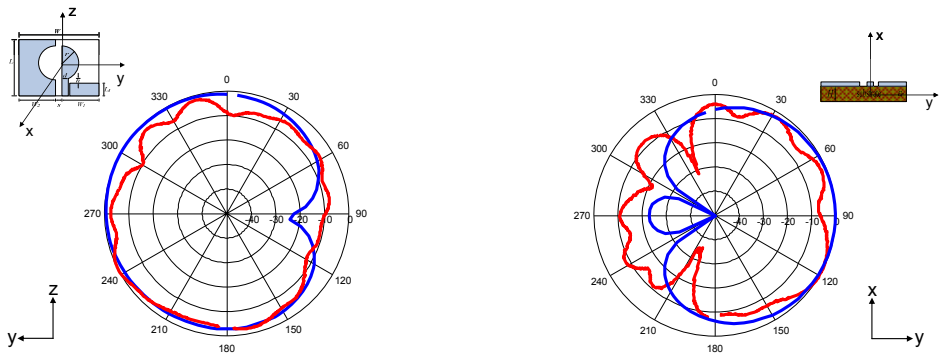


Figure 6.5: Measured (red line) and simulated (blue line) radiation patterns of the quasi-self-complementary antenna at 1.47 GHz.

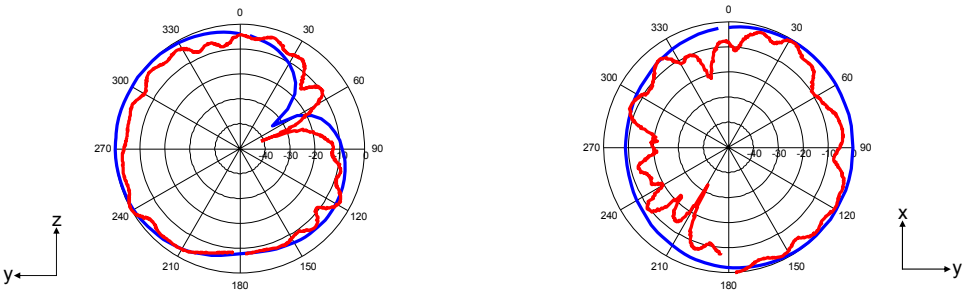


Figure 6.6: Measured (red line) and simulated (blue line) radiation patterns of the quasi-self-complementary antenna at 2.63 GHz.

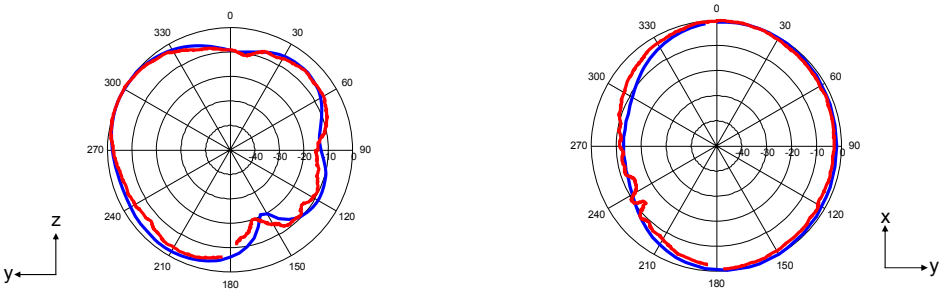


Figure 6.7: Measured (red line) and simulated (blue line) radiation patterns of the quasi-self-complementary antenna at 4.64 GHz.

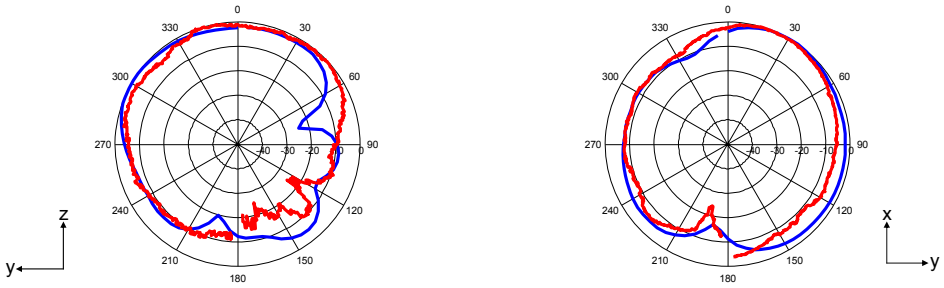


Figure 6.8: Measured (red line) and simulated (blue line) radiation patterns of the quasi-self-complementary antenna at 8.1 GHz.

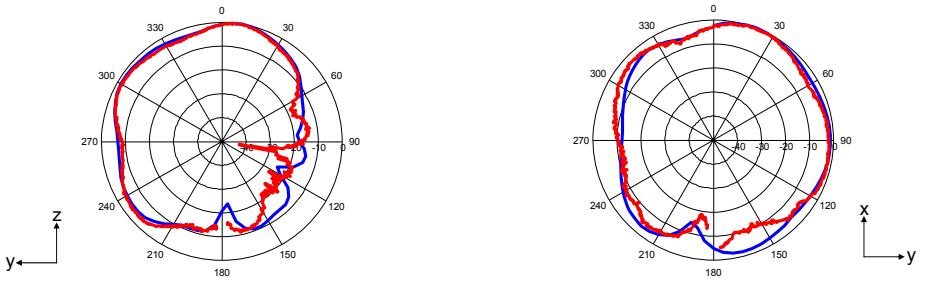


Figure 6.9: Measured (red line) and simulated (blue line) radiation patterns of the quasi-self-complementary antenna at 9.83 GHz.

It is noticed that the measured patterns agree well with those obtained in the simulation. The *H*-plane (*x*-*y* plane) patterns are nearly omni-directional in the half circular disc hemisphere whereas their slot hemisphere counterparts get distorted.

The measured *E*-plane (*z*-*y* plane) patterns are also close to the simulated ones. They exhibit irregular shaped patterns due to the complicated current distributions on the antenna.

### 6.2.2 Antenna Characteristics

In the theory, self-complementary antennas should exhibit the constant input impedance, i.e. 188.5 Ω and they tend to be frequency-independent. However, it is found that practical SCAs still have impedance variations with frequency due to the finite size of the structure [8]. Therefore, instead of a constant value, less variable input impedance characteristic will be expected. Figure 6.10 presents the simulated input impedance of the proposed antenna. It is clearly seen that the real part of the input impedance exhibits a small variation around 50 Ω within the 1.3 – 12 GHz frequency band. The imaginary part of the input impedance shows a similar trend with a small variation around 0 Ω. The matching issue is considered in detail later in this chapter.

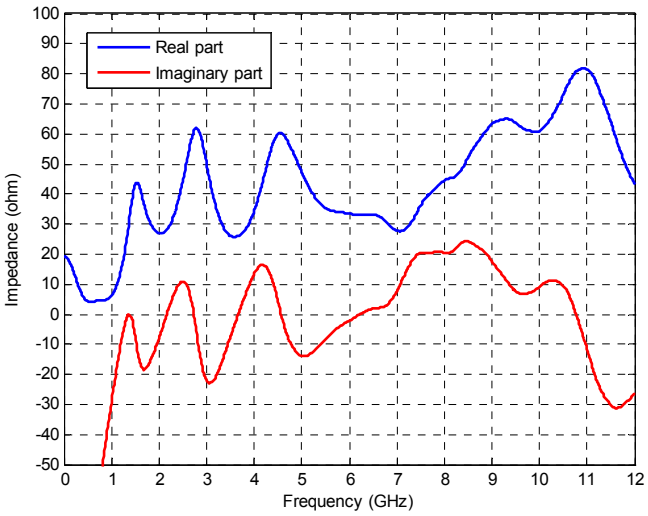


Figure 6.10: Simulated input impedance curve of the quasi-self-complementary antenna with the optimal design.

The simulated Smith Chart curve of the quasi-self-complementary antenna is plotted in figure 6.11. It is seen that the input impedance loops around impedance matching point within the circle of voltage standing wave ratio (VSWR)=2, which demonstrates the minor fluctuation of the input impedance of the antenna.

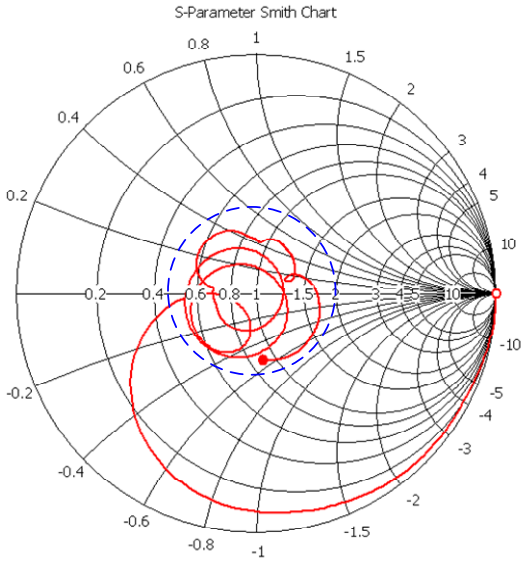


Figure 6.11: Simulated Smith Chart of the quasi-self-complementary antenna with the optimal design.

The simulated current distributions at different frequencies for the antenna with optimal design are shown in figure 6.12. Figure 6.12 (a) displays the current pattern near the first local minimum at 1.47 GHz. The current pattern near the second local minimum at 2.63 GHz is given in figure 6.12 (b) while figure 6.12 (c) and figure 6.12 (d) illustrate more complicated current patterns at 4.64 GHz and 8.1 GHz, respectively. Current distribution at 9.83 GHz is depicted in figure 6.12 (e).

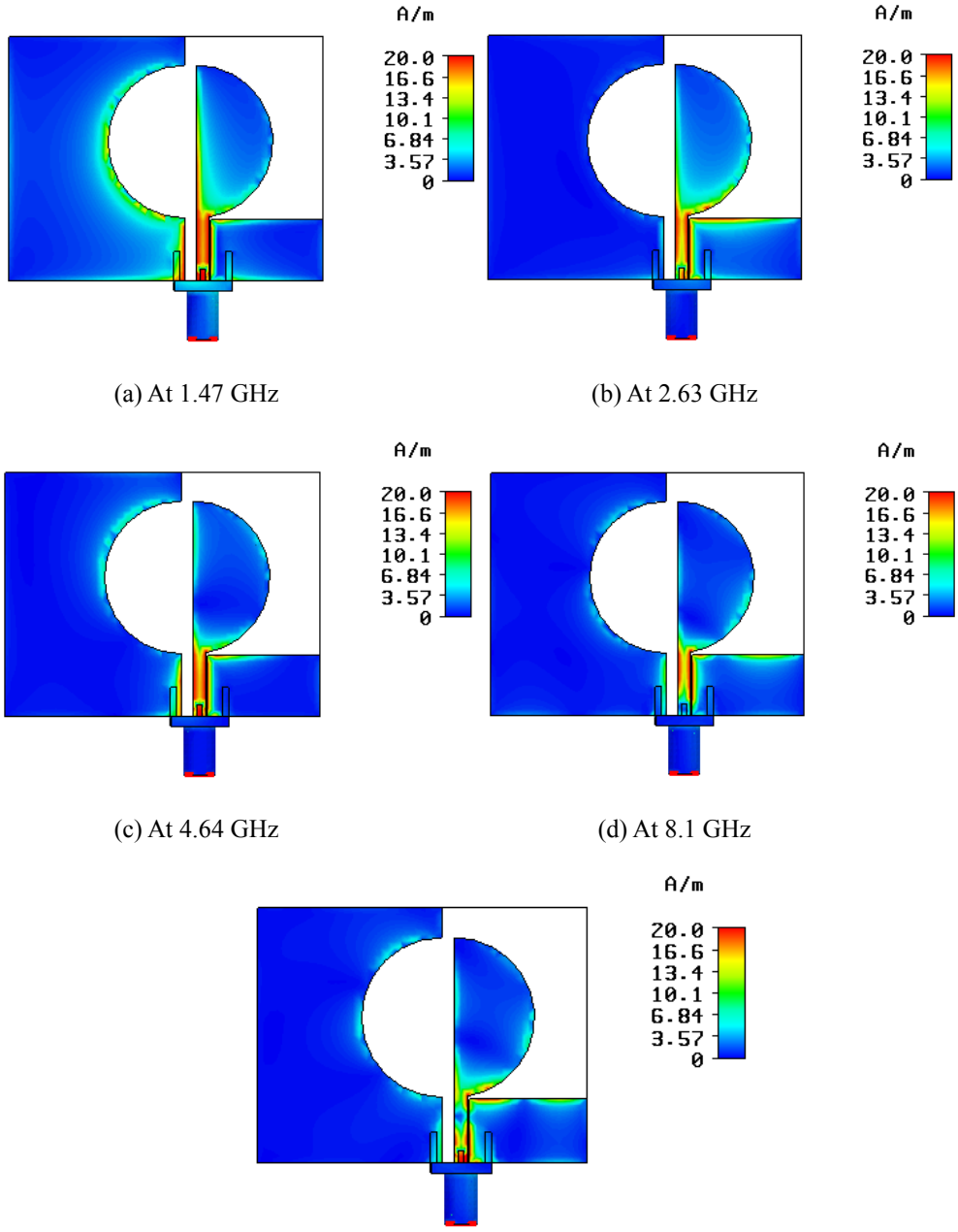


(a) At 1.47 GHz

(b) At 2.63 GHz

(c) At 4.64 GHz

(d) At 8.1 GHz

(e) At 9.83 GHz

Figure 6.12: Simulated current distributions of the quasi-self-complementary antenna with the optimal design.

As shown in figure 6.12, the current is primarily concentrated on the edges of both half circular disc and half circular slot as well as on the CPW-like matching section. However, with the increase of the frequency, less current is observed in half circular slot part. It is also noticed that a strong current flow distributes on the CPW-

like matching section across the entire frequency band. Therefore, the performance of the antenna is pivotally dependent on the matching section. In addition, since the current is not symmetrically spread on the antenna, with majority of the current dwelling on the half circular disc part, hence results in the asymmetry of radiation patterns.

Figure 6.13 illustrates the simulated peak gain of the quasi-self-complementary antenna with the optimal design across the UWB frequency band. It is shown that when the frequency increases from 1.3 GHz to 6 GHz, the gain rises from -4.132 dBi to 5.026 dBi; with the further increase of the frequency from 6 GHz to 9 GHz, the gain reduces from 5.026 dBi to 3.11 dBi and within 9 GHz to 10.6 GHz band, there again shows a climbing trend with gain peaking at 5.004 dBi. Figure 6.14 depicts the orientation of the peak gain with the increase of frequency. It is noticed that at the low and mid operational band the maximum gains occur at around $\varphi = 90^{\circ}$ cut plane with a variation of $\theta$ mainly from $45^{\circ}$ to $140^{\circ}$. At the higher operational band, the peak gains emerge at a range of $\theta$ mainly from $5^{\circ}$ to $25^{\circ}$ with $\varphi$ at around $260^{\circ}$ cut plane.

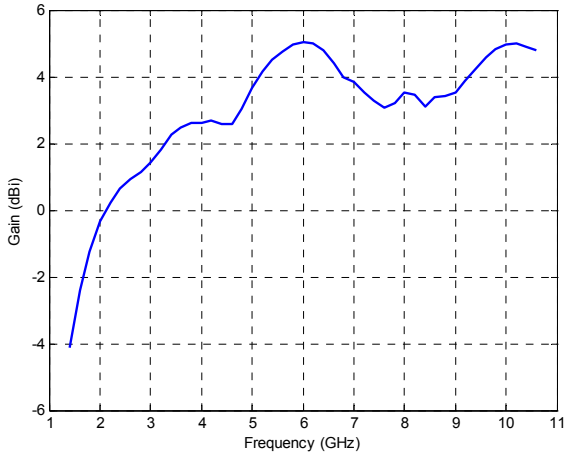


Figure 6.13: Simulated peak gain of the quasi-self-complementary antenna with the optimal design.

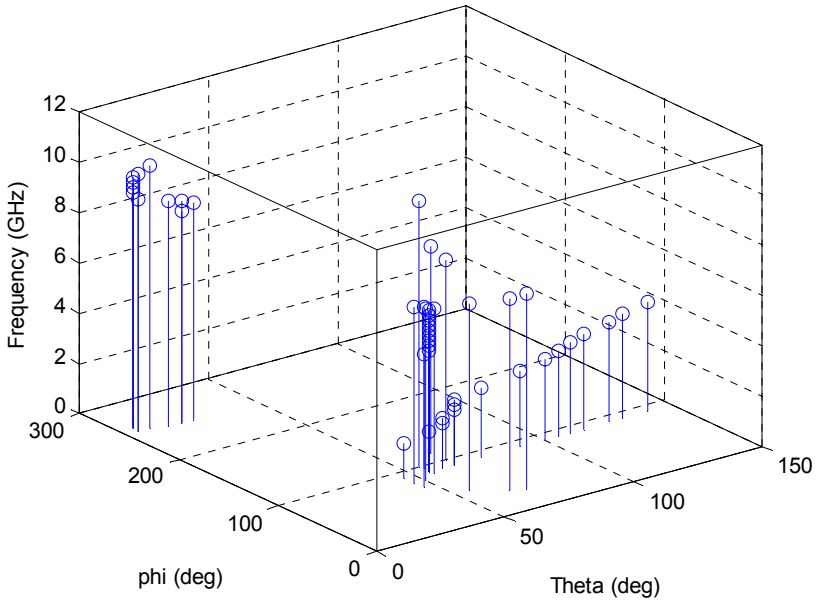


Figure 6.14: Simulated peak gain orientation of the quasi-self-complementary antenna with the optimal design.

### 6.2.3 Design Parameters

In this subsection, the important parameters that determine the antenna performance will be analysed to generate some design rules.

The first parameter is the matching section width $W_1$. As shown in figure 6.15, when $r$ is fixed at 12.5mm, $W_2$=28.77mm and $s$=2.03mm, the performance of the quasi-self-complementary antenna is quite sensitive to $W_1$. It is observed that the $|S_{11}|$ curves have similar shape for the four different $W_1$, but the -10 dB bandwidth of the antenna varies remarkably with the variation of $W_1$. This is because $W_1$, as a part of the matching section, tunes the input impedance and therefore the operating bandwidth while it is changed, as shown in figure 6.15. Also, it is noticed that the variation of $W_1$ shifts all the other resonance modes across the spectrum except the first one. The first local minimum will not be shifted by altering the value of $W_1$ but will be enhanced with the decrease of $W_1$.

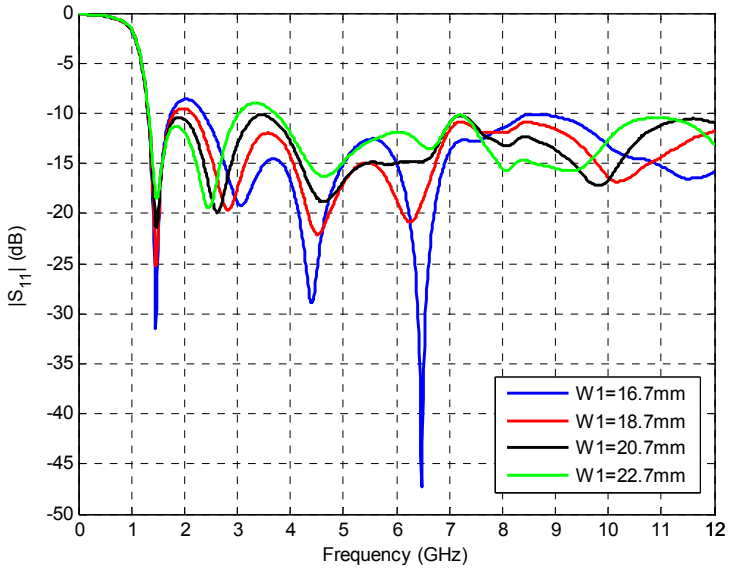


Figure 6.15: Simulated $|S_{11}|$ curves for different widths of the matching section with $W_2$=28.77mm, $s$=2.03mm and $r$=12.5mm.

Another design parameter affecting the antenna behaviour is the slotted rectangular patch width $W_2$. The simulated $|S_{11}|$ curves with $r$=12.5mm, $W_1$=20.7mm and $s$=2.03mm for different width $W_2$ are plotted in figure 6.16.

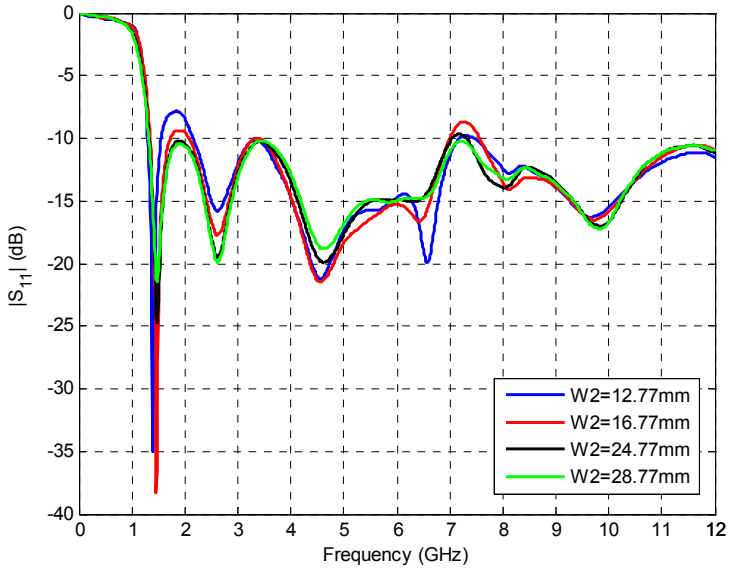


Figure 6.16: Simulated $|S_{11}|$ curves for different widths of the slotted rectangular patch with $W_1$=20.7mm, $s$=2.03mm and $r$=12.5mm.

It can be seen in figure 6.16 that $|S_{11}|$ curves again feature similar shape for the four various $W_2$ whereas the -10 dB bandwidth of the antenna changes, particularly at the lower end. In addition, it is observed that the first local minimum is slightly moved up with the increase of $W_2$. Therefore, the parameter $W_2$ presents an influence on the lower end of the antenna bandwidth.

The simulated $|S_{11}|$ curves of the quasi-self-complementary antenna for different $s$ with $W_1$=20.7mm, $W_2$=28.77mm and $r$=12.5mm are illustrated in figure 6.17.

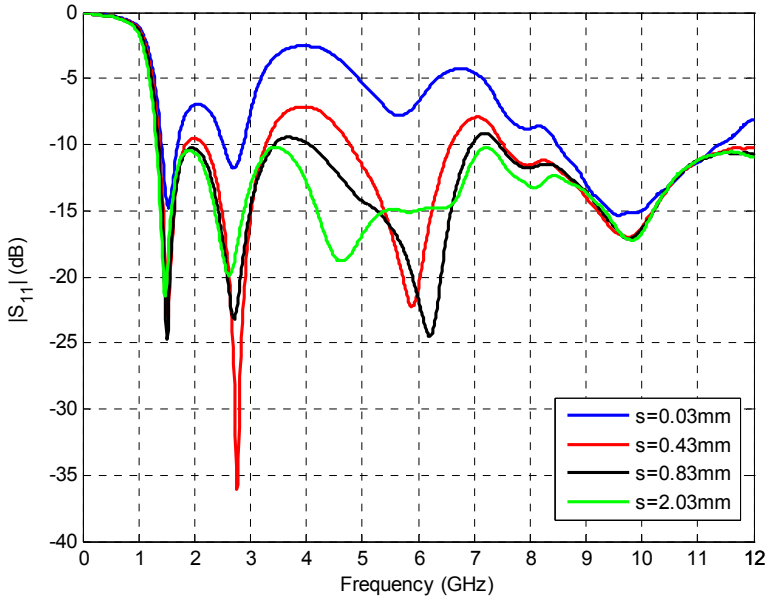


Figure 6.17: Simulated $|S_{11}|$ curves for different spacings with $W_1$=20.7mm, $W_2$=28.77mm and $r$=12.5mm.

It is seen in figure 6.17 that the -10 dB bandwidth varies dramatically with the change of $s$. When the spacing $s$ is too narrow, the impedance matching within the UWB band is disastrous with most of $|S_{11}|$ values higher than -10 dB. With the increase of the spacing $s$, better impedance matching performances can be achieved and the optimal spacing is found to be at $s$=2.03mm.

Furthermore, an intriguing phenomenon is observed in figure 6.15, figure 6.16 and figure 6.17 that the first local minimum always emerges at around 1.47 GHz for different $W_1$, $W_2$ and $s$ when the half disc / slot radius $r$ is fixed at 12.5mm.

Figure 6.18 depicts the simulated $|S_{11}|$ curves for various dimensions of the half disc / slot with their respective optimal designs, which are provided in table 6-A. It can be seen that the ultra wide impedance bandwidth can be achieved in all of these designs.

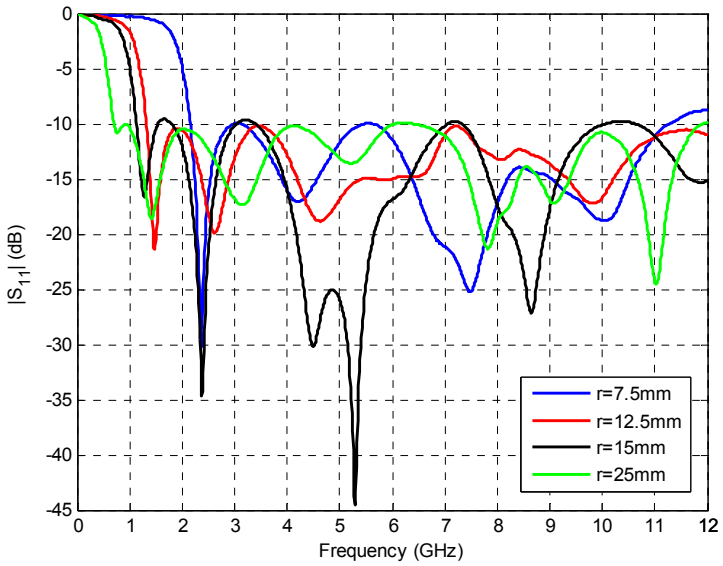


Figure 6.18: Simulated $|S_{11}|$ curves for different disc dimensions of the quasi-self-complementary antenna in the optimal designs.

Table 6-A: Optimal design parameters of the quasi-self-complementary antenna and relationship between the diameter and the first local minimum.

| Diameter $2r$ | 15 | 25 | 30 | 50 |
|---|---|---|---|---|
| First local minimum $f_1$ (GHz) | 2.36 | 1.47 | 1.27 | 0.77 |
| Wavelength $\lambda$ at $f_1$ (mm) | 127.12 | 204.08 | 236.22 | 389.61 |
| $2r / \lambda$ | 0.118 | 0.123 | 0.127 | 0.128 |
| Optimal $W_1$ (mm) | 12 | 20.7 | 25 | 41 |
| $W_1 / 2r$ | 0.8 | 0.828 | 0.833 | 0.82 |
| Optimal $W_2$ (mm) | 18.47 | 28.77 | 34.97 | 52.97 |
| $W_2 / 2r$ | 1.231 | 1.151 | 1.166 | 1.06 |
| Optimal $W$ | 32.5 | 51.5 | 62 | 94.5 |
| $W / 2r$ | 2.17 | 2.06 | 2.07 | 1.89 |
| Optimal $s$ | 2.03 | 2.03 | 2.03 | 1.43 |

The relationship between the disc diameters and the first local minimums is also listed in table 6-A. It is demonstrated that the first local minimum relates to the half circular disc / slot with an approximate relationship of $2r = \lambda / 8$, where $\lambda$ corresponds to the free space wavelength of the first local minimum. Furthermore, it is observed that the optimal width of the matching section $W_1$ is just less than the

diameter of the disc / slot, ranging from 0.8 to 0.833, while the counterpart of the slotted ground $W_2$ is just more than the diameter of the disc / slot, spanning from 1.06 to 1.231. Also, it is noticed that the optimal footprint width of the quasi-self-complementary antenna $W$ is just about twice the diameter of the disc /slot while the optimal spacing $s$ remains 2.03mm for $r$=7.5mm, $r$=12.5mm and $r$=15mm scenarios, which is close to the central strip width $d$ (2mm), and only with a slight variation to 1.43 for the $r$=25mm scenario.

### 6.2.4 Evolution of the Printed Quasi-Self-Complementary Antenna

To clearly demonstrate the mechanism of the built-in CPW-like matching section, an investigation into the impedance matching evolution of the printed quasi-self-complementary antenna is performed.

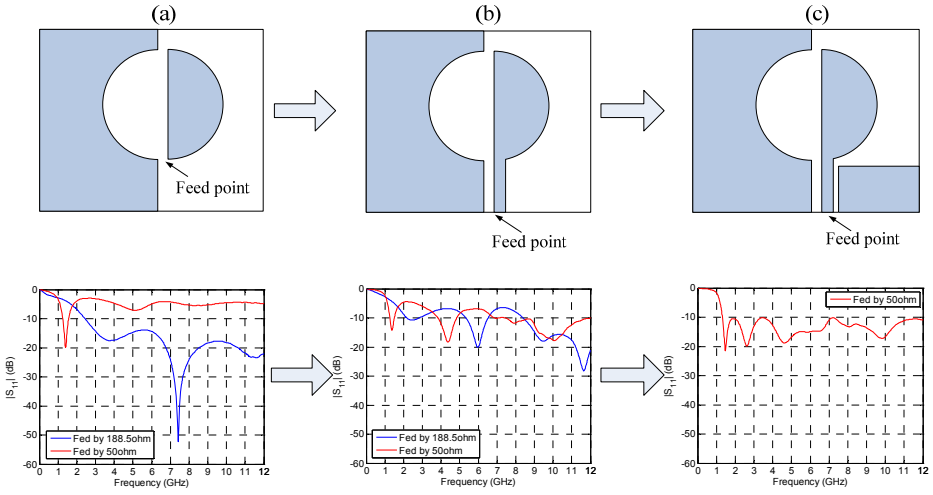


Figure 6.19: Impedance matching evolution of the quasi-self-complementary antenna.

The evolution of the printed quasi-self-complementary antenna is illustrated in figure 6.19. As the starting point, no matching section is attached to the self-complementary structure in figure 6.19 (a). A discrete port which locates over the bottom end of both the disc and slot is used to excite the antenna in the simulation. For the comparison purpose, the antenna is fed by 188.5Ω and 50Ω characteristic

impedance, respectively. It is evident from the $|S_{11}|$ curves in figure 6.19 (a) that the impedance is mismatched to the 50Ω feed, but well-matched to the 188.5Ω feed over the wide bandwidth. With a central strip of the matching section adhered to the half circular disc in figure 6.19 (b), the impedance matching to the 50Ω feed becomes better, however, the matching to the 188.5Ω feed gets degraded. Finally, with the entire CPW-like matching section attached in figure 6.19 (c), the $|S_{11}|$ curve shows a good impedance matching to the 50Ω feed over the UWB band. That is due to the fact that the slot formed by the lower edge of the half disc and the ground plane can support a travelling wave well in this antenna, which has been addressed in the previous chapter. Therefore, this results in an ultra wide -10 dB bandwidth and verifies the effectiveness of the built-in matching section.

## 6.3 Microstrip Line-Fed Quasi-Self-Complementary Antenna

In the last section, the printed CPW-Fed quasi-self-complementary antenna has been investigated and it exhibits an ultra-wide -10 dB impedance bandwidth as well as reasonable radiation properties. However, it presents a relatively large physical size which still could be a challenge for integration into space-limited systems.

In this section, a very-small-size printed quasi-self-complementary antenna fed by a microstrip line is studied. A triangular slot is inserted on the ground plane to enhance the impedance matching of the antenna. It has been shown that the optimal design of this type of antenna can offer an ultra wide impedance bandwidth with satisfactory radiation properties. Key parameters that influence the performance of the antenna are investigated. Most importantly, the proposed antenna features both

physically and electrically small dimensions, 16mm×25mm in physical size and 0.24λ in electrical size, respectively.

### 6.3.1 Antenna Design and Performance

The proposed small printed quasi-self-complementary antenna is shown in figure 6.20.

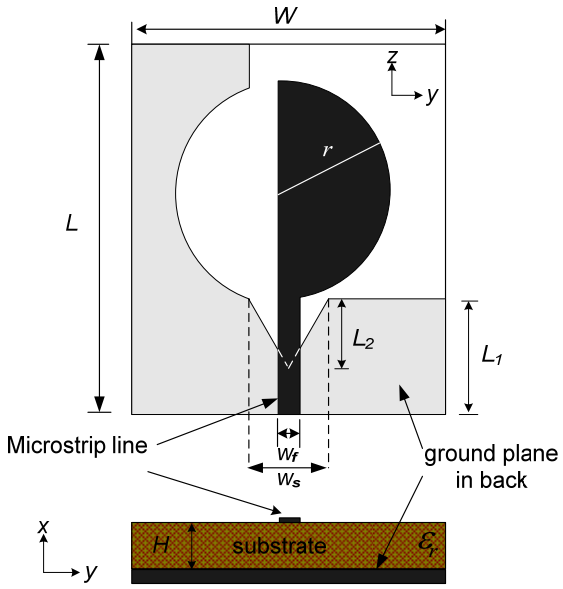


Figure 6.20: Geometry of the proposed micro-strip line fed quasi-self-complementary antenna.

A half circular disc with a radius of $r$ and its complementary magnetic counterpart are printed on the different side of the dielectric substrate (in this study, the substrate of thickness $H$=1.6mm and relative permittivity $\varepsilon_r$=3.0 was used). $L$ and $W$ represent the length and the width of the dielectric substrate, respectively. In addition, a triangular notch is cut on the ground plane in order to improve the impedance matching. $W_s$ and $L_2$ denote the width and height of the triangular notch respectively.

A prototype of the proposed printed quasi-self-complementary antenna with

optimal design, i.e., $r$=6mm, $W$=16mm, $L$=25mm, $W_s$ =6mm, $W_f$ =2.4mm, $L_1$ =8.9mm, $L_2$ =4.8mm, was constructed in the Antenna Measurement Laboratory, as shown in figure 6.21. The $|S_{11}|$ were measured by using a HP 8720ES network analyser and the radiation pattern measurements were performed inside an anechoic chamber.

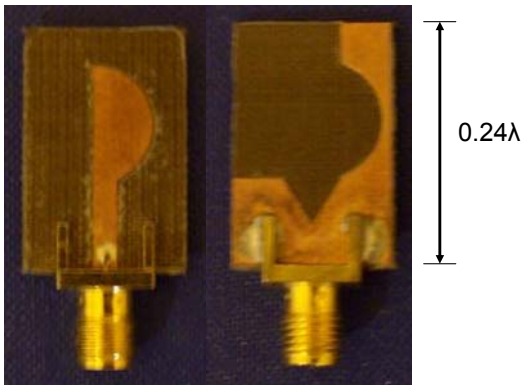


(a) (b)

Figure 6.21: The prototype of the proposed micro-strip line fed quasi-self-complementary antenna (a) Front side and (b) Back side.

Figure 6.22 displays the simulated and the measured $|S_{11}|$ curves of the proposed antenna. The measured 10 dB $|S_{11}|$ bandwidth is from 2.86 GHz to 10.7 GHz, while in simulation from 2.8 GHz to 11.3 GHz. The measurement confirms the UWB characteristic of the proposed printed quasi-self-complementary antenna, as predicted in the simulation. The minor discrepancy between the simulation and the measurement is due to the effect of the feeding cable as the antenna is rather small. It is also noticed that the antenna size is not only physically small but also electrically small, only 0.24λ at 2.86 GHz.

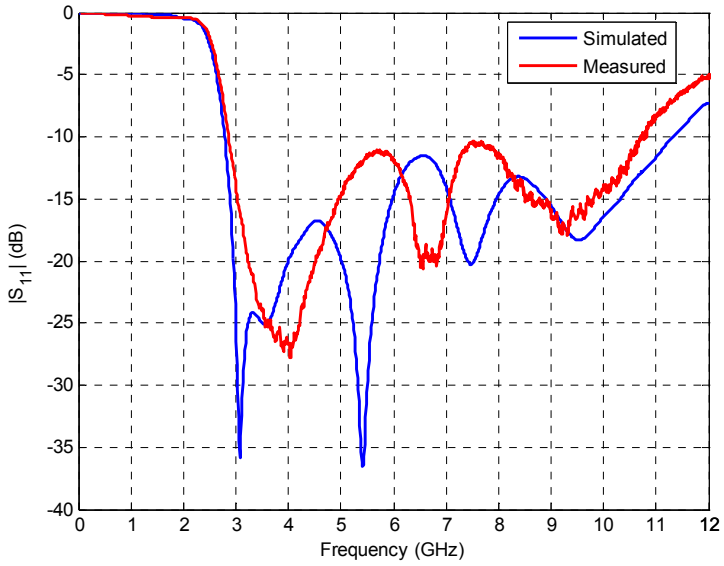


Figure 6.22: Simulated (blue) and measured (red) $|S_{11}|$ curves of the proposed printed quasi-self-complementary antenna.

The measured and the simulated normalised radiation patterns at 3.07 GHz and 9.31 GHz are plotted in figure 6.23 and figure 6.24, respectively. The patterns obtained in the measurement are close to those in the simulation. It is observed that the *H*-plane patterns are reasonable over the entire operating bandwidth. The simulated peak gain of the proposed antenna is plotted in figure 6.25, it is seen that a satisfactory gain level is achieved through the whole band. Figure 6.26 illustrates the orientation of the peak gain with the increase of frequency. It is observed that at the low and mid operational band the maximum gains occur at around $\varphi = 90^{\circ}$ cut plane with a variation of $\theta$ from $80^{\circ}$ to $130^{\circ}$. At the higher operational band, the peak gains emerge at a range of $\theta$ from $55^{\circ}$ to $80^{\circ}$ with $\varphi$ at around $0^{\circ}$ or $130^{\circ}$ cut plane.

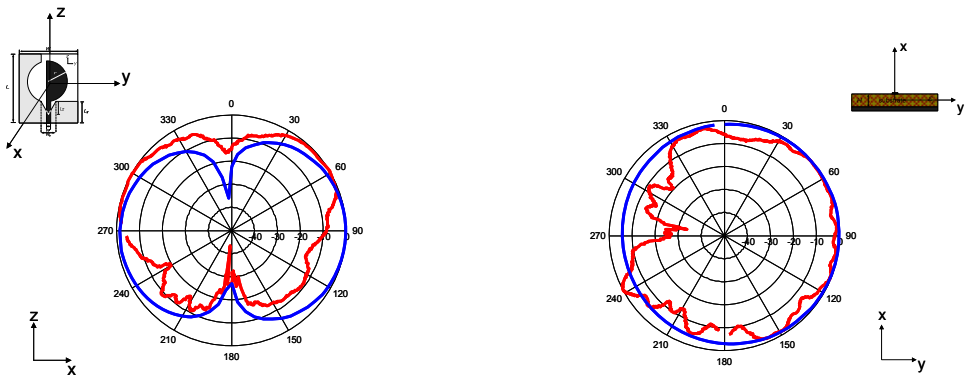


(a) (b)

Figure 6.23: Simulated (blue) and measured (red) radiation patterns with the optimal design at 3.07 GHz (a) *E*-plane (b) *H*-plane.

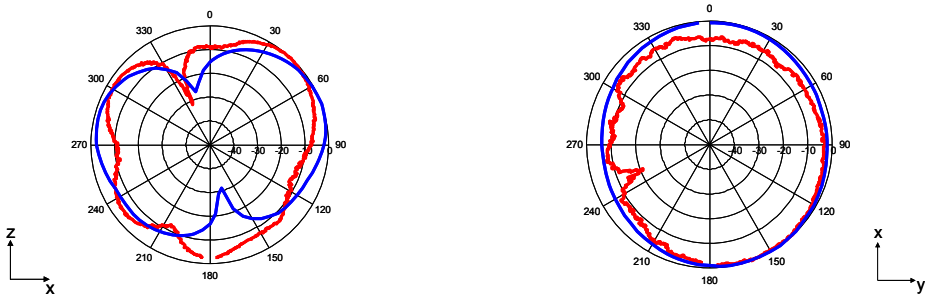


(a) (b)

Figure 6.24: Simulated (blue) and measured (red) radiation patterns with the optimal design at 9.31 GHz (a) *E*-plane (b) *H*-plane.

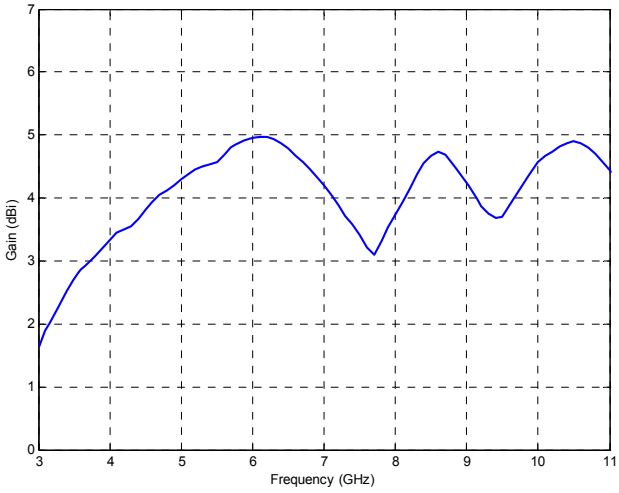


Figure 6.25: Simulated peak gain of the proposed antenna.

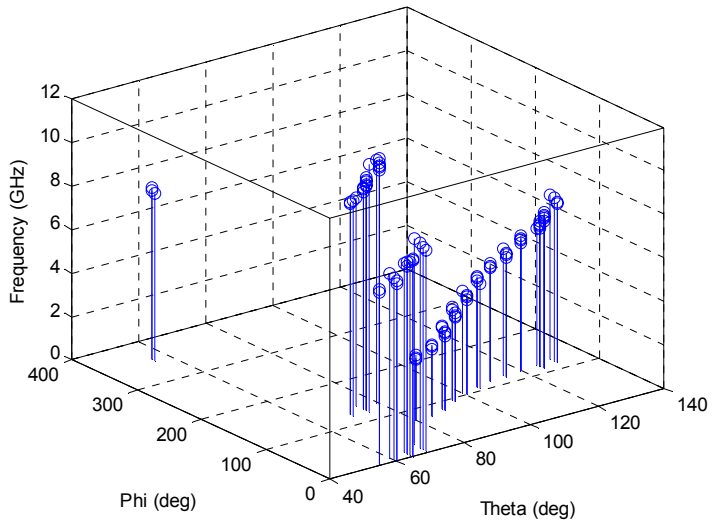


Figure 6.26: Simulated peak gain orientation of the proposed antenna.

### 6.3.2 Effects of Design Parameters

It has been shown in the simulation that the operating bandwidth of the printed quasi-self-complementary antenna is primarily dependent on the width of the antenna $W$, the width of the triangular slot $W_s$ and the height of the triangular slot $L_2$. So these parameters should be optimised for maximum bandwidth.

#### *A. The Effect of Antenna Width W*

Figure 6.27 plots the simulated $|S_{11}|$ curves with different antenna width ($W$=15, 16, 20 and 24mm) when $W_s$ is fixed at 6mm and $L_2$ at 4.8mm, respectively. It can be seen that the $|S_{11}|$ curves vary significantly and exhibit various shapes for the four different $W$. When $W$ is changed, the first local minimum frequency does not change much, however the higher local minimum frequencies vary dramatically, leading to the variations of the operating bandwidth of the antenna, as shown in figure 6.27. The optimal antenna width is found to be at $W$=16mm.

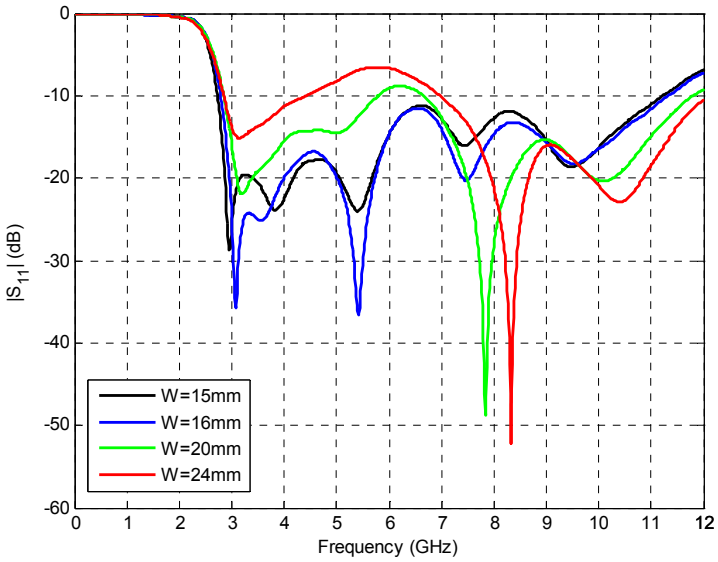


Figure 6.27: Simulated $|S_{11}|$ curves for different widths of the antenna with $W_s$=6mm and $L_2$=4.8mm.

### *B. The Effect of the Width of the Triangular Slot $W_s$*

The simulated $|S_{11}|$ curves with $L_2$=4.8mm and optimal antenna width $W$ of 16mm for different triangular slot widths $W_s$ are presented in figure 6.28. It is observed in figure 6.28 that the $|S_{11}|$ curves change substantially with the variation of $W_s$. When $W_s$ increases from 2mm to 6mm the impedance matching of the antenna gets better, however the higher edge of the bandwidth decreases. With the further increase of $W_s$ from 6mm to 8mm the impedance matching of the antenna becomes worse and the higher end of the bandwidth keeps reducing. The optimised triangular slot width is found to be at $W_s$=6mm.

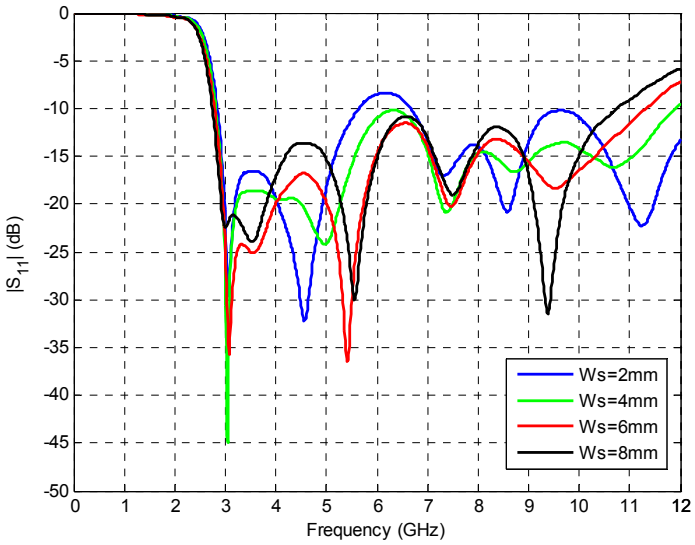


Figure 6.28: Simulated $|S_{11}|$ curves for different widths of the triangular slot with $W$=16mm and $L_2$=4.8mm.

### C. *The Effect of the Height of the Triangular Slot* $L_2$

Figure 6.29 shows the simulated $|S_{11}|$ curves for different triangular height $L_2$ when $W$=16mm and $W_s$ =6mm, respectively. It is observed that the impedance matching is also greatly dependent on the height of the triangular slot. When $L_2$ is equal to 4.8mm, the -10 dB bandwidth covers an ultra wide frequency band; when $L_2$ decreases to 2.8mm and 0.8mm, the lower edge of the bandwidth increases and the impedance matching for $L_2$ =0.8mm becomes worse. When $L_2$ rises to 6.8mm the lower edge of the bandwidth reduces, however, the impedance matching for mid band is degraded. The optimal triangular slot height is found to be at $L_2$ =4.8mm.

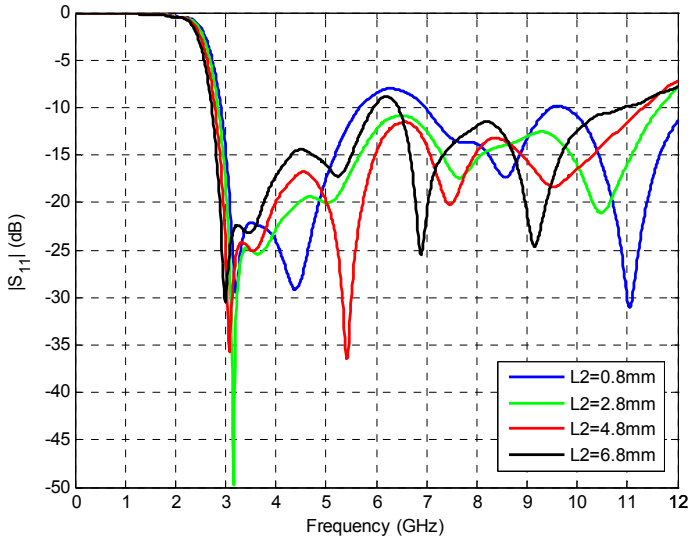


Figure 6.29: Simulated $|S_{11}|$ curves for different heights of the triangular slot with $W$=16mm and $W_s$=6mm.

## 6.4 Summary

A printed CPW-Fed quasi-self-complementary antenna is firstly investigated in this Chapter. It is demonstrated numerically and experimentally that the proposed printed quasi-self-complementary antenna can achieve an ultra wide impedance bandwidth, from 1.3 GHz to 13.1 GHz. The antenna also exhibits a compact and small dimension, only 0.22 $\lambda$ at 1.3 GHz. The important parameters of the quasi-self-complementary antenna are studied to derive the design rules. It has been shown that the performance of the antenna is critically dependent on the matching section width $W_1$, slotted ground width $W_2$, spacing $s$ and the size of the half circular disc / slot $r$. Furthermore, an evolution of the proposed antenna is depicted to gain some insights into the mechanism of the built-in CPW-like matching section. In addition, a microstrip line-fed quasi-self-complementary antenna is also proposed and investigated. It presents an even smaller dimension, 16mm×25mm in physical size and 0.24λ in electrical size, respectively. Also, an ultra wide impedance bandwidth

with reasonable radiation patterns is obtained. The results show that both types of printed quasi-self-complementary antennas are good candidates for the UWB applications.

## References

[1] Y. Mushiake, "Self-Complementary Antennas", *IEEE Antennas and Propagation Magazine*, vol. 34, no. 6, December 1992, pp. 23-29.

[2] Y. Mushiake, "A Report on Japanese Development of Antennas: From the Yagi-Uda Antenna to Self-Complementary Antennas", *IEEE Antennas and Propagation Magazine*, vol. 46, no. 4, August 2004, pp. 47-60.

[3] J. Kraus, "Antennas for all applications", © 2002, McGraw-Hill, INC.

[4] P. Xu, K. Fujimoto, S. Lin, "Performance of Quasi-Selfcomplementary Antenna Using a Monopole and a Slot", *2002 IEEE Antennas and Propagation Society International Symposium*, San Antonio, Texas, U.S.A, 16-21 June 2002.

[5] F. Kuroki, H. Ohta, M. Yamaguchi and E. Suematsu, "Wall-Hanging Type of Self-Complementary Spiral Patch Antenna for Indoor Reception of Digital Terrestrial Broadcasting", *2006 IEEE MTT-S International Microwave Symposium Digest*, San Francisco, CA, U.S.A, 11-16 June, 2006.

[6] K. Wong, T. Wu, S. Su and J. Lai, "Broadband Printed Quasi-Self-Complementary Antenna for 5.2 / 5.8 GHz WLAN Operation", *Microwave and Optical Technology Letters*, vol. 39, no. 6, December 20, 2003.

[7] Z. Chen, T. See and X. Qing, "Small Printed Ultrawideband Antenna with Reduced Ground Plane Effect", *IEEE Transaction on Antennas and Propagation*, vol. 55, no. 2, February 2007, pp. 383-388.

[8] P. Xu, K. Fujimoto, "L-shaped Self-complementary Antenna", *2003 IEEE*

*Antennas and Propagation Society International Symposium, Columbus*, Ohio, U.S.A, 22-27 June 2003.

# Chapter 7 Time Domain Behaviour of UWB Antennas

As described in chapter 2, UWB systems often employ short pulses to deliver information, in other words, enormous bandwidth is occupied. Therefore the influence of the antenna on the transmitted signal emerges as a vital issue. The antenna can not be treated as a "spot filter" any more but a "band-pass filter". In this regard, antenna parameters will have to be evaluated as functions of frequency and some elemental antenna parameters need to be re-addressed or re-assessed within the UWB definition scope and due to UWB's unique features, it is essential to study UWB antennas from a time domain perspective [1-10]. Ideally, the received UWB signal should maintain exactly the same shape as the source pulse. Practically, the signal waveforms reaching the receiver usually do not resemble the input pulse at the transmitter. The received signals normally are distorted in shape and sometimes present a long tail termed the "ringing effect". The antenna, therefore, should be carefully designed to avoid unwanted distortions and a time domain study of UWB antennas is indispensable.

In addition, according to the FCC regulations, emission limits should also be taken into account. The spectra of radiated pulses should abide by the regulation to evade potential interference between UWB and other existing wireless systems. Thus, the source pulses also play a pivotal role on the performance of UWB systems. Appropriately choosing the source pulse shape can maximise the radiated power within the UWB band and satisfy the required emission limit [11, 12].

In this chapter, the CPW-Fed disc monopole antenna, illustrated in chapter 5,

is exemplified to analyse its time domain characteristics. Firstly, the behaviour of this antenna is assessed from a system point of view. Secondly, transmit and receive responses of the CPW-Fed disc monopole are studied. Thirdly, the radiated power spectral density of the antenna is examined in contrast to the FCC emission mask. Finally, a convolution approach is applied to obtain the measured received signals and the antenna system is evaluated by the "pulse fidelity".

## 7.1 Behaviour of UWB Antenna System

### 7.1.1 Description of UWB Antenna System

Consider a typical transmitting / receiving antenna system in UWB radio systems [12], as shown in figure 7.1.

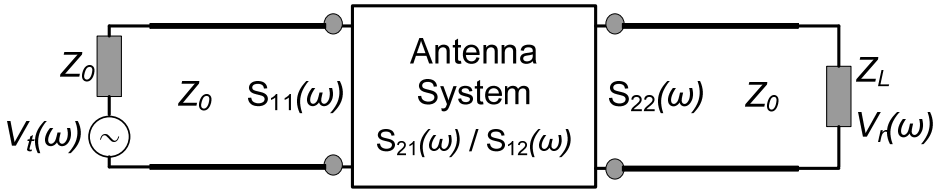


Figure 7.1: Schematic diagram of UWB antenna system.

The Friis Transmission Equation relates the received power to the transmitted power between two antennas [13], as given in equation 7.1.

$$\frac{P_r}{P_t} = (1-|\Gamma_t|^2)(1-|\Gamma_r|^2) G_r G_t \left| \hat{\rho}_t \cdot \hat{\rho}_r \right|^2 \left( \frac{\lambda}{4\pi d} \right)^2 \qquad (7.1)$$

where $P_t$, $P_r$: time average input power of the transmitting antenna and time average output power of the receiving antenna; $\Gamma_t$, $\Gamma_r$: reflection coefficient at the input of the transmitting antenna and the output of the receiving antenna; $G_t$, $G_r$: gain of the transmitting antenna and the receiving antenna; $\left| \hat{\rho}_t \cdot \hat{\rho}_r \right|^2$: polarisation matching

factor between the transmitting and receiving antenna; $\lambda$ : operating wavelength; and *d*: distance between the two antennas.

As UWB systems operate over a huge frequency range, all of the parameters in equation 7.1 are frequency-dependent. The formula can be rewritten as follows:

$$\frac{P_r(\omega)}{P_t(\omega)} = (1-|\Gamma_t(\omega)|^2)(1-|\Gamma_r(\omega)|^2)G_t(\omega)G_r(\omega)\left|\hat{\rho}_t(\omega)\cdot\hat{\rho}_r(\omega)\right|^2\left(\frac{\lambda}{4\pi d}\right)^2 \qquad (7.2)$$

For reflection and polarisation matched antennas aligned for maximum directional radiation and reception, equation 7.2 reduces to:

$$\frac{P_r(\omega)}{P_t(\omega)} = (\frac{\lambda}{4\pi d})^2 G_t(\omega)G_r(\omega) \qquad (7.3)$$

The system transfer function, i.e. $S_{21}$, is defined to describe the relation between the source and the output signal. According to figure 7.1, $[V_t(\omega)/2]^2 = P_t(\omega)Z_0$, $V_r^{\,2}(\omega)/2 = P_r(\omega)Z_L$, so $S_{21}$ is given by:

$$S_{21}(\omega) = \frac{V_r(\omega)}{V_t(\omega)} = \left|\sqrt{\frac{P_r(\omega)}{P_t(\omega)}\frac{Z_L}{4Z_0}}\right| e^{-j\phi(\omega)} = |S_{21}(\omega)|e^{-j\phi(\omega)}$$

$$\phi(\omega) = \phi_t(\omega) + \phi_r(\omega) + \frac{\omega d}{c} \qquad (7.4)$$

In equation 7.4, *c* denotes velocity of light, $\phi_t(\omega)$ and $\phi_r(\omega)$ are the phase variation related to the transmitting and receiving antennas, respectively.

It is evident in equation 7.2 and equation 7.4 that the transfer function is determined by the characteristics of both transmitting and receiving antennas, such as impedance matching, gain, polarisation matching and the spacing between the two antennas. $S_{21}$ also integrates all of the important system performance, such as path loss and phase delay. Thus, it can be used to assess the behaviour of antenna systems.

In addition, the system response can be fully determined when the transfer

function is known. To repress distortions in the received waveform, the transfer function should feature a flat magnitude and linear phase response across the operating band.

### 7.1.2 Measured Results of UWB Antenna System

The measurements of the antenna system were conducted inside an anechoic chamber by using a HP 8720ES vector network analyser. The antenna system consists of two identical UWB antennas, as illustrated in figure 7.2. As UWB technology will be mainly deployed in short distance communications, thus in the measurements the transmitting antenna and the receiving antenna are vertically placed with a separation of $d$=1.2m. Furthermore, in order to evaluate the system performances in different directions, the two antennas are measured in two various orientations, namely face to face and side by side, respectively, as displayed in figure 7.3.

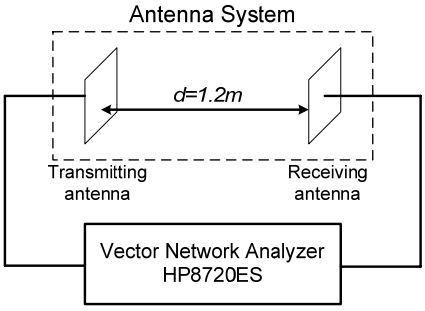


Figure 7.2: Antenna system set-up.

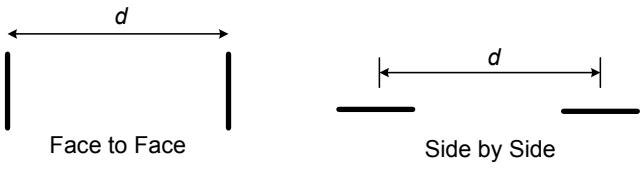


Figure 7.3: Antenna orientations (top view).

For the CPW-Fed disc monopole antenna, the two discs face to each other in

"face to face" orientation while in "side by side" scenario, the two CPW-Fed disc monopoles are aligned along the same line with the two discs facing towards the same direction.

The measured transfer function of the CPW-Fed disc monopole pair is plotted in figure 7.4 and figure 7.5, respectively.

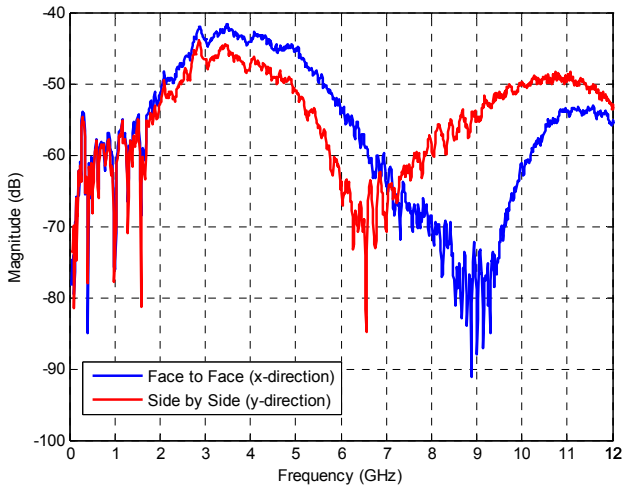


Figure 7.4: Magnitude of measured transfer function of the CPW-Fed disc monopole pair.

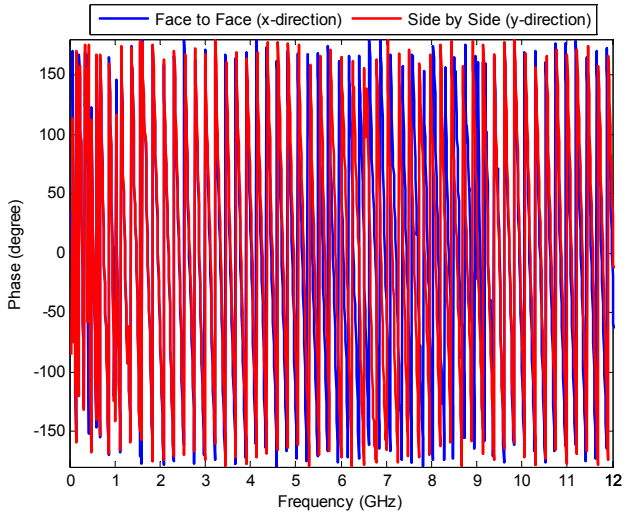


(a)

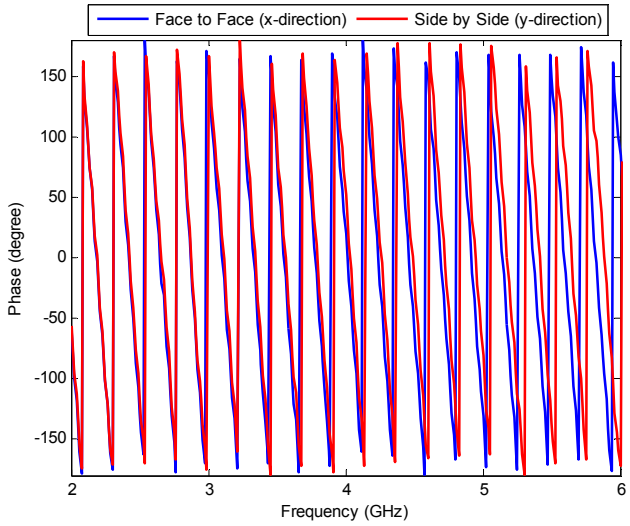


(b)

Figure 7.5: (a) Phase of measured transfer function of the CPW-Fed disc monopole pair (b) Zoomed in to 2 GHz – 6 GHz.

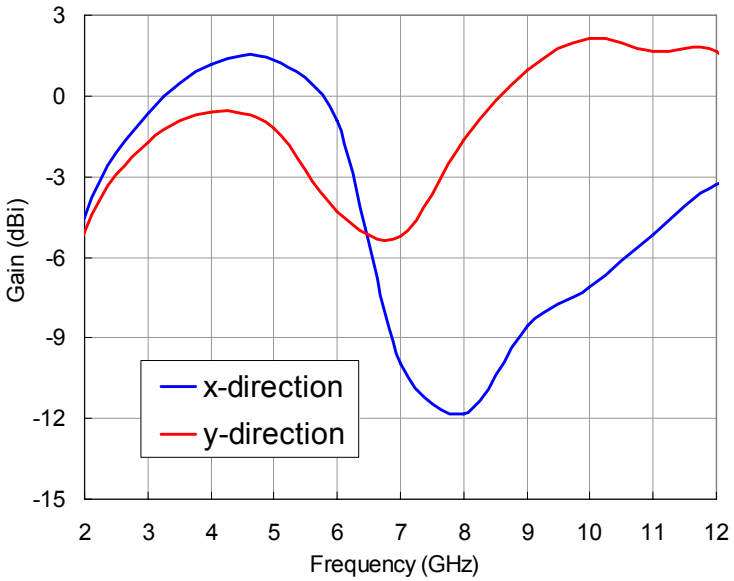


Figure 7.6: Simulated gain of the CPW-Fed disc monopole antenna in the *x*-direction and the *y*-direction.

It is seen in figure 7.4 that the magnitude curves of the transfer functions coincide well with the antenna gain (as shown in figure 7.6). At lower frequency range (less than 3 GHz), the *y*-direction (the direction which is parallel to the disc

radiator) gain is quite close to that of the *x*-direction (the direction which is normal to the disc radiator), consequently, the two magnitude curves for both cases, i.e. face to face and side by side, are almost equivalent. Within the frequency range from 3 GHz to 6.4 GHz, the *y*-direction gain gets smaller than that of the *x*-direction, therefore the magnitude curve of face to face scenario is slightly higher than that of the side by side scenario. Nevertheless, at higher frequencies (more than 6.4 GHz), the *x*-direction gain declines dramatically with the increase of the frequency, in the meantime, the *y*-direction gain rises significantly. So, the magnitude of the side by side scenario becomes higher than the face to face scenario.

It is also observed that the operating band (-10 dB below the peak) of transfer function for the face to face case ranges from 2 GHz to 5.8 GHz. Outside this band, the magnitude curve wanes rapidly. This indicates the signal within the frequency range of 2 GHz to 5.8 GHz will be received almost intact. For frequencies higher than 5.8 GHz the frequency components will be further attenuated, which leads to distortion of the total received signal. The operating band of side by side case is narrower than the face to face case, from 2 GHz to 5.2 GHz and the magnitude curve experiences a deep null at around 6 GHz.

As noticed in figure 7.5, the phase curves of the transfer functions for both face to face and side by side scenarios are very alike. They are nearly linear over an ultra wide frequency range from about 2 GHz to 6 GHz, as shown in figure 7.5 (b). The non-linear attributes outside this range will result in distortions of the received waveforms.

Usually, the radiation pattern, transfer function and gain (single direction) are used as a metric to evaluate the UWB disc monopoles' performance. However, these measures are either taken at specific frequencies (radiation patterns) or at fixed

directions (transfer functions). Therefore, an overall gain pattern is desired to facilitate the antenna analysis. With this pattern, the gain is plotted against the angle and frequency in one figure and it would be more revealing to examine the antenna radiation behaviour with respect to parameters, i.e. frequency and azimuth angle.

Figure 7.7 depicts the azimuth gain pattern of the CPW-Fed disc monopole antenna. It is shown in figure 7.7 that at lower frequencies, i.e. from 3 GHz to 5.5 GHz, the radiation patterns at *x*-*y* plane are omni-directional. With the increase of the frequency from 5.5 GHz, non-omni-directional radiation characteristics occurs and the notch will be firstly formed in the *y*-direction and eventually generated in the *x*-direction. After 6 GHz, the gain starts to go up in the *y*-direction and it will reach another peak at 10 GHz. In the *x*-direction, the gain also begins to rise after around 9 GHz. This behaviour again agrees perfectly with the plot of the transfer function, as illustrated in figure 7.4. Clearly, with the help of this gain pattern, more information about the antenna radiation behaviours can be obtained in all directions.

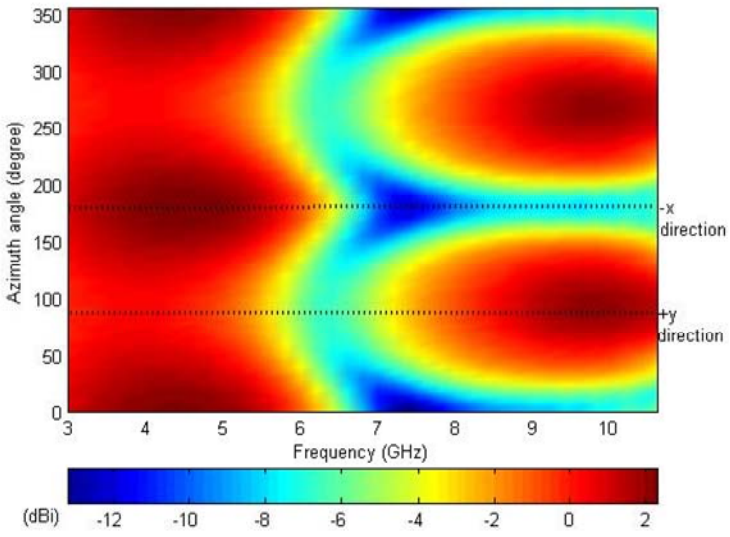


Figure 7.7: Azimuth gain pattern of the CPW-Fed disc monopole antenna.

The gain drop in the *y*-direction could be explained as follows. From the current distribution of this antenna, it is clearly seen that the current is mostly

concentrated on the two edges of circular disc. Thus it can be treated as an antenna array with two simple current elements, as shown in figure 7.8.

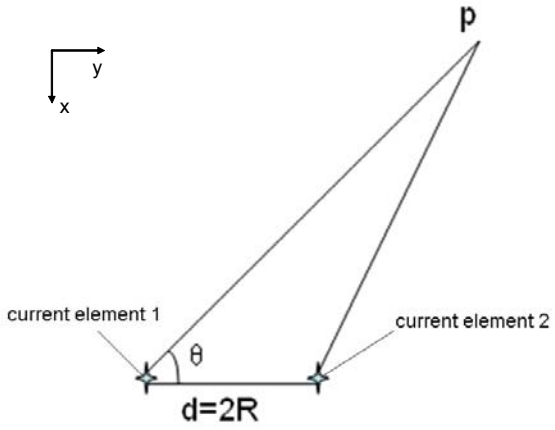


Figure 7.8: Circular disc approximated by two current elements.

The total electric field in the far field region can be expressed by equation 7.5:

$$E = E_1 + E_1 e^{j\beta d\cos\theta} \tag{7.5}$$

where $E_1$ is the radiated field by current element 1 and $\beta d\cos\theta$ is the current element 2 phase advanced than current element 1, so equation 7.5 can be written as:

$$E = E_1(1 + e^{j\beta d\cos\theta}) \tag{7.6}$$

when $\theta = 0^\circ$ ($y$-direction), equation 7.6 reduces to:

$$E = E_1(1 + e^{j\beta d}) \tag{7.7}$$

And there will be a null (no radiation) in the $y$-direction only if $\beta d = \pi$. So when $\lambda = 2d$, the dip of gain will appear at that corresponding frequency. This approximation can be applied to the CPW-Fed disc monopole case. As the diameter of the disc $2r$ is 25mm, the null of gain will show up at

$$\lambda = 2d = 2 \times 25mm = 50mm \tag{7.8}$$

So,

$$f = c/\lambda = 3\times10^{8}/50\times10^{-3} = 6GHz \tag{7.9}$$

Therefore, this verifies the gain drop in the *y*-direction around 6 GHz. A current distribution plot at 6 GHz is also plotted in figure 7.9.

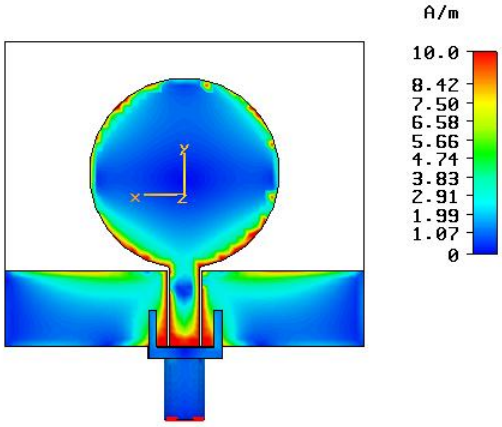


Figure 7.9: Current distribution of CPW-Fed disc monopole antenna at 6 GHz.

## 7.2 Impulse Response of UWB Antenna

In section 7.1, the behaviour of the CPW-Fed disc monopole antenna is assessed from a system point of view. The system transfer function $S_{21}$ has integrated the effects of both transmitting and receiving antennas. This section will investigate the impulse response of the CPW-Fed disc monopole when it is used as transmitter and receiver, respectively.

### 7.2.1 Transmitting and Receiving Responses

Consider a practical antenna whose performance is frequency-dependent. The transmitting and receiving frequency (time) characteristics are expressed by $A(\omega)$ ($a(t)$) and $H(\omega)$ ($h(t)$), respectively, as displayed in figure 7.10.

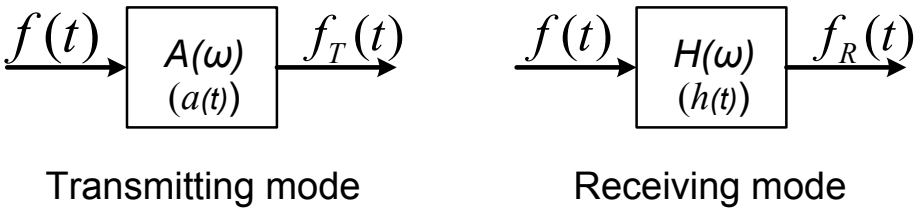


Figure 7.10: Antenna operating in transmitting and receiving modes.

In addition, applying the principle of reciprocity, it can be shown that the transmitting and receiving characteristics are linked by [14, 15]:

$$A(\omega) \propto j\omega H(\omega) \tag{7.10}$$

For the same stimulus *f(t)* ( $F(\omega)$ ), the transmitting response $f_T(t)$ and receiving response $f_R(t)$ can be represented by:

$$f_T(t) \overset{\Delta}{=} \int F(\omega) A(\omega) e^{j\omega t} d\omega \tag{7.11}$$

$$f_R(t) \overset{\Delta}{=} \int F(\omega) H(\omega) e^{j\omega t} d\omega \tag{7.12}$$

Using equation 7.10, equation 7.11 can be rewritten as:

$$f_T(t) \propto \int F(\omega) j\omega H(\omega) e^{j\omega t} d\omega = \frac{\partial}{\partial t} f_R(t) \tag{7.13}$$

Equation 7.13 indicates that the transmitting response is proportional to the temporal derivative of the receiving response. As a result, $f_T(t)$ and $f_R(t)$ will present different shapes to the same stimulus *f(t)* ( $F(\omega)$ ).

If the bandwidth $B(\Omega, \omega_c)$ of the stimulus $F(\omega)$ is defined as [14]:

$$B(\Omega, \omega_c) \overset{\Delta}{=} \left\{ \omega : \left| |\omega| - \omega_c \right| \le \Omega / 2 \right\}$$

where $\omega_c$, $\Omega > 0$, $\omega_c$ is the centre frequency of the bandwidth.

Then equation 7.13 can be modified as:

$$f_T(t) \propto \frac{\partial}{\partial t} f_R(t) = \int F(\omega) j\omega H(\omega) e^{j\omega t} d\omega = \int |\omega| F(\omega) H(\omega) e^{j\omega(t+\frac{\pi}{2|\omega|})} d\omega \quad (7.14)$$

In narrow band scenario, $\Omega << \omega_c$, $|\omega| \approx \omega_c$, therefore equation 7.14 can be approximated to:

$$f_T(t) \propto \frac{\partial}{\partial t} f_R(t) \approx \omega_c \int F(\omega) H(\omega) e^{j\omega(t+\frac{\pi}{2\omega_c})} d\omega \propto f_R(t + \frac{\pi}{2\omega_c}) \quad (7.15)$$

In the extreme case of a sine wave signal $f_R(t) = \cos(\omega_c + \phi)$,

$$\frac{\partial}{\partial t} f_R(t) \propto f_R(t + \frac{\pi}{2\omega_c}) \quad (7.16)$$

which is not an approximation, but exact.

Thus, the antenna transmitting and receiving responses are approximately equal up to scaling and shifting when the signal bandwidth is sufficiently narrow.

For ultra wide band case, the approximation ($\Omega << \omega_c$) leading to equation 7.15 is not valid. The transmitting response is proportional to the temporal derivative of the receiving response, as shown in equation 7.13. However, this derivative relationship can not be represented by scaling and shifting.

### 7.2.2 Transmitting and Receiving Response of CPW-Fed Disc Monopole Antenna

The transmitting and receiving response of the CPW-Fed disc monopole antenna can be obtained based on the frequency domain measurement results.

Consider the antenna system shown in figure 7.2 and figure 7.3 and assume the two antennas are placed in free space, thus the system transfer function $S_{21}(\omega)$ with face to face orientation can be expressed as [14]:

$$S_{21}(\omega) = A(\omega)H(\omega)\frac{e^{-jkd}}{d} \tag{7.17}$$

where $A(\omega)$ and $H(\omega)$ represents the transmitting and receiving characteristics of the antenna, respectively; $d$ is the spacing between the two antennas.

Applying the derivative relationship between $A(\omega)$ and $H(\omega)$, equation 7.17 may be given in various forms as:

$$S_{21}(\omega) = A(\omega)H(\omega)\frac{e^{-jkd}}{d} \propto \frac{1}{j\omega}A(\omega)A(\omega)\frac{e^{-jkd}}{d} \propto j\omega H(\omega)H(\omega)\frac{e^{-jkd}}{d} \tag{7.18}$$

Therefore, the transmitting characteristic $A(\omega)$ ($a(t)$) and the receiving characteristic $H(\omega)$ ($h(t)$) can be calculated when the measured system transfer function $S_{21}(\omega)$ is known.

The transmitting and receiving characteristics of the CPW-Fed disc monopole are shown in figure 7.11 and figure 7.12, respectively. The signal waveforms have already been normalised to their respective maximum value. The results confirm the disc monopole exhibits different but related characteristics when operating in transmitting and receiving modes.

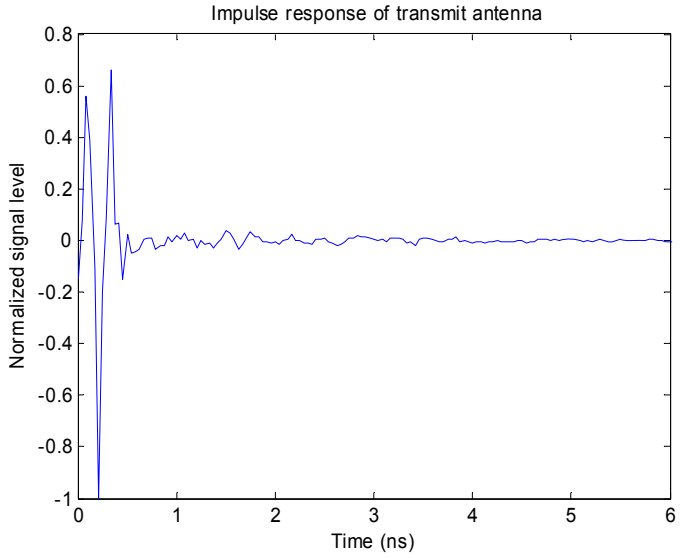


Figure 7.11: Transmitting characteristic of CPW-Fed disc monopole antenna.

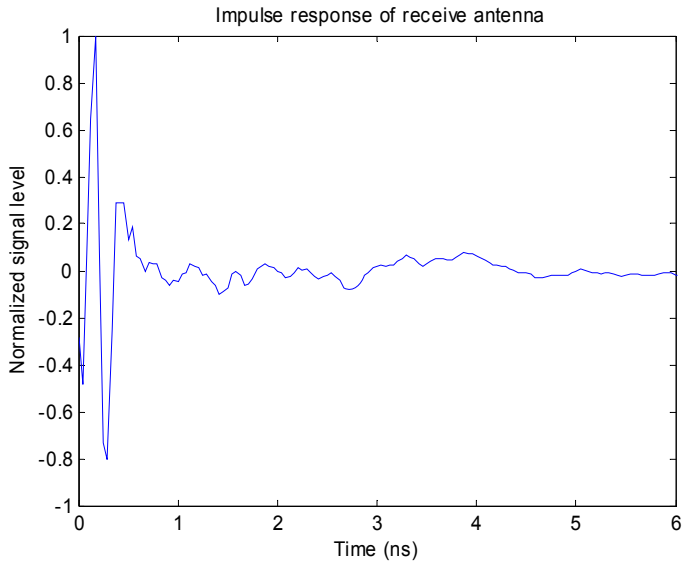


Figure 7.12: Receiving characteristic of CPW-Fed disc monopole antenna.

If a first-order Rayleigh pulse with pulse parameter of $a$=45ps, as given in equation 7.19 and figure 7.13, is used as the stimulus, the radiated pulse from the CPW-Fed disc monopole can be obtained by convolving the stimulus with the transmitting impulse response of the antenna, as illustrated in figure 7.14.

$$f(t) = -\frac{2t}{a^2} e^{-(\frac{t}{a})^2} \tag{7.19}$$

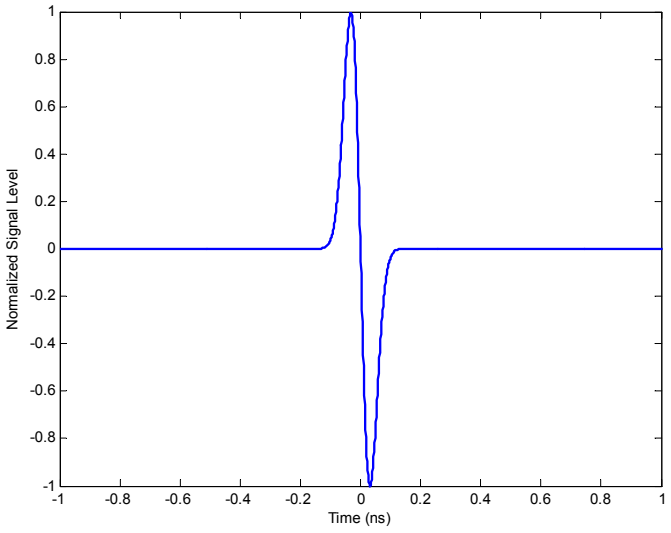


Figure 7.13: First-order Rayleigh pulse with $a$=45ps.

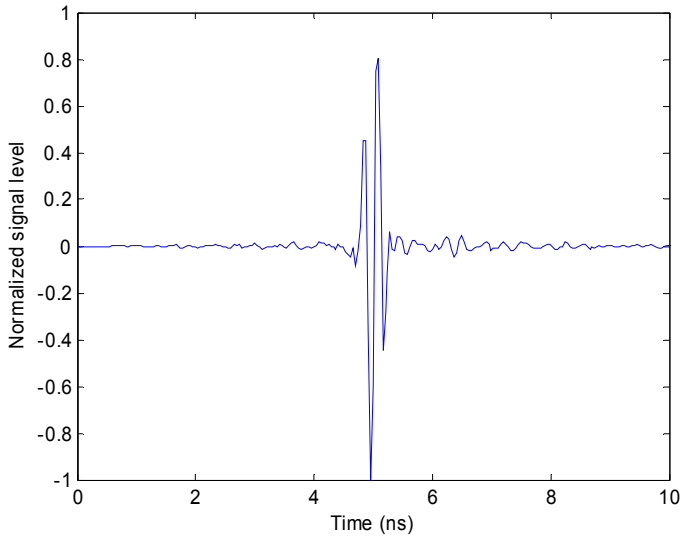


Figure 7.14: Radiated pulse from the CPW-Fed disc monopole antenna.

## 7.3 Radiated Power Spectral Density

As mentioned in chapter 2, UWB systems may incur interference to other existing wireless systems since they operate over a huge frequency range, which covers many occupied bands. Therefore, the emission limit is an important issue for the design of both source pulses and UWB antennas.

### 7.3.1 Design of Source Pulses

The first order Rayleigh pulse, as given in equation 7.19, is widely used as the source signal to excite the transmitter in UWB systems. The pulse parameter *a* denotes the characteristic time. Large *a* corresponds to wide waveform in the time domain but narrow bandwidth in the frequency domain. Figure 7.15 displays the normalised source pulses with three various pulse parameters. Their respective power spectral densities (PSD) against the FCC mask are given in figure 7.16.

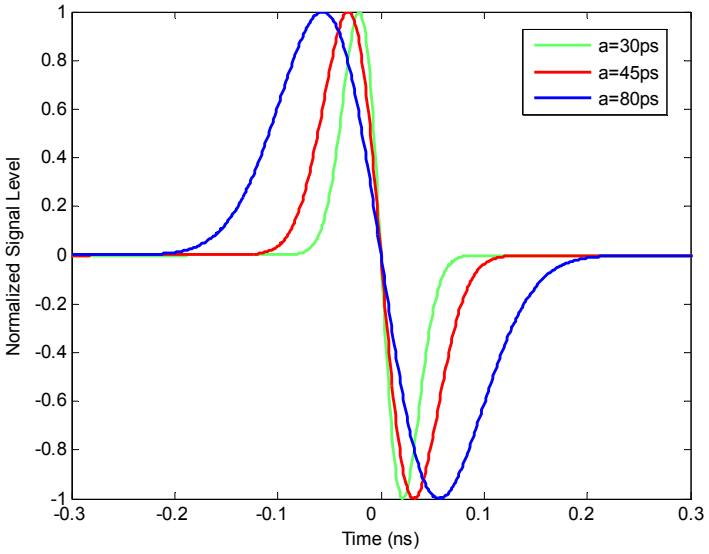


Figure 7.15: First order Rayleigh pulses with different *a*.

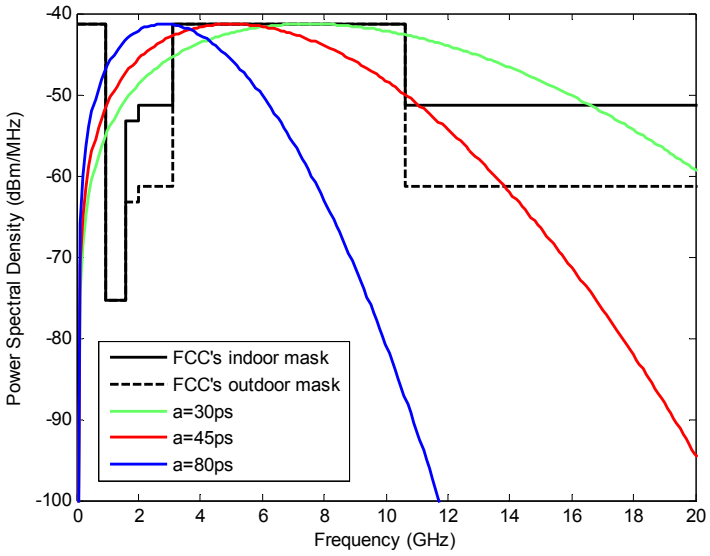


Figure 7.16: Power spectral densities of first order Rayleigh pulses with different *a*.

As shown in figure 7.16, the peak value position of the PSD as well as the 10 dB bandwidth, i.e. the frequency range confined by the points that are 10 dB below the peak emission , increases with the decrease of *a*. When *a*=30ps, the PSD curve culminates at 7.7 GHz with its 10 dB bandwidth spanning from 1.5 GHz to 16.6 GHz;

when *a* increases to 45ps, the maximum value of PSD appears at 5 GHz with the 10 dB bandwidth reduced to 10.1 GHz, from 1 GHz to 11.1 GHz; with the further increase of *a* to 80ps, the 10 dB bandwidth only ranges from 0.55 GHz to 6.2 GHz with PSD peaking at 2.8 GHz.

Figure 7.16 also demonstrates that none of the three pulses can completely comply with the FCC defined emission mask due to the high PSD at frequencies lower than 3.1 GHz. Moreover, the pulse with *a*=30ps exhibits a high PSD level within the frequency range between 10.6 GHz and 16.4 GHz. Comparatively, the pulse with *a*=45ps is more adequate for UWB systems as its bandwidth matches the UWB band better while the bandwidth of *a*=80ps is a bit narrow.

It is feasible to shift the spectra of the first order Rayleigh pulse to UWB band to fully satisfy the FCC's emission limits by using continuous sine wave carrier if the carrier frequency and the pulse parameter are properly chosen [16]. In addition, it is shown that some higher order Rayleigh pulses [12] can conform to the FCC's indoor emission mask directly such as the fourth order Rayleigh pulse with a pulse parameter of *a*=70ps, as presented in equation 7.20, figure 7.17 and figure 7.18.

$$f(t) = [\frac{12}{a^4} - \frac{48}{a^6}(t-1)^2 + \frac{16}{a^8}(t-1)^4]e^{-(\frac{t-1}{a})^2} \tag{7.20}$$

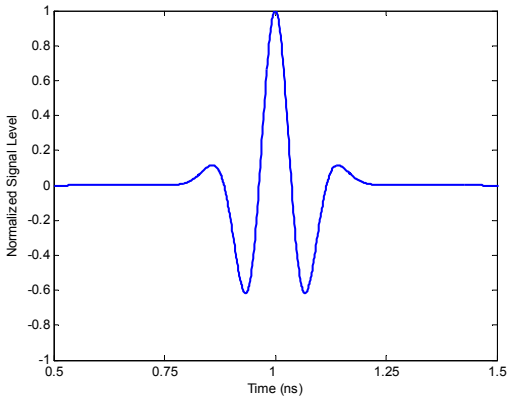


Figure 7.17: Fourth order Rayleigh pulse with *a*=70ps.

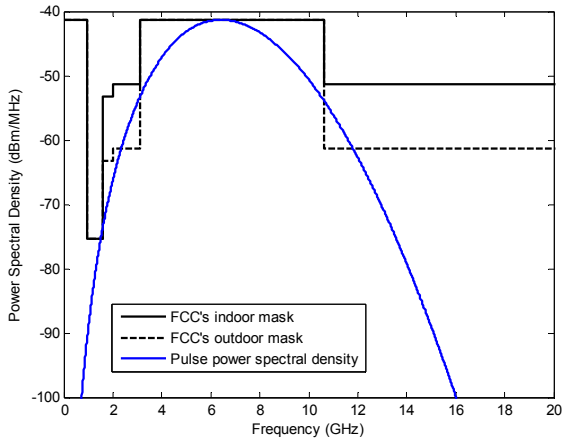


Figure 7.18: Power spectral density of fourth order Rayleigh pulse with *a*=70ps.

Despite the power spectral density of the first order Rayleigh pulse can not completely meet the FCC's emission mask, it is widely employed in UWB systems because of its simple monocycle waveform which can be easily produced by RF circuits. Therefore in this chapter, this type of signal is still used as the source pulse to investigate the time domain performances of the UWB antenna.

### 7.3.2 Radiated Power Spectral Density of CPW-Fed Disc Monopole Antenna

In the previous section, it has been demonstrated that the antenna transmitting characteristic can be calculated based on the measured system transfer function. Therefore, the radiated pulse can be easily obtained through the convolution of input pulse and the antenna transmitting response.

The power spectral densities of the radiated pulses for face to face orientation against the FCC emission mask are plotted in figure 7.19 and figure 7.20, respectively. Here, the first order Rayleigh pulse with *a*=45ps and the fourth order Rayleigh pulse with *a*=70ps, as discussed in the previous section, are employed as

the source signals to drive the CPW-Fed disc monopole. Their corresponding power spectral densities are also depicted in the figures to compare with the radiated ones accordingly.

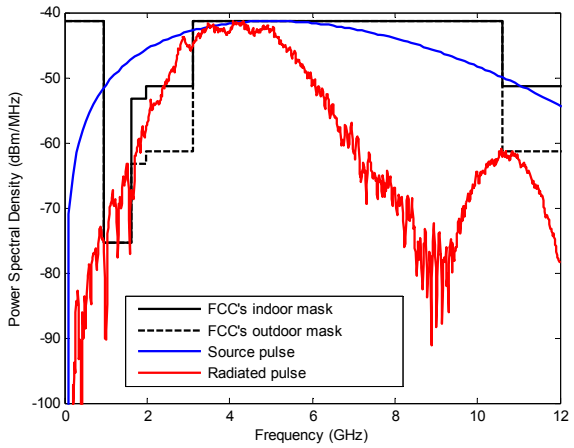


Figure 7.19: Radiated power spectral density with the first order Rayleigh pulse of $a$=45ps.

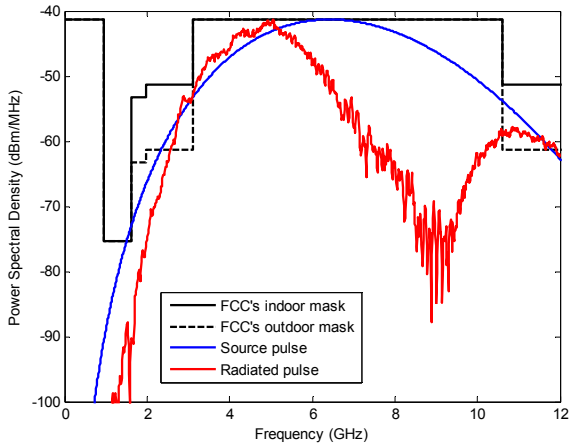


Figure 7.20: Radiated power spectral density with the fourth order Rayleigh pulse of $a$=70ps.

As shown in figure 7.19, when the source signal is the first order Rayleigh pulse with $a$=45ps, the radiated PSD is compliant with the FCC emission mask at most part of the frequency band except at the frequencies lower than 3.1 GHz, which is mainly owing to the high spectra level of the source pulse within this frequency

range. At around 9 GHz, the radiated PSD undergoes a deep null, which agrees well to the system transfer function $S_{21}$, as given in figure 7.4.

It is comprehensible that the fourth order Rayleigh pulse with $a$=70ps can result in a radiated PSD fully compliant with the FCC indoor mask since the source pulse spectra completely satisfy this emission limit, as shown in figure 7.20.

## 7.4 Received Signal Waveforms

For a UWB system, as shown in figure 7.2, the received signal is desired to resemble the source pulse with minimum distortions. The received waveform is determined by both the source pulse and the system transfer function which has already considered the effects from the entire system including the transmitting and receiving antennas.

The transfer function measured by the vector network analyser is a frequency response of the system. However, the frequency domain information can be transformed to the time domain. Here, Hermitian processing is used for the data conversion [17], as illustrated in figure 7.21. Firstly, the pass-band signal is obtained with zero padding from the lowest frequency down to DC (Direct Current). Secondly, the conjugate of the signal is taken and reflected to the negative frequencies. The resulting double-sided spectrum corresponds to a real signal, i.e. the system impulse response. It is then transformed to the time domain using Inverse Fast Fourier Transform (IFFT). Finally, the system impulse response is convolved with the input signal to obtain the received pulse.

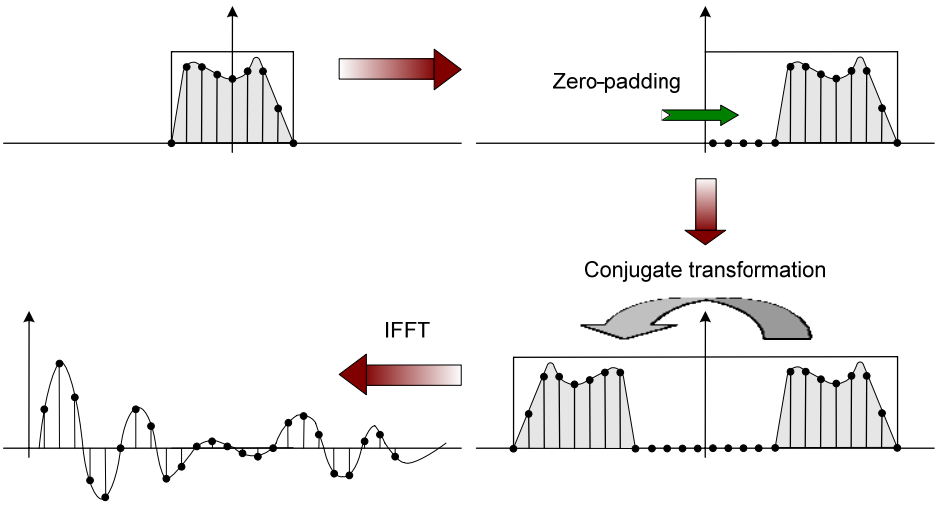


Figure 7.21: Hermitian processing (Reproduced from [17]).

As previously mentioned, the received UWB signal pulses practically do not resemble the source pulses and normally are distorted in shape. Therefore a measure of the similarity between the received pulse and the input pulse is highly desirable and valuable to indicate how good the performance of the UWB antenna system is. A well-defined parameter termed fidelity [7] is proposed to evaluate the quality of a received pulse waveform, as given in equation 7.21.

$$F = \max_{\tau}\left[\frac{\int_{-\infty}^{+\infty} f(t)s_R(t+\tau)dt}{\sqrt{\int_{-\infty}^{+\infty} f^2(t)dt\int_{-\infty}^{+\infty} {s_R}^2(t)dt}}\right] \tag{7.21}$$

where the source pulse $f(t)$ and the received pulse $s_R(t)$ are normalised by their energy. The fidelity factor $F$ is the maximum correlation coefficient of the two signals by changing the time delay $\tau$. It denotes the similarity between the source pulse and the received pulse. When the two signal waveforms are equivalent to each other, the fidelity reaches its peak, i.e. unity, which indicates the antenna system does not distort the input pulse at all. In the extreme scenario that the two pulses are totally different in shape, the fidelity reduces to the minimum value of zero.

Practically, a UWB system yields a fidelity between 0 and 1. Clearly, a high fidelity is always desirable.

When the first order Rayleigh pulse with $a$=45ps is selected as the input signal, the received pulse of the CPW-Fed disc monopole antenna are illustrated in figure 7.22.

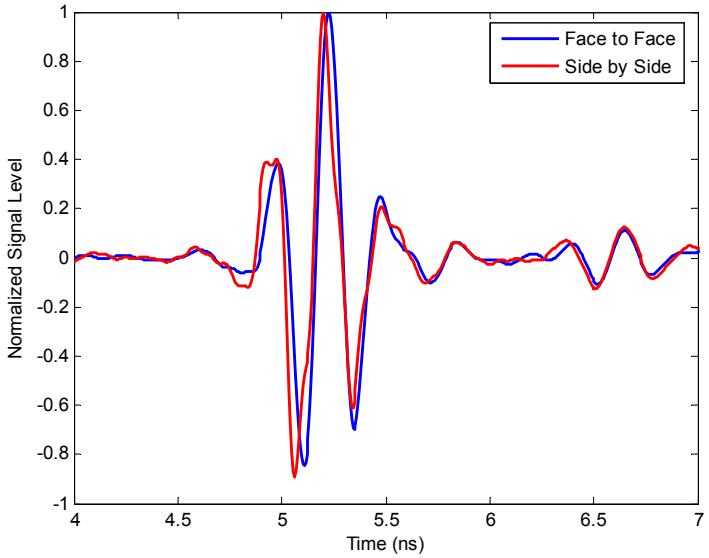


Figure 7.22: Received signal waveforms by the CPW-Fed disc monopole antenna with the first order Rayleigh pulse of $a$=45ps as the input signal.

The received waveforms of the two cases, i.e. face to face and side by side, match with each other very well. The pulse waveforms generally follow the shape of the source pulse with slight distortions. The calculated fidelity $F$ is 0.75 for face to face scenario and 0.63 for side by side scenario.

The distortions of the received pulse waveforms can be explained by comparing the bandwidths between the system transfer function $S_{21}$ and the spectrum of the source pulse, as illustrated in figure 7.23.

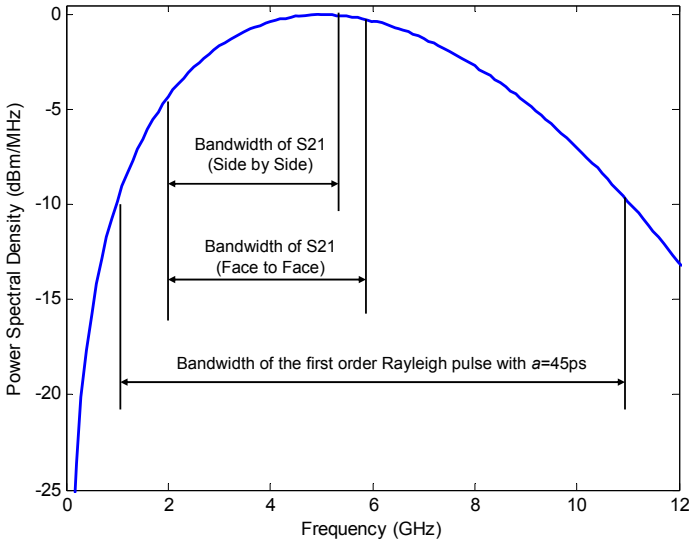


Figure 7.23: Spectrum of transfer functions and the first order Rayleigh pulse with $a$=45ps.

The input signal possesses a power spectrum from 1 GHz to 11.1 GHz at -10 dB points. However, the operating band of the transfer functions, as presented in figure 7.4, are much less than that of the source pulse spectrum. That indicates the input signal frequency components outside the transfer function bandwidth can not be efficiently transmitted by the CPW-Fed disc monopole. In addition, it is observed there are some non-linear parts in the phase curves of the transfer functions, as displayed in figure 7.5. As a result, the received waveforms suffer some distortions.

Moreover, the transfer function curves (both the magnitude and the phase) of the two cases are very similar within their corresponding operating bands, resulting in similar received pulse waveforms. However, face to face scenario features a flatter magnitude curve, which means the signal frequency components are received more equally, leading to a higher fidelity than side by side scenario.

The further investigation shows that the distortions of the received signals may be mitigated if the source pulse bandwidth were to fully fit into the band of the system transfer function.

Consider a Gaussian pulse modulated by a continuous sine wave carrier, as given in equation 7.22.

$$f(t) = \sin(2\pi f_c t) e^{-(t/a)^2} \tag{7.22}$$

where the carrier frequency $f_c$ is set at 4 GHz and pulse parameter *a* at 380ps.

The pulse waveform of the modulated Gaussian pulse and its corresponding spectrum are plotted in figure 7.24 and figure 7.25, respectively. It is seen that the spectrum peaks at 4 GHz with a -10 dB bandwidth from 2.7 GHz to 5.2 GHz, which indicates the major energy of the signal is completely shifted into the operating band of the system transfer function.

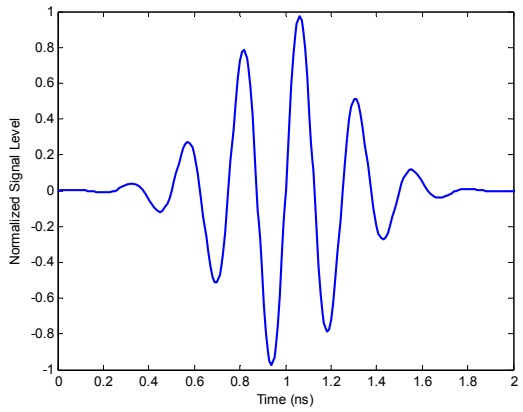


Figure 7.24: Modulated Gaussian pulse with *fc*=4 GHz and *a*=380ps.

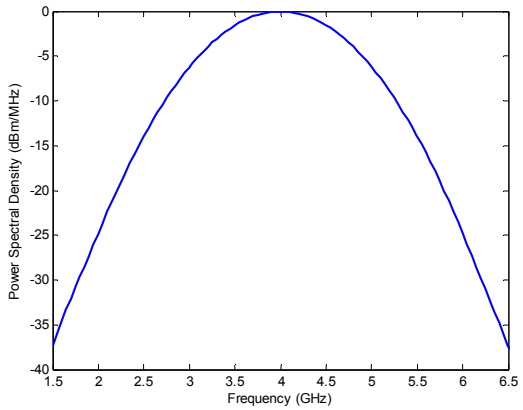


Figure 7.25: Spectrum of modulated Gaussian pulse with *fc*=4 GHz and *a*=380ps.

When the modulated Gaussian pulse is excited to the CPW-Fed disc monopole pair, the received signal waveforms are very similar to the source pulse in both orientations, as shown in figure 7.26.

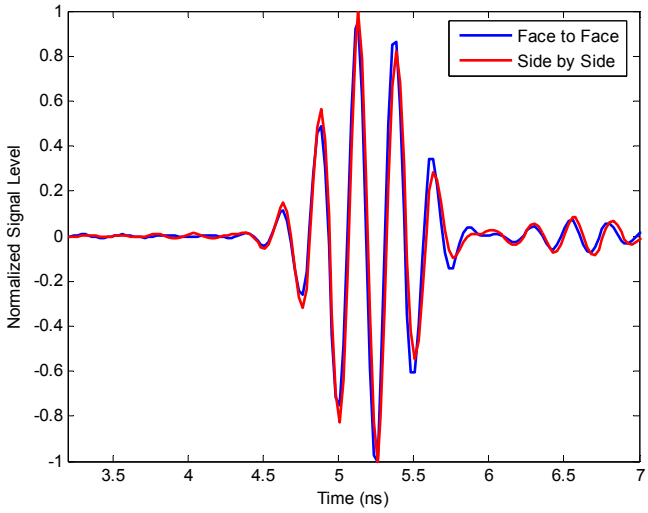


Figure 7.26: Received signal waveforms by the CPW-Fed disc monopole with modulated Gaussian pulse (*fc*=4 GHz, *a*=380ps) as the input signal.

The calculated fidelity is 0.9958 for face to face case and 0.9956 for side by side case, much higher than those when the first order Rayleigh pulse is applied as the source signal. A remarkable improvement of received signal quality has been achieved by using the modulated Gaussian pulse.

The calculated fidelities for different source pulses are tabulated in table 7-A.

Table 7-A: Fidelity for the CPW-Fed disc monopole antenna pair.

| | 1st order Rayleigh *a*=30ps | 1st order Rayleigh *a*=45ps | 1st order Rayleigh *a*=80ps | 4th order Rayleigh *a*=70ps | Modulated Gaussian *a*=380ps |
|---|---|---|---|---|---|
| Face to Face | 0.6315 | 0.7474 | 0.8369 | 0.9006 | 0.9958 |
| Side by Side | 0.6229 | 0.6303 | 0.8599 | 0.9250 | 0.9956 |

According to the table 7-A, a fidelity greater than 0.995 is achieved for both orientations when the modulated Gaussian pulse is employed as the source pulse. This is well understood because the pulse spectrum is fully located within the band of the system transfer function. Most of frequency components can be received efficiently and equally. Therefore, the antenna system does not incur distortions to the signal.

For the fourth order Rayleigh pulse with $a$=70ps, its spectrum matches well with the 3.1 GHz – 10.6 GHz UWB frequency band, as plotted in figure 7.18. The upper end of the transfer function operating band is at about 6 GHz, less than 10.6 GHz. Signal frequency components between 6 GHz and 10.6 GHz are attenuated dramatically, resulting in some distortions in the received signal waveforms.

The spectrum of the first order Rayleigh pulse is critically dependent on the pulse parameter $a$. A larger $a$ corresponds to a wider waveform in the time domain but a narrower spectrum bandwidth in the frequency domain, as illustrated in equation 7.19. For $a$=80ps, the spectrum bandwidth ranges from 0.55 GHz to 6.2 GHz. The upper frequency end of the signal spectrum is close to that of the transfer function, but the lower end is smaller than that of the transfer function. That indicates some low frequency components of the pulse are filtered by the antenna system. With the decrease of $a$, the spectrum bandwidth becomes wider, and some high frequency components are also filtered. Consequently, the fidelity value gets smaller and it is even lower than 0.7 for both orientations when $a$=30ps.

## 7.5 Summary

In UWB systems, the antenna serves as a bandpass filter and reshapes the signal spectrum. The antenna transmitting response is related to its receiving response by a

temporal derivative. As a result, the signal waveform arriving at the receiver usually does not resemble the input pulse.

To achieve a high fidelity, which represents the similarity between the input pulse and the received one, the system transfer function should feature a flat magnitude with linear phase within the operating band. Furthermore, the spectrum of the source pulse should match the transfer function. Therefore, the received pulse waveform is dependent on both the antenna system and the source pulse.

The first order Rayleigh pulse has a simple monocycle shape. However, its power spectral density can not completely abide by the FCC defined emission mask. In addition, the acquired fidelity may be quite low owing to the mismatch between the pulse spectrum and the operating band of the transfer function. Some higher order Rayleigh pulses (for instance, the fourth order pulse with $a$=70ps) can fully meet the FCC emission mask, which makes it competent for DS-UWB systems. Applying the modulated Gaussian pulse, a very high fidelity can be obtained and the received signal does not suffer many distortions. Thus, this relatively narrow band pulse with carrier is appropriate for MB-OFDM UWB systems.

## References

[1] X. Wu and Z. Chen, "Design and Optimization of UWB Antennas by a Powerful CAD Tool: PULSE KIT", *IEEE Antennas and Propagation Society International Symposium*, vol. 2, 20-25 June 2004, pp. 1756-1759.

[2] F. Talom, B. Uguen, L. Rudant, J. Keignart, J. Pintos and P. Chambelin, "Evaluation and Characterization of an UWB Antenna in Time and Frequency Domains", *IEEE International Conference on Ultra-Wideband (ICUWB 2006)*, Waltham, U.S.A, September 2006, pp. 669-673.

[3] K. Yazdandoost, H. Zhang and R. Kohno, "Ultra-wideband Antenna and Pulse Waveform for UWB Applications", *2006 International Conference on ITS Telecommunications*, Chengdu, China, June 2006, pp. 345-348.

[4] W. Malik, D. Edwards and C. Stevens, "Angular-spectral antenna effects in ultra wideband communications links", *IEE Communications*, vol. 153, issue 1, 2nd February 2006, pp. 99-106.

[5] A. Abbosh and M. Bialkowski, "Design of Ultrawideband Planar Monopole Antennas of Circular and Elliptical Shape", *IEEE Transactions on Antennas and Propagation*, vol. 56, no. 1, January 2008, pp. 17-23.

[6] X. Wu and Z. Chen, "Comparison of Planar Dipoles in UWB Applications", *IEEE Transactions on Antennas and Propagation*, vol. 53, no. 6, June 2005, pp. 1973-1983.

[7] T. Ma and S. Jeng, "Planar Miniature Tapered-Slot-Fed Annular Slot Antennas for Ultrawide-Band Radios", *IEEE Transactions on Antennas and Propagation*, vol. 53, no. 3, March 2005, pp. 1194-1202.

[8] Y. Cho, K. Kim, D. Choi, S. Lee and S. Park, "A Miniature UWB Planar Monopole Antenna With 5-GHz Band-Rejection Filter and the Time-Domain Characteristics", *IEEE Transactions on Antennas and Propagation*, vol. 54, no. 5, May 2006, pp. 1453-1460.

[9] T. Ma and S. Wu, "Ultrawideband Band-Notched Folded Strip Monopole Antenna", *IEEE Transactions on Antennas and Propagation*, vol. 55, no. 9, September 2007, pp. 2473-2479.

[10] S. Cheng, P. Hallbjorner and A. Rydberg, "Printed Slot Planar Inverted Cone Antenna for Ultrawideband Applications", *IEEE Antennas and Wireless Propagation Letters*, vol. 7, 2008, pp. 18-21.

[11] G. Lu, P. Spasojevic and L. Greenstein, "Antenna and Pulse Designs for Meeting UWB Spectrum Density Requirements", *2003 IEEE Conference on Ultra Wideband Systems and Technologies*, Reston, U.S.A, 16-19 November 2003, pp. 162-166.

[12] Z. Chen, X. Wu, H. Li, N. Yang and M. Chia, "Considerations for Source Pulses and Antennas in UWB Radio Systems", *IEEE Transactions on Antennas and Propagation*, vol. 52, no. 7, July 2004, pp. 1739-1748.

[13] C. Balanis, "Antenna Theory Analysis and Design", © 2005, by John Wiley & Sons, INC.

[14] J. Kunisch and J. Pamp, "UWB radio channel modelling considerations", *Proc. International Conference on Electromagnetics in Advanced Applications* (ICEAA'03), pp. 277-284, Torino, Italy, September 2003.

[15] J. Kunisch and J. Pamp, "Considerations regarding the correlation between transmit and receive response of UWB antennas", *2004 URSI International Symposium on Electromagnetic Theory*, Pisa, Italy, 23-27 May 2004.

[16] K. Siwiak and D. McKeown, "Ultra-Wideband Radio Technology", © 2004, by John Wiley & Sons, Ltd.

[17] I. Oppermann, M. Hamalainen and J. Iinatti, "UWB Theory and Applications", © 2004, by John Wiley & Sons, Ltd.

# Chapter 8 Conclusions and Future Work

## 8.1 Summary

UWB is a promising technology which will bring the convenience and mobility of wireless communications to high-speed interconnections in devices throughout the digital home and office. As a critical part of the entire UWB system, the antenna presents a particular challenge since there are more strict requirements for a competent UWB antenna compared with its narrow band counterpart. In addition, in order to be easily integrated into space-limited systems, UWB antennas with small and compact size are highly desirable and essential to a wide variety of applications. Therefore, the antenna miniaturisation and analysis for UWB systems are conducted in this thesis.

The loaded orthogonal half disc monopole antenna stems from an original orthogonal half disc monopole by inserting a pair of loading strips between the half disc and the ground plane. Studies show that the loading strip width and position as well as the ground plane are the three prime parameters affecting the performance of the loaded orthogonal half disc monopole antenna. It has also been demonstrated that the ground plane size can be properly reduced for making the antenna more compact. The emergence and enhancement of the first resonance due to the loading technique result in the widened bandwidth at the lower frequency band and a summary of the design rules has been given for achieving the ultra wide impedance bandwidth in a loaded orthogonal half disc monopole antenna. Both simulation and measurement have demonstrated that the loaded orthogonal half disc monopole can achieve an ultra wide impedance bandwidth, covering the frequency band allocated by the FCC,

and maintain omni-directional radiation patterns over the entire operating band. Most importantly, the loaded orthogonal half disc monopole antenna has realised 64% physical size reduction and 68.8% equivalent size reduction in volume compared with the original design therefore demonstrating the feasibility of the loading technique to the miniaturisation of UWB antennas.

The printed half disc monopole antenna evolves from an original printed CPW-Fed circular disc monopole. It has been shown that a remarkable 65% physical size reduction in area can be achieved for the printed disc monopole antenna for UWB systems by simply halving the original antenna and adjusting the width of the coplanar ground plane. The printed half disc monopole antenna exhibits an even wider impedance bandwidth at the lower band. It has been revealed that the prolonged current path due to the removal of the right-hand side ground plane causes the wider impedance bandwidth at the lower end. Investigations also indicate that the half disc element is capable of supporting multi resonant modes and these modes are closely distributed. The overlapping of these resonances leads to the UWB characteristic. The half disc monopole behaves like a pure standing wave mode at the first resonance and a hybrid mode of standing and travelling waves at higher order resonances. Thus the printed half disc monopole features a similar operating principle with the original UWB antenna. In addition, design rules are also provided to achieve the ultra wide impedance bandwidth in a printed half disc monopole antenna.

The printed CPW-Fed quasi-self-complementary antenna excited by a $50\Omega$ coaxial cable without additional matching circuit can achieve an ultra wide impedance bandwidth, from 1.3 GHz to more than 12 GHz. The antenna presents a compact and small dimension, only $0.22\lambda$ at 1.3 GHz. The vital parameters of the

quasi-self-complementary antenna are also investigated to derive the design rules. It has been shown that the antenna performance is primarily dependent on the matching section width, slotted ground width, spacing between the disc and the slot, and the size of the half circular disc / slot. In addition, an evolution of the antenna is illustrated to acquire some insights into the mechanism of the built-in CPW-like matching section. It has been demonstrated that by adding a CPW-like matching section, a good impedance matching to the 50Ω feed can be achieved over the UWB band therefore the effectiveness of the built-in matching section is verified. Furthermore, it is presented that a massive 74% equivalent size reduction in area can be realised in the printed quasi-self-complementary antenna compared with the original CPW-Fed disc monopole design. The microstrip line-fed quasi-self-complementary antenna exhibits both physically and electrically small dimensions, 16mm×25mm in physical size and 0.24λ in electrical size, respectively. Also, an ultra wide impedance bandwidth with reasonable radiation patterns is obtained.

The time domain performance of the CPW-Fed circular disc monopole antenna is also studied in this thesis. The received signal waveform is determined by both the transmitting / receiving antennas and the source pulse. The antenna system transfer function should feature a flat magnitude and linear phase response over the operating band in order to obtain high fidelity. In addition, the spectrum of the source signal should match the operating band of the system transfer function. Various pulses, i.e. the first order Rayleigh pulse, the fourth order Rayleigh pulse and the carrier-modulated Gaussian pulse, are studied and chosen as the source pulse for the CPW-Fed circular disc monopole antenna system. Investigations have indicated that a high signal fidelity is obtained by applying the carrier-modulated Gaussian pulse since its spectrum matches the antenna system transfer function well.

## 8.2 Key Contributions

The major contributions in this thesis are detailed as follows.

Firstly, a loaded orthogonal half disc monopole antenna is proposed and realised by introducing a pair of loading strips. The loaded antenna exhibits 64% physical size reduction and 68.8% equivalent size reduction compared with the original design. In the meantime, the loaded antenna can still achieve ultra wide impedance bandwidth covering 3.1 GHz – 10.6 GHz and maintain omni-directional radiation properties.

Secondly, a printed half disc monopole antenna is proposed and realised by simply halving the original antenna design and tuning the ground plane width. The printed half disc monopole can still retain an ultra wide impedance bandwidth and even exhibit a bit wider bandwidth at the lower band. The operating principle as well as the reason for the widened bandwidth at the lower end is illustrated.

Thirdly, novel and simple printed quasi-self-complementary antennas are proposed and realised by exploiting a half circular self-complementary structure. The CPW-Fed printed quasi-self-complementary antenna features an ultra wide impedance bandwidth, ranging from 1.3 GHz to more than 12 GHz. Also, compared with current UWB antenna designs published in the literature, this quasi-self-complementary antenna offers a rather small electrical size, only $0.22\lambda$ at the lowest frequency of the bandwidth. Moreover, the microstrip line-fed quasi-self-complementary antenna presents both physically and electrically small dimensions, 16mm×25mm in physical size and $0.24\lambda$ in electrical size, respectively. Most importantly, the proposed printed quasi-self-complementary antennas are excited by a $50\Omega$ coaxial cable without using an extra matching network. Thus, these antennas can be easily integrated with the RF front end.

Lastly, the time domain behaviour of the CPW-Fed disc monopole antenna is evaluated in this thesis.

All of these antennas proposed in the thesis demonstrate the feasibility of UWB antenna miniaturisation by using different methods which makes them suitable for space-limited systems.

## 8.3 Future Work

UWB antenna miniaturisation and analysis is a hot topic at present. Some aspects of the work presented here can be further investigated and improved. Future work can be performed in the following areas:

Firstly, it has been noticed that both the printed half disc monopole antenna and the printed quasi-self-complementary antenna exhibit distorted radiation patterns at higher frequencies. Further research may focus on finding out methods to overcome this problem.

Secondly, all the antenna measurements in this thesis are conducted inside an anechoic chamber. However, in practical UWB systems, antennas may be embedded inside a laptop or other terminals. Therefore, devices' effects on antenna performances need to be studied. In addition, the human body impact on antennas mounted on portable devices should also be considered.

Thirdly, this thesis only focuses on the research for single UWB antenna elements. Nevertheless, for some directional systems, a high gain is required to achieve the quality of the communication link. Thus, the research on antenna array can be carried out in the future work.

Fourthly, with the self-complementary structure, antennas can be scaled down to a very compact size for other applications, such as 2.45 GHz band on-body

communications. Therefore, potential compact antenna designs exploiting the self-complementary structure for on-body communications can be studied in the future work.

Lastly, good time domain behaviour is a vital requirement for UWB antennas. Further investigations can be conducted to evaluate the time domain performance of the other three UWB antennas, i.e. the loaded orthogonal half disc monopole antenna, the printed half disc monopole antenna and the printed quasi-self-complementary antenna.

# Author's Publications

## *Journal Papers*

1. **L. Guo**, S. Wang, X. Chen and C. G. Parini, "Study of a compact antenna for UWB applications", *IET Electronics Letters*. (Accepted)
2. **L. Guo,** S. Wang, X. Chen and C. G. Parini, "A Small Printed Quasi-Self-Complementary Antenna for Ultrawideband Systems", *IEEE Antennas and Wireless Propagation Letters*, vol. 8, 2009, pp. 554-557.
3. **L. Guo**, S. Wang, X. Chen and C. G. Parini, "Study of A Miniaturised Quasi-Self-Complementary UWB Antenna in Frequency and Time Domain", *Radioengineering*, vol. 18, no. 4, December 2009, pp. 381-387.
4. **L. Guo**, S. Wang, Y. Gao, Z. Wang, X. Chen and C. G. Parini, "Study of a printed quasi-self-complementary antenna for ultra wideband systems", *IET Electronics Letters*, vol. 44, no. 8, April 10$^{th}$, 2008, pp. 511-512.
5. **L. Guo**, J. Liang, C. C. Chiau, X. Chen, C.G. Parini and J. Yu, "Performance of UWB disc monopoles in time domain", *IET Proceedings on Microwaves, Antennas & Propagation*, vol. 1, no. 4, August 2007, pp. 955-959.
6. S. Wang, **L. Guo**, X. Chen, C. G. Parini and J. McCormick, "Design of Compact Broadband TSA Arrays by Using Element Mutual Coupling", *IET Electronics Letters*, vol. 44, August 2008, pp. 1049-1051.
7. J. Liang, **L. Guo**, C. C. Chiau, X. Chen and C. G. Parini, "Study of CPW-fed circular disc monopole antenna for ultra wideband applications", *IEE Proceedings on Microwaves, Antennas & Propagation*, vol. 152, no. 6, December 2005, pp. 520-526.

## *Conference Papers*

1. **L. Guo**, S. Wang, X. Chen and C.G.Parini, "A Time Domain Study of A Small Quasi-Self-Complementary UWB Antenna", *2010 International Workshop on Antenna Technology: Small Antennas, Innovative Structures and Materials (iWAT2010)*, Lisbon, Portugal, March 1-3, 2010. (Accepted)
2. **L. Guo**, S. Wang, X. Chen and C.G.Parini, "A Printed Miniaturised Antenna for Ultra Wideband Systems", *2010 International Workshop on Antenna Technology: Small Antennas, Innovative Structures and Materials (iWAT2010)*, Lisbon, Portugal, March 1-3, 2010. (Accepted)
3. **L. Guo**, S. Wang, X. Chen and C. G. Parini, "Miniaturised Antennas for UWB Communications", *3rd European Conference on Antennas and Propagation (EuCAP 2009)*, Berlin, Germany, March 23-27, 2009.
4. **L. Guo**, S. Wang, X. Chen and C. G. Parini, "A Miniature Quasi-Self-Complementary Antenna for UWB Applications", *Asia Pacific Microwave Conference 2008 (APMC 2008)*, HongKong & Macau, China, December 16-20, 2008.
5. **L. Guo**, X. Chen and C.G. Parini, "A Printed Quasi-Self-Complementary Antenna for UWB Applications", *2008 IEEE AP-S International Symposium on Antenna and Propagation*, San Diego, U.S.A, July 5-12, 2008.
6. **L. Guo**, S. Wang, Y. Gao, X. Chen and C.G. Parini, "Miniaturisation of Printed Disc UWB Monopoles", *IEEE International Workshop on Antenna Technology: Small Antennas and Novel Metamaterials*, 4-6, March 2008, Chiba University, Japan.
7. **L. Guo**, S. Wang, C.C.Chiau, X. Chen and C.G. Parini, "On Small UWB Antennas", *2007 European Conference on Antennas & Propagation (EuCAP*

*2007)*, Edinburgh, UK, 12-16 November 2007.

8. **L. Guo**, M. Rehman, J. Liang, X. Chen and C.G. Parini, "A Study of Cross Ring Antenna for UWB Applications", *IEEE International Workshop on Antenna Technology: Small Antennas and Novel Metamaterials*, 21-23, March 2007, Cambridge, U.K.
9. **L. Guo**, Z. Yang, J. Liang, X. Chen and C.G. Parini, "An Improved Design of Orthogonal Half Disc UWB Antenna", *The first European Conference on Antennas and Propagation (EuCAP 2006)*, Nice, France, 6-10 November, 2006.
10. **L. Guo**, J. Liang, C.G. Parini and X. Chen, "Transmitting and Receiving Characteristics of A CPW-Fed Disc Monopole for UWB Applications", *2006 IEEE AP-S International Symposium on Antenna and Propagation*, Albuquerque, U.S.A, July 9-14, 2006.
11. **L. Guo**, J. Liang, X. Chen and C.G. Parini, "Time Domain Behaviors of Artimi's UWB Antenna", *IEEE International Workshop on Antenna Technology: Small Antennas and Novel Metamaterials*, March 6-8, 2006, White Plains, NY, U.S.A.
12. **L. Guo**, J. Liang, C.C. Parini and X. Chen, "A time domain study of CPW-Fed disk monopole for UWB applications", *Asia-Pacific Microwave Conference 2005*, 4-7 December 2005, Suzhou, China.
13. **L. Guo**, J. Liang, X. Chen and C.G. Parini, "Study of tapering effects on the CPW-Fed of a circular disk monopole antenna", *2005 Loughborough Antennas & Propagation Conference (LAPC' 05)*, Loughborough, U.K, 4-6 April 2005.
14. S. Wang, **L. Guo**, X. Chen, C.G. Parini and J. McCormick, "Analysis of Mutual Coupling in Broadband Arrays", *2008 IEEE AP-S International Symposium on Antenna and Propagation*, San Diego, U.S.A, July 5-12, 2008.
15. S. Wang, **L. Guo**, X. Chen, C.G. Parini and J. McCormick, "Design of Broadband

Phased Array Using Tapered Slot Antenna", *IEEE International Workshop on Antenna Technology: Small Antennas and Novel Metamaterials*, 4-6, March 2008, Chiba University, Japan.

16. X. Chen, **L. Guo**, J. Liang and C.G. Parini, "On the Performance of UWB Monopole Antennas", *2007 IEEE International Conference on Ultra-Wideband (ICUWB 2007)*, Singapore, 24-26 September 2007.
17. J. Liang, **L. Guo**, C.C.Chiau and X. Chen, "Time domain characteristics of UWB disc monopole antennas", *35th European Microwave Conference*, 3-7 October, 2005, Paris, France.
18. J. Liang, **L. Guo**, C.C.Chiau and X. Chen, "CPW-fed circular disc monopole antenna for UWB applications", *IEEE International Workshop on Antenna Technology: Small Antennas and Novel Metamaterials*, March 7-9, 2005, Singapore.
19. S. Wang, X. Chen, **L. Guo** and C.G. Parini, "Towards Miniaturisation of UWB Antennas", *UWB 2007 European Workshop*, 10-11 May 2007, Grenoble, France.
20. X. Chen, J. Liang, **L. Guo**, P. Li, C.C.Chiau and C.G. Parini, "Planar UWB monopoles and their operation", *The first European Conference on Antennas and Propagation (EuCAP 2006)*, Nice, France, 6-10 November, 2006.
21. X. Chen, J. Liang, P. Li, **L. Guo**, C.C.Chiau and C.G. Parini, "Planar UWB monopole antennas", *Asia-Pacific Microwave Conference 2005*, 4-7 December 2005, Suzhou, China.